ANALYSIS OF SHEAR HEATING AND EFFECT OF TEMPERATURE DEPENDANT VISCOSITY ON HYDRODYNAMIC LIFT OF OIL BRUSH SEALS

by

ERTUĞRUL TOLGA DURAN

Submitted to the Graduate School of Engineering and Natural Sciences
in partial fulfillment of
the requirements for the degree of
Master of Science

SABANCI UNIVERSITY

August 2006

ANALYSIS OF SHEAR HEATING AND EFFECT OF TEMPERATURE DEPENDANT VISCOSITY ON HYDRODYNAMIC LIFT OF OIL BRUSH SEALS

APPROVED BY:

Assoc. Prof. Dr. Mahmut F. AKŞİT   ....
  (Thesis Advisor)

Prof. Dr. Asıf ŞABANOVİÇ   ....

Assist. Prof. Dr. Kemalettin ERBATUR   ....

Assist. Prof. Dr. Güllü Kızıltaş ŞENDUR   ....

Assist. Prof. Dr. İlyas KANDEMİR   ....

DATE OF APPROVAL: ....

ANALYSIS OF SHEAR HEATING AND EFFECT OF TEMPERATURE DEPENDANT VISCOSITY ON HYDRODYNAMIC LIFT OF OIL BRUSH SEALS

Ertuğrul Tolga DURAN

EECS, MS Thesis, 2006

Thesis Advisor: Assoc. Prof. Dr. Mahmut F. AKŞİT

ABSTRACT

Due to their superior performance and stable leakage characteristics, brush seals are one of the dynamic seals used in oil and oil mist applications in aero-engines and turbines. The viscous medium between the high speed rotor surface and brush seal bristles generates a hydrodynamic lifting force that determines seal clearance and leakage rate in oil sealing applications. The analytical solution to bristle lifting force can be obtained by using Reynolds formulation. Following a short bearing approximation, a closed form solution of the lifting force has been previously presented. However, solution to hydrodynamic lift force suggests a strong dependence on oil temperature and viscosity. This work presents an analytical solution to oil temperature rise due to shear heating. Starting with continuity and Navier Stokes equations, temperature distribution is derived by solving thermal energy equation. The hydrodynamic lift force relation has been expanded to include oil temperature and viscosity variability due to rotor speed and lift clearance. Results are also compared with the experimental data obtained from the dynamic oil seal test rig. In addition to temperature analysis, pressure distribution for the brush seal is also derived by tracking three different ways, all of which gives consistent results with each other and real life applications. Derivation of shear heat effect included lift clearance, which is the most important parameter for leakage performance of brush seals, is also done and compared with experimental lift clearance data.

FIRÇA YAĞ KEÇELERİNDE SICAKLIĞA BAĞLI VİSKOZİTENİN HİDRODİNAMİK KALDIRMAYA ETKİSİ VE VİSKOZ ISI KAYBI ANALİZİ

Ertuğrul Tolga DURAN

EECS, Yüksek Lisans Tezi, 2006

Tez Danışmanı: Doç. Dr. Mahmut F. AKŞİT

Anahtar kelimeler: Fırça keçe, Viskoz Isı Kaybı, Hidrodinamik Kaldırma Yüksekliği, Yağ Basıncı, Yataklama Teorisi

ÖZET

Yüksek performansları ve kararlı akış karakteristikleri sebebiyle fırça keçeler, uçak motorlarında ve türbinlerde yağ ve yağ buharı sızdırmazlığında kulanılan dinamik sızdırmazlık elemanı türlerinden biridir. Yağ sızdırmazlığı uygulamalarında yüksek hızlı rotor yüzeyi ile fırça keçe telleri arasındaki viskoz ortam hidrodinamik kaldırma kuvveti oluşturur. Bu kuvvet fırça keçe ile rotor arasındaki mesafeyi, dolayısıyla yağ kaçak miktarını belirler. Hidrodinamik kaldırma kuvvetinin analitik çözümü Reynolds formülasyonu kullanılarak yapılabilir. Kısa yatak kabulü yapılarak kaldırma kuvveti için analitik çözüm daha önce elde edilmiştir; ancak hidrodinamik kaldırma kuvveti fonksiyonu yağ sıcaklığına ve viskoziteye bağlıdır. Bu çalışma viskoz ısı kaybından ötürü yağ sıcaklığı artışı için analitik çözüm sunmaktadır. Süreklilik ve Navier Stokes denklemlerinden başlanmış; termal enerji denklemi çözülerek sıcaklık dağılımı türetilmiştir. Hidrodinamik kaldırma kuvveti bağıntısı, rotor hızıyla ve hidrodinamik kaldırma yüksekliğiyle değişen yağ sıcaklığı etkisini içerecek şekilde genişletilmiştir. Sonuçlar dinamik yağ sızdırmazlık test düzeneğinden elde edilen deneysel verilerle karşılaştırılmıştır. Sıcaklık dağılımının yanı sıra, fırça keçe için basınç dağılımı üç ayrı yol izlenerek türetilmiştir. Basınç dağılımı için bulunan çözümlerin birbirleriyle ve gerçek uygulamalarla tutarlı olduğu görülmüştür. Fırça keçelerin sızdırmazlık performansının belirlenmesinde en önemli parametre olan hidrodinamik kaldırma yüksekliği, vizkos ısı kaybının etkisini de içerecek şekilde teorik olarak türetilmiş ve deneysel verilerle karşılaştırılmıştır.

"To my family…"

ACKNOWLEDGEMENT

TABLE OF CONTENTS

LIST OF TABLES

LIST OF FIGURES

LIST OF SYMBOLS

BH	Free bristle height
FH	Fence height
β	Constant for viscosity relation for a given oil
C, C_1, C_2	Integration constants
c_p	Specific heat at constant pressure
E	Elasticity modulus of the bristle
F_b	Component of the lifting force normal to the bristle section
g_x	Gravitational acceleration in x-direction
g_y	Gravitational acceleration in y-direction
g_z	Gravitational acceleration in z-direction
H	Hydrodynamic lift clearance
h	Distance between bristle and rotor surfaces
h_i	Distance between the rotor and i^{th} bristle surfaces
I	Second moment of inertia for bristle section
L	Circumferential length of the rotor
L_b	Bristle length
μ	Dynamic viscosity
$\mu_{eff\text{-}z}$	Dynamic viscosity at certain z-coordinate
μ_{eff}	Effective dynamic viscosity
n_r	Number of bristles in one row of the bristle pack
η	Integration factor
P	Pressure
P^*	Normalized pressure
P_u	Upstream pressure
P_d	Downstream pressure
P_a	Atmospheric pressure
P_i	Local pressure distribution for each bristle
ΔP	Pressure difference between upstream and downstream sides
R_b	Bristle radius
R_{rotor}	Rotor radius

R_{eq}	Equivalent bristle bending curvature
R_a	Equivalent bristle bending curvature for infinite boundary
R_{bend}	Bent bristle radius
Re	Reynolds number
ρ	Density
T	Temperature
T_u	Upstream temperature
T_d	Downstream temperature
$T_{mean\text{-}z}$	Mean temperature with respect to z
$T_{dmean\text{-}z}$	Mean downstream temperature with respect to z
T_{eff}	Effective temperature
θ	Cant angle
u	Rotor surface speed
v_x	Velocity of the fluid in x-direction
v_y	Velocity of the fluid in y-direction
v_z	Velocity of the fluid in z-direction
v_x^{*}	Normalized velocity of the fluid in x-direction
v_y^{*}	Normalized velocity of the fluid in y-direction
v_z^{*}	Normalized velocity of the fluid in z-direction
w	Width of the bristle pack
W	Hydrodynamic lifting force
y_d	Deflection of the beam normal to rotor surface
(x, y, z)	Global coordinates
(x_i, y_i, z_i)	Local coordinates for each bristle

ABBRAVATIONS

N-S   Navier-Stokes

1   INTRODUCTION

Sealing technology plays an important role in controlling turbo machinery leakages and coolant flows in turbines and compressors. They also help control overall rotor dynamic stability during transient conditions. Improvements in fluid film sealing lead to 0.2 to 0.6% reduction in heat rate and 0.3 to 1% increase in power output in compressor applications. Seal clearance is the most important parameter in determining leakage performance, where excessive clearances cause efficiency losses and flow instabilities. Brush seals recently emerged as a seal technology in oil and oil mist applications in order to avoid clearance related problems and to achieve higher efficiences. Labyrinth seals, carbon seals or oil rings are other sealing elements that are commonly used around the bearings and oil sumps. Tighter clearances are required at these locations to avoid oil contamination of the downstream turbine components, or to minimize oil consumption levels. In some generator applications, these requirements are accentuated by the presence of explosive cooling gas. Due to their superior leakage performance, stable leakage characteristics and superior performance in accommodating transient conditions, brush seals are becoming more and more popular in sealing applications.

1.1   Brush Seal Structure

Brush seal is a dense pack of fine diameter *(0,05 to 0,15mm)* wire bristles which are sandwiched and welded between backing plate and the retaining plate *(front plate)*. Fiber density is around 785fiber/cm *(2000 fibers/in)*. The weld on the seal outer diameter is machined to obtain tight tolerances at the outer sealing surface which is fitted into a suitable housing. The bristles are extended radially inward beyond the backing plate, and machined to form a bore fit with the mating rotor. Typically, brush seals are mounted around a rotor with a slight interference. Selection of interference

must be properly done to avoid catastrophic rotor overheating and excessive rotor thermal growth problems.
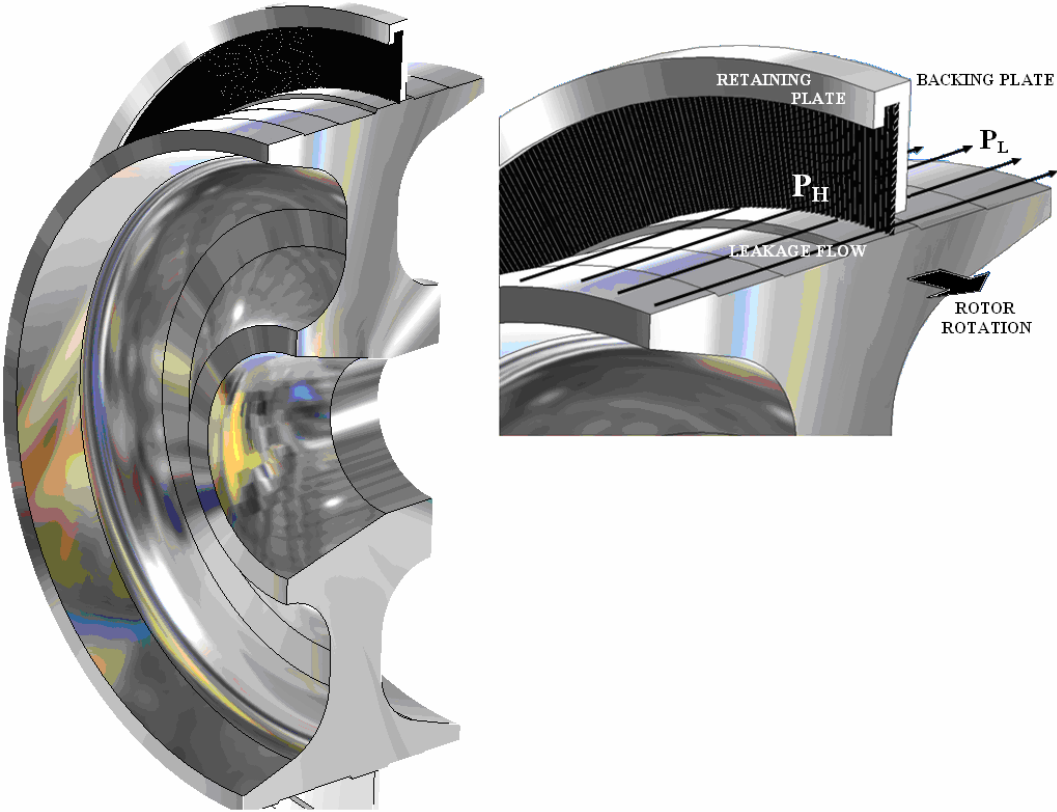
Figure 1.1 Brush seal geometry

Low pressure occurs at the downstream side while high pressure is applied at the upstream side of the brush seal. Pressure difference between upstream and downstream sides is called the *"pressure load"*. Under the pressure load, fluid flows from upstream side to downstream side, which corresponds to rotor axial direction, in the presence of pressure load. Shaft rotation is perpendicular to the leakage flow direction.

Backing plate is placed at the downstream side of the brush seal to provide a mechanical support to bristles under differential pressure loads. Retaining plate tightly clamps the bristles and holds them in plane. Brush seal is mounted around a mating rotor with a slight interference where bristles touch the rotor with an acute angle, which is so called cant angle, in the direction of the rotor rotation. Brush seals perform very well under rotor transients owing to the inherent compliance of bristles. Cant angle allows bristles to bend without buckling so that radial shaft movements can be

accommodated. Typically, cant angle, Θ, changes between 35° to 55°. Decreasing Θ causes bristles to behave much stiffer during rotor excursions.

BH is the distance between the front plate and the rotor surface, and defined as *"free bristle height"*. FH, which is defined as *"Fence height"*, is the distance between the rotor surface and the backing plate. Bristles have most lack of restriction in fence height region.
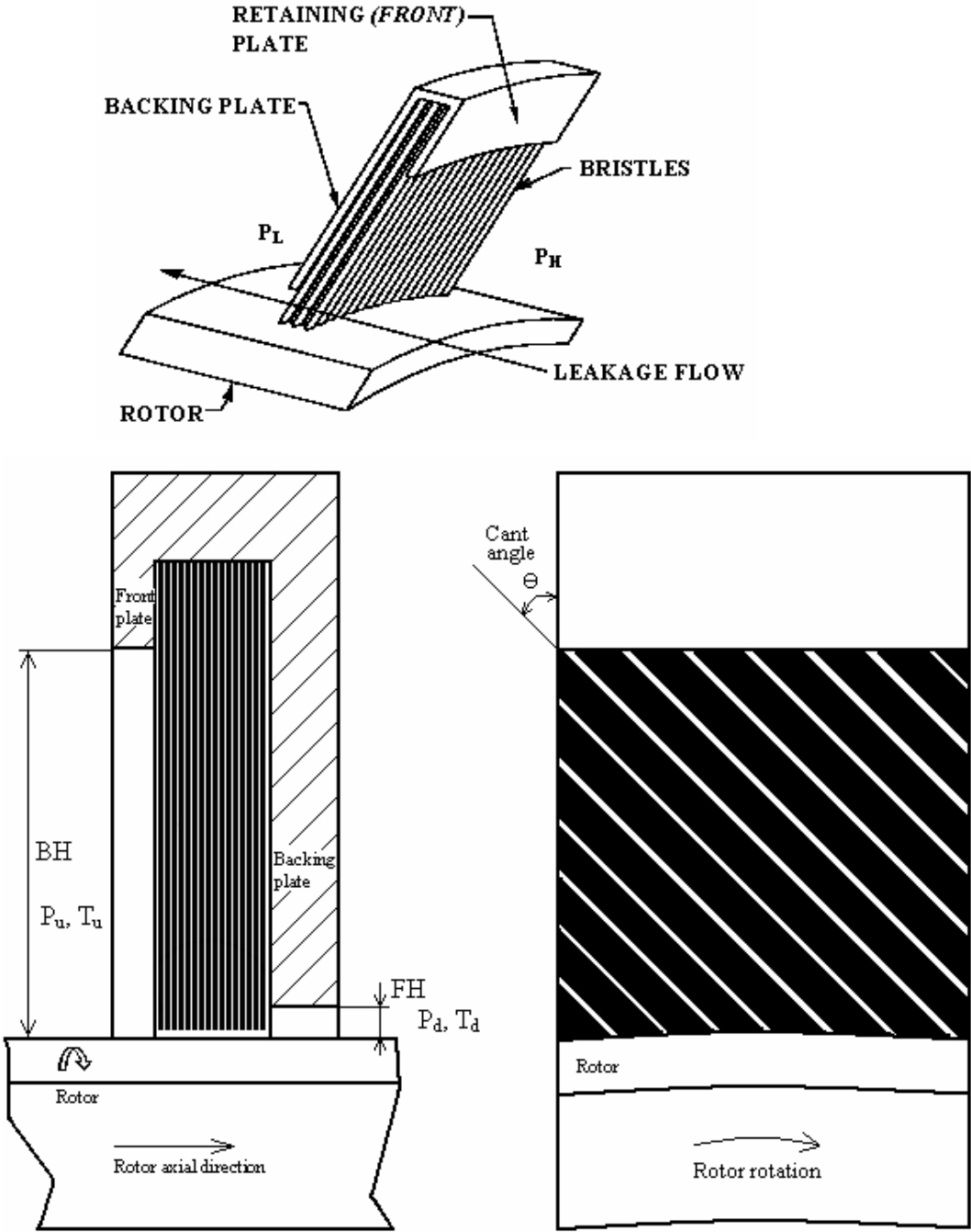
Figure 1.2 Brush seal parameters

1.2 Main Phenomenon in Brush Seals

In brush seal applications, pressure difference between upstream and downstream sides results in fluid flow in rotor axial direction. In addition, a small amount of radial flow can also be observed in brush seals since there is a pressure difference between the upper and bottom sides of the brush pack as well. In brush seals, leakage performance of the seal is mostly determined by the dominant axial flow.
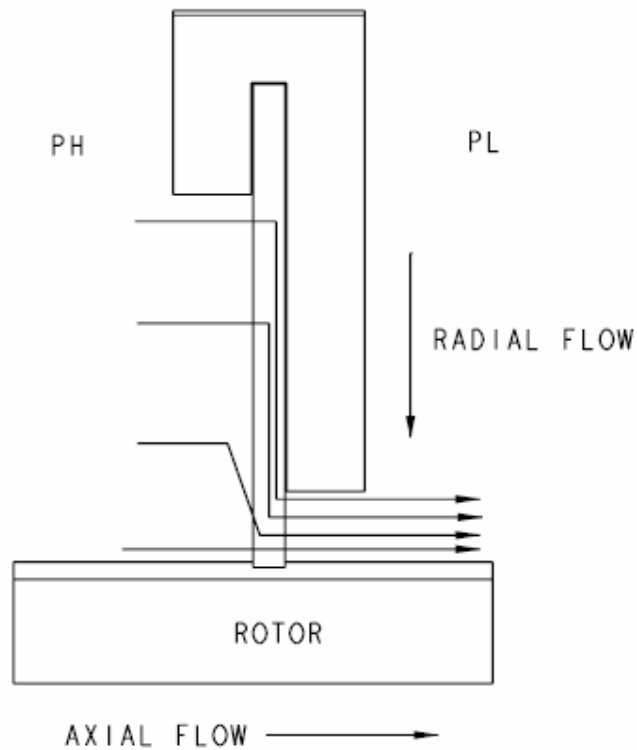
Figure 1.3 Leakage flow in a brush seal, Aksit [33]

Together with frictional forces, loads generated by leakage flows and pressure gradients in radial and axial directions cause mainly four phenomenon in brush seal applications,

- Bristle stiffening
- Hysteresis
- Blow-down *(Pressure closure)*
- Bristle fluttering

4

1.2.1   Bristle Stiffening

As a consequence of pressure load in axial direction and friction mechanism, frictional forces are generated in between the bristles and between the bristle pack and the backing plate. During transient operation, rotor excursion takes place because of maneuver loads, thermal expansion and elastic deformation of the rotor. Frictional forces cause bristles to behave much stiffer when they are pushed radially during a rotor excursion. Bristle stiffening leads to increase in contact loads at the rotor surface, which cause high wear rates.

In steady state conditions of oil seals, frictional forces take a role in determining seal clearance as they contribute to reaction forces, which balance the hydrodynamic lift force.

1.2.2   Hysteresis

There are two types of hysteresis, one of which occurs after a rotor excursion and called dynamic hysteresis. During rotor excursion, bristles are pushed radially out in order to compensate eccentric and thermally expanded rotor. After steady conditions are reached, rotor returns to its steady state position and dimension whereas radially displaced bristles can not follow the rotor, and remain hung-up due to pressure load and friction mechanism. This time, frictional forces prevent bristles to track rotor motion. Dynamic hysteresis creates a leakage problem since it causes leakage rate to increase by increasing seal clearance.

Other type of hysteresis is static hysteresis, which is observed without any rotor excursion. If a simple pressurization-depressurization cycle is applied to a brush seal, leakage rate for each leg of the cycle differs from each other. During pressurization leg, bristles are pushed radially out and locked in a certain position, again as a result of pressure load and friction mechanism. Therefore, same seal clearance can not be obtained during depressurization leg which results in different leakage rate. Change in leakage rate with pressure load for a pressurization-depressurization cycle is called hysteresis curve.
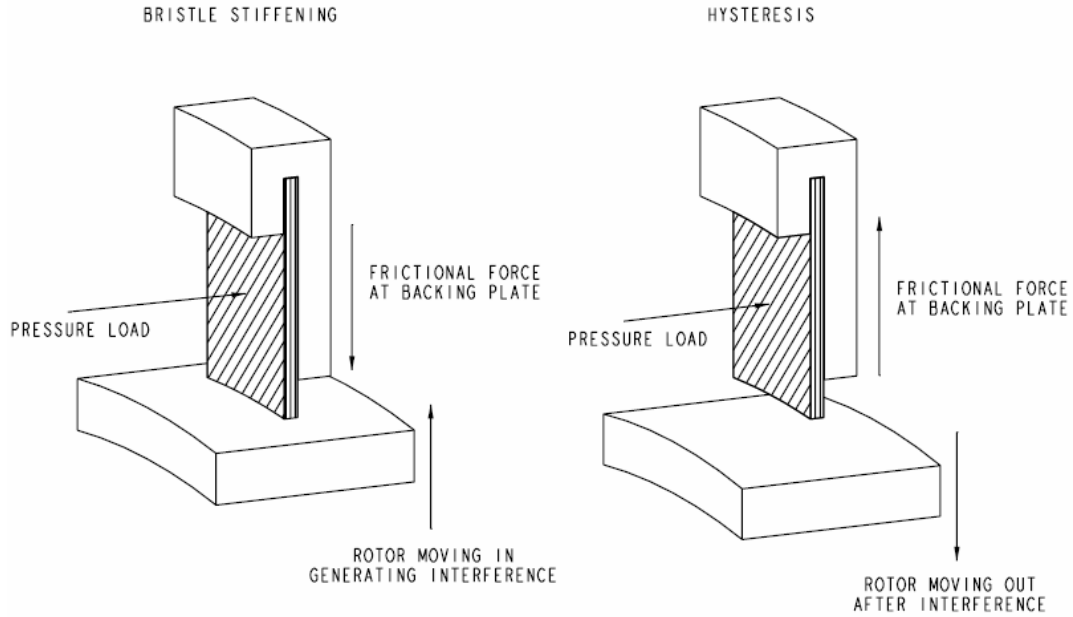
Figure 1.4 Bristle stiffening and dynamic hysteresis, Aksit [33]

1.2.3 Blow-down

As it was mentioned in the previous pages, a limited amount of radial flow within the bristle pack occurs due to slight pressure difference in the radial direction. Therefore, when a pressure load is applied to a brush seal, bristles at high pressure side are prone to move towards the rotor. This is called "blow-down" or "pressure closure". Radial flow and blow-down force increases as moved downstream within the bristle pack. Bristles at high pressure side are less restricted compared to the bristles at downstream side due to increasing cumulative axial pressure and inter bristle contact forces. However, downstream bristles are subject to higher radial pressure loads.

In order to control pressure closure, extended retaining plates can be used. Although usage of extended retaining plates eliminates most radial flow, pressure closure can still be observed. The reason for this pressure closure is the tendency of inclined bristles to bend towards the rotor under axial load. Increasing pressure load and cant angle increases pressure closure.

In steady state conditions, blow down force driven by radial pressure gradients takes an important role in determining seal clearance and contact forces.

1.2.4 Bristle Fluttering

As a result of lack of restriction, upstream side bristles tend to flutter under the aerodynamic disturbances at inlet region such as turbulence or jet flow coming from an upstream brush seal in a cascade setup. Flutter problem is generally observed in air brush seal applications, and causes sudden loss of high pressure side bristles uneven seal wear. Damping shims and extended retaining plates can be used in order to avoid bristle fluttering problem.

1.3 Problem Statement

The leakage performance of the brush seal is directly related to seal clearance. Therefore, seal clearance becomes the most important parameter in steady state. When air is the sealing medium, aerodynamic lift forces, which are generated on very small bearing surface, can not overcome blow-down and friction forces driven within the brush pack. The small bearing surface and the low viscosity of the air are the reasons for weak aerodynamic forces. If the sealing medium is oil, hydrodynamic lifting force becomes dominant, and the associated clearance becomes important.

In oil brush seals, lifting force deflect the bristles off the rotor surface. Hydrodynamic lift clearance is determined when the balance between the hydrodynamic lifting force and reaction forces is reached. Reaction forces mainly consists of three components: Reaction forces due to bristle deflection, blow-down forces occuring due to radial pressure gradients and frictional forces in between the bristles and between the bristle pack and the backing plate.

Shear heating of the oil is the main phenomena in brush seals which causes high speed lift stabilization. Hydrodynamic lift clearance increases with rotor surface speed up to a certain value due to considerable lifting effect with rotation. Effect of shear heat dissipation on viscosity can not overcome the lifting effect of rotation at low surface speeds. Increasing shear heating effect at moderate and high speeds yields to a significant drop in viscosity, which stabilizes the lift clearance, and therefore leakage flow.

1.4 Literature Survey

Literature on thermal aspects of brush seal remain limited, despite their increasing use in secondary flow sealing applications during the last few decades. In one of the early works, Gorelov et al. [1] showed that with the decrease in airflow rate, there is a marked heating of the brush. At the same time, very little airflow is sufficient for cooling at low-pressure differentials. Hendricks et al. [2] were the first to consider the frictional heat flux by employing a formula as products of spring force, surface speed, and interface heat coefficient. They calculated increasing heat flux as a function of interference. Owen et al. [3] developed a formula to calculate the heat generation; however, their analysis requires the rotor surface temperature as an input. It was assumed that heat was conducted towards bristles and dissipated to the airflow. Chew and Guardino [4] developed a computational model for flow between the bristle tips and the rotor to calculate tip force, wear, and temperature. The model includes heat conduction and heat generation due to contact friction. Demiroglu [5] developed a closed form equation to calculate heat generation. He measured the temperature field over the rotor rim and fence height region using an infrared thermograph technique. In a more recent work, Dogu et al. [6] provided analytical and numerical investigations of brush seal temperature distribution after providing an outline for the seal heat transfer mechanism. The full flow and temperature field solution has been obtained using a two-dimensional axisymmetric CFD model.

All of the above mentioned literature deals with air as the sealing medium, and studies frictional heat related problems at rotor bristle contacts. On the other hand, when a liquid medium needs to be sealed such as hydrogen generator buffer oil seals or liquid hydrogen/oxygen seals in rocket turbo pumps, problem gets more complicated as hydrodynamic lift prevents bristle rotor contact, and shear heating gets into the picture. Although there had been some early experimental works to use brush seals under cryogenic conditions for liquid hydrogen/oxygen sealing [7], only a few data points have been published on thermal aspects [8]. Rumors on some early coking failures with stiff metallic brush seals, which were actually designed for air applications, hindered brush seal oil applications. Renewed attempts for oil and oil mist sealing applications are rather new starting with Ingistov [9], who reported use of brush seal in a bearing oil sealing application. Later, Bhate et al. [10] reported success in a similar gas turbine

8

bearing oil sealing application. Both of these applications involved use of nonmetallic brush seals to prevent bearing oil from being ingested in to the compressor. However, these seals were designed to work with buffer air or oil mist. Therefore, the work by Ingistov [9] did not include any oil temperature rise issues. Bhate et al. [10] reported that heating across the seal was not excessive. Although limited, their tests did not reveal any apparent oil coking.

Brush seal applications for liquid oil flow appeared first in patent disclosures [11-14]. Detailed performance characteristics of oil brush seals were reported by Aksit et al. [15]. They have demonstrated feasibility of metal brush seals for oil sealing applications if the seal had been designed properly. Their experimental data clearly indicated presence of hydrodynamic lift appearing as increased oil leakage with speed. They studied the temperature rise in oil brush seal applications. Their findings indicated that oil temperature rise levels at high speeds due to shear thinning.

When oil is the sealing medium, hydrodynamic lift becomes dominant, and associated clearance can not be omitted. Seal clearance generated by hydrodynamic lift bears critical importance in oil seals, as it affects leakage performance and amount of shear heat generated. In an attempt to help designers with brush seal applications when sealing medium is liquid, Aksit et al. [16] provided a simple analytical formulation that does not rely on any empirical constants or correlations. Their analysis is developed based on Reynolds relation typically used for hydrodynamic bearings. Although simple and easy to use, their analysis required the knowledge of effective viscosity of the oil for a given speed and lift clearance. As indicated at the early experiments, shear heating becomes dominant at high rotor speeds. Strong temperature-viscosity dependency of lube oils presses the need for a detailed analysis and understanding of the effect of shear heat on hydrodynamic lift of brush seals in oil sealing applications. To provide a better understanding about the critical balance of hydrodynamic lift force with speed, viscosity and pressure difference, this work presents an analytical study to investigate shear heat temperature rise in liquid sealing medium within the hydrodynamic lift clearance. A closed-form solution to temperature distribution in axial and radial directions has been obtained by solving thermal energy equation. Effective temperature has been calculated for different values of rotor surface speed, pressure difference and hydrodynamic lift clearance. Calculated speed dependent viscosity values have been adopted into the

bearing theory to calculate hydrodynamic lifting force. Results have been compared with lifting force obtained by Aksit et al. [16] through beam and short bearing analyses.

In addition to boundary layer and temperature analysis for the oil under the bristle pack, pressure distribution under each bristle is also derived by applying Reynolds bearing theory.

As mentioned before, hydrodynamic lift clearance is the most important parameter which affects the brush seal steady state leakage performance. Therefore, hydrodynamic lift clearance is analytically derived, and compared with the available experimental lift data.

In this study, design and design considerations for high speed seal test rig is also given.

2   TEST RIG DESIGN AND EXPERIMENTAL LEAKAGE DATA

In steady state, seal clearance is the most important parameter for the brush seal. If the sealing medium is oil, hydrodynamic lifting force becomes dominant, and the associated clearance becomes significant. Hydrodynamic lift clearance is the main parameter in determining leakage performance of the oil brush seal. Lift clearance changes with rotor surface speed and pressure load. In engine applications, clearance increases as rotor speed increases, and stabilizes after a certain rotor speed. The reason for this stabilization is the shear heating of the oil. A better understanding of shear heat dissipation can be achieved by means of thermal analysis and hydrodynamic bearing theory. A seal test rig is designed to obtain leakage data for hydrodynamic lift clearance evaluation, pressure and temperature data, which will be used to validate theoretical results of thermal and hydrodynamic bearing analysis. In this chapter, information about design and assembly of the test rig is given.

2.1   Test Rig Design

Design and production of the components of the seal test rig allows tight tolerance control on critical dimensions. Every part of the assembly is made of stainless steel, which permits testing at high temperatures. Since balancing of the rotating sections has a great importance, test rig components are produced with tight tolerance and minimal surface roughness.

2.1.1 Seal Housing Design

Seal housing assembly is the part of test rig where brush seals are placed. Exploded view of housing assembly is shown in Figure 3.1.
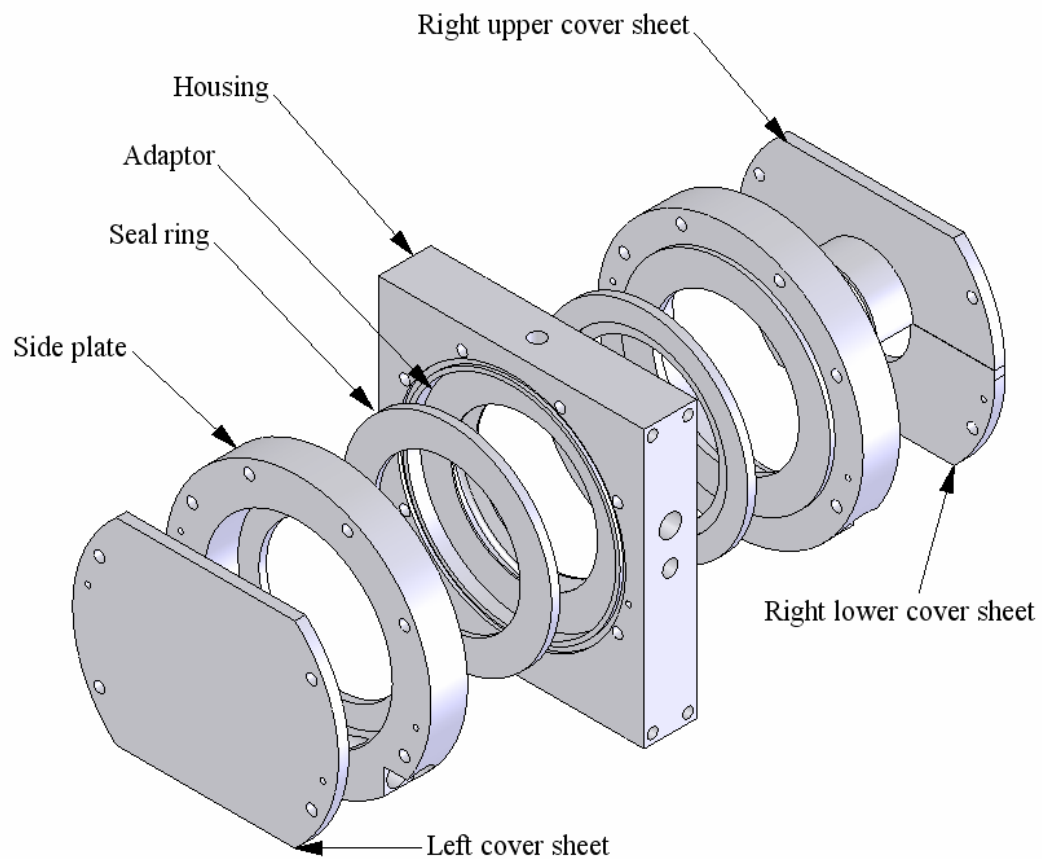
Figure 2.1 Exploded view of the seal housing assembly

2.1.1.1 Housing

Housing is the base part for the seal housing assembly. Test oil is supplied through an oil inlet hole to the cavity between rotor and brush pack surfaces, and in between bristles. Three probe holes are threaded in accordance with 3/8-24UNJF-3B standard, two of which are for pressure gauges, and the third one is for the thermocouple. ETM-375-7BAR-A types of GE pressure transducers are used, which have 707.927mV/BAR sensitivity and -18°C to 100°C compensated temperature range.

Thermocouples are K-type with $1000^{\circ}C$ full scale range. Measured pressure and temperature values are transferred to the computer by means of 20-channel data acquisition system, and monitored in an EXCEL sheet.

Since the testing medium is pressurized oil, O-rings have to be used between mating housing parts to avoid bias leakages. For this purpose, O-ring grooves are opened on both sides of the housing.

Seal housing components are assembled using bolt-nut combination. Bolt holes are drilled through the side surfaces of the housing. Seal housing assembly is fixed to a graduated moveable slide from the bottom of the housing with M16 bolts.
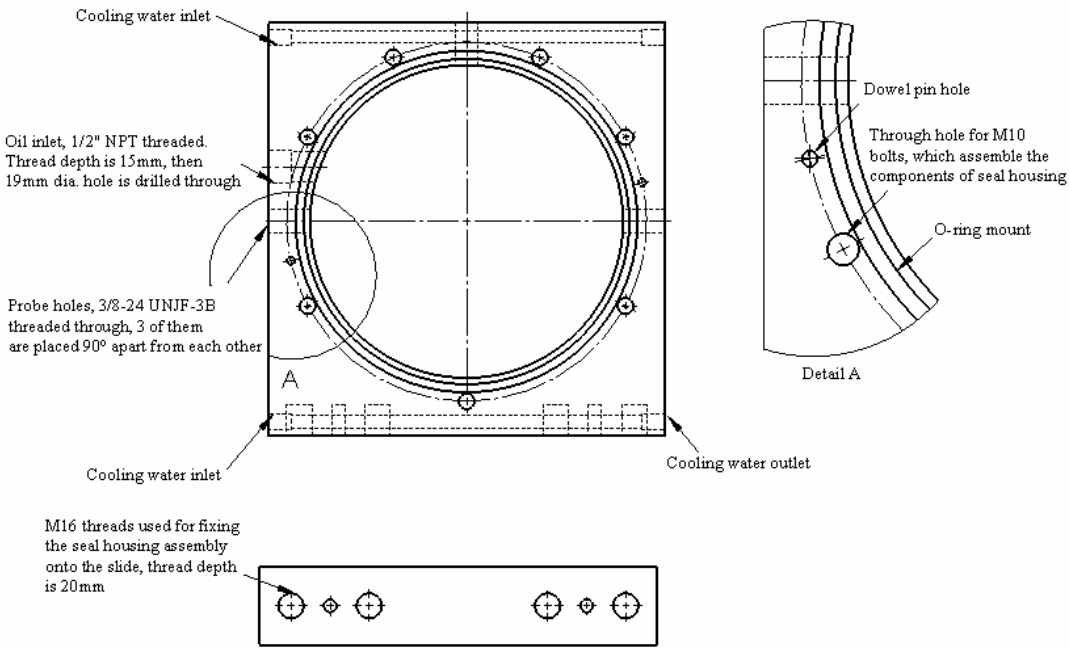
Figure 2.2 Detailed view of housing

In cases where leakage is small and test speed is high, shear heat developing within oil can not be removed quickly. Therefore, heating of the housing constitutes a problem arising from elevated oil temperatures during leakage tests. In order to overcome heating problem, water is used as a cooling fluid, which is circulated within the housing through a set of water cooling holes. Cooling water at the outlet is send to a heat exchanger than a water tank with the aid of a circulation pump. A detailed drawing of housing is given in Figure 2.2.

2.1.1.2 Adaptor and Seal Rings

Adaptor is designed to support brush seals and to form a sump to collect the oil leaking through the test seals. Inlet region of the adaptor is manufactured with a recess in order to provide satisfactory space for the oil inlet chamber. Outer surface of the adaptor is mated to the inner surface of the housing, and brush seals are mounted at either sides of the adaptor. Together with seal rings, adaptor forms the high pressure inlet cavity for brush seals. Seal rings clamp the brush seals to the adaptor. The simple geometry of the seal rings makes their replacement convenient bringing the flexibility of working with different brush seal geometries. Adaptation of different brush seals can be achieved by only changing the seal ring dimensions. Detailed view of adaptor and seal rings assembly is given in Figure 2.3.
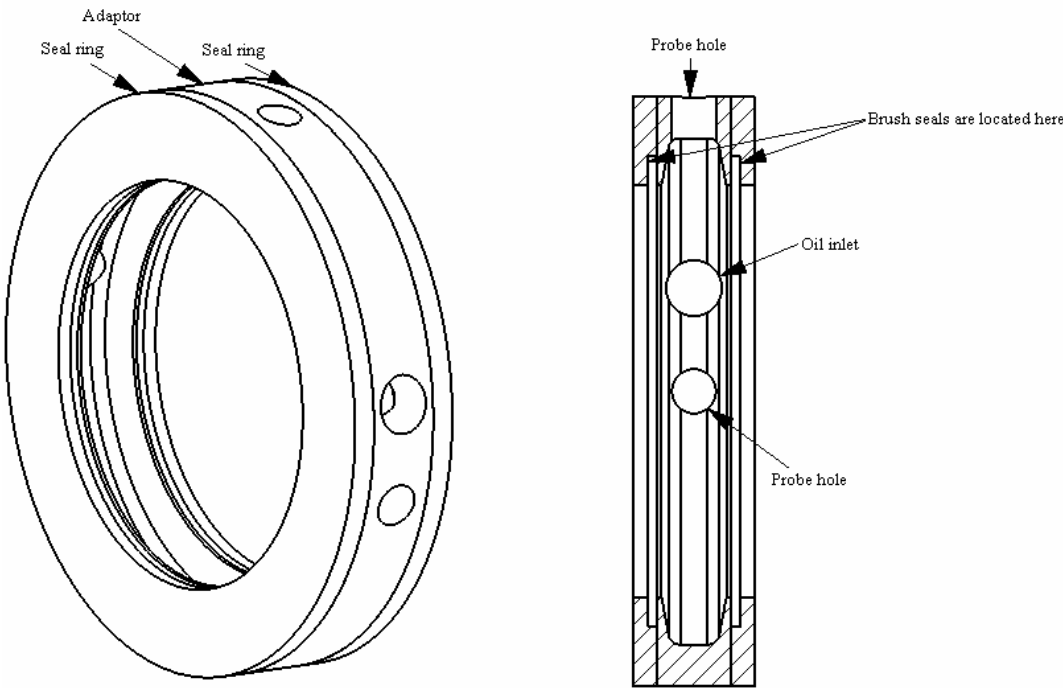
Figure 2.3 Detailed view of assembly of adaptor and seal rings

2.1.1.3 Side Plates

Side plates are mounted at either sides of the housing and bolted through in order to tighten seal rings. During leakage tests, high pressure is obtained at the inlet region of the adaptor. Therefore, oil flows from this inlet region towards the side plates, and gets collected in the sump region, which is formed between side plates and cover sheets. Excess oil is pumped backed to the oil tank from oil outlet, so that continuous circulation of oil is maintained.
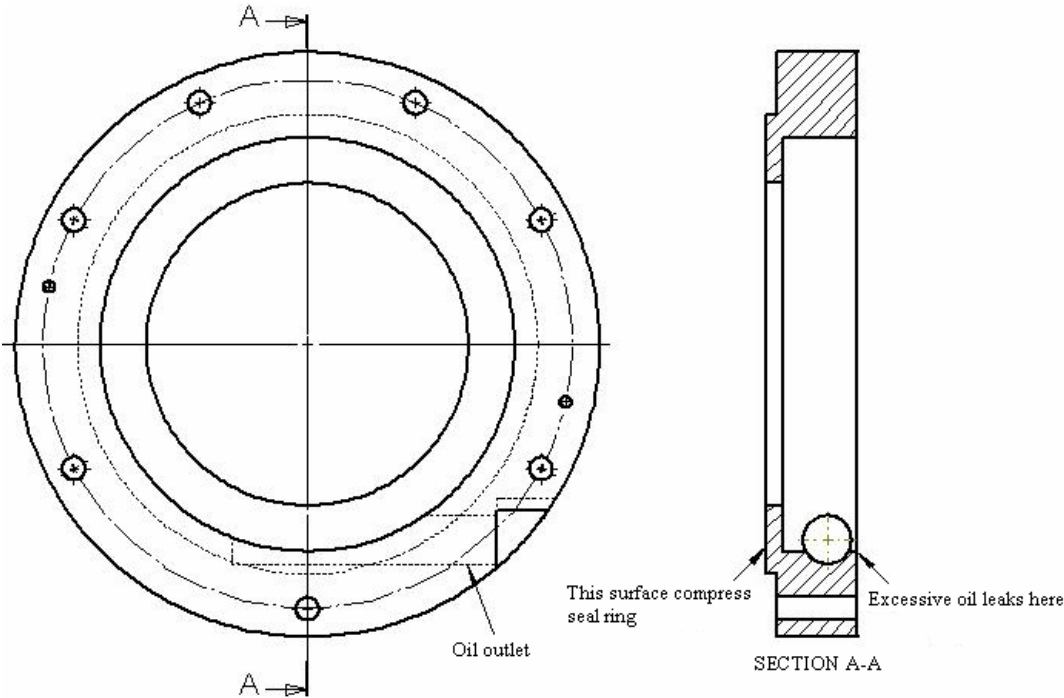
Figure 2.4 Detailed view of left side plate

2.1.1.4 Cover Sheets

Since test medium is oil, contamination problem may arise from exposure to environment. Together with the side plates, cover sheets avoid contamination by forming a closed sump region. Left cover sheet is produced as a single part whereas right cover sheet consists of two distinct components. Upper half of the right cover sheet has an extension, which prevents oil leakage to spil or drip on rotating shaft. During leakage tests, rotor spins inside the seal housing assembly. Circular opening on the right cover sheet allows rotor placement into the assembly.

Cover sheets are assembled onto side plates with M10 bolts. They can be removed without disassembling seal housing. Therefore, intervention to the seal assembly in the case of any problem can be achieved by simply removing one of the cover sheets. Detailed view of left and right cover sheets are shown in Figure 2.5 and 2.6 respectively.

Upper and lower parts are cut in order to create gap for bolt head

Holes for 4*M10 bolts

Dowel pin holes
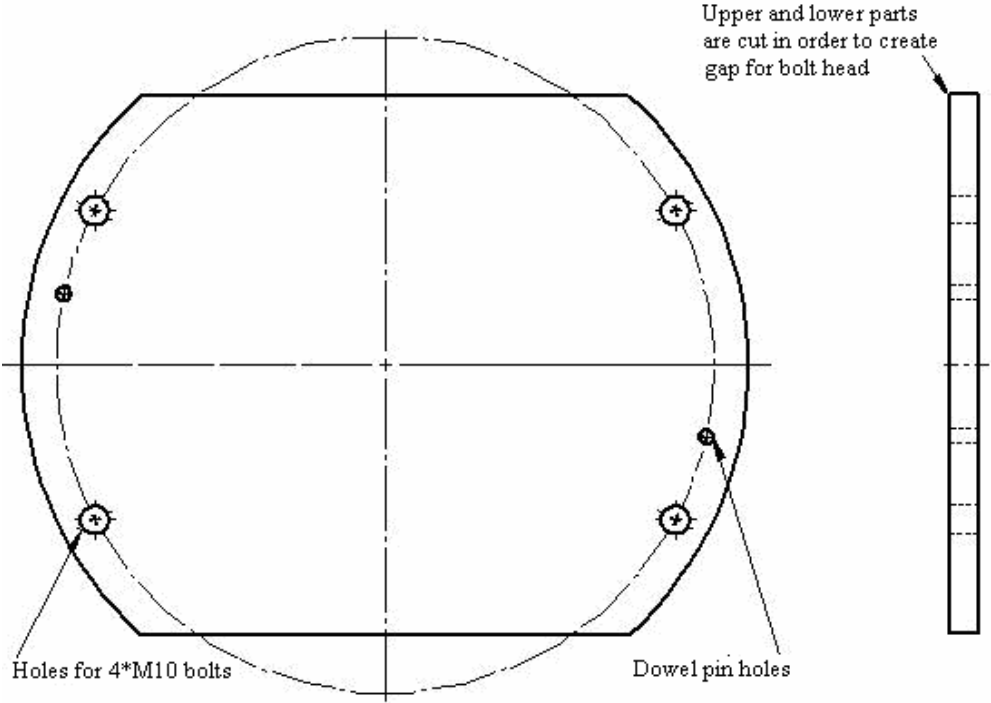
Figure 2.5 Detailed view of left cover sheet

Extended part that prevents rotor from oil leakage

Circular hollow which allows rotor placement
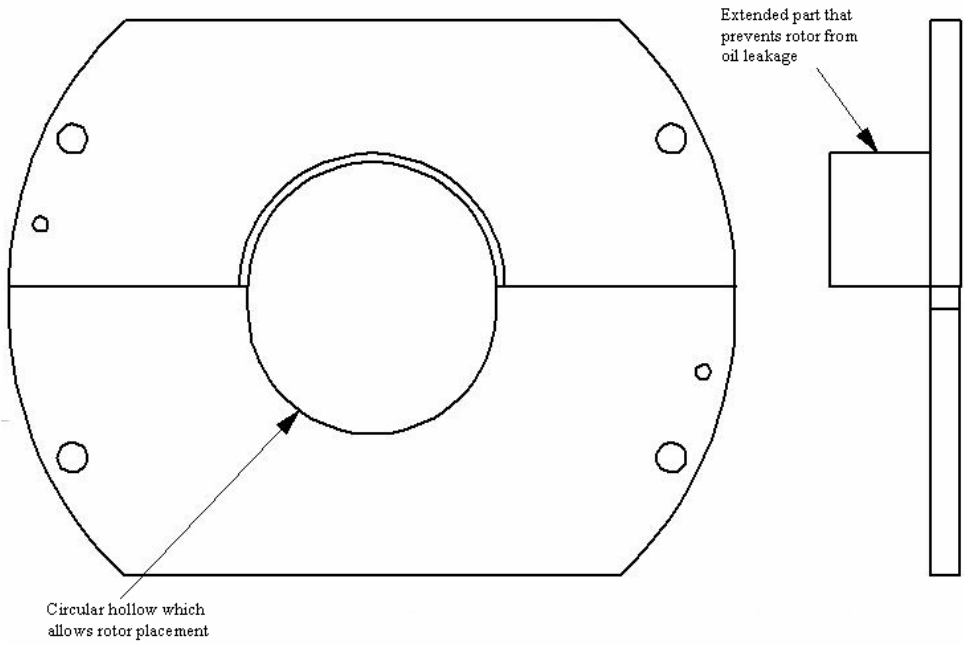
Figure 2.6 Detailed view of right cover sheet

2.1.1.5 Seal Housing Assembly

The seal housing assembly is designed to test two seals at the same time. Symmetric location of two brush seals eliminates any axial loading on the rotor. This brings the advantage of high speed testing at elevated pressures which are typically experienced in gas turbine brush seal applications. Use of through bolts provides easy assembly and disassembly. Removable seal rings allow testing of different brush seal geometries and facilitate testing of other rotary seals.
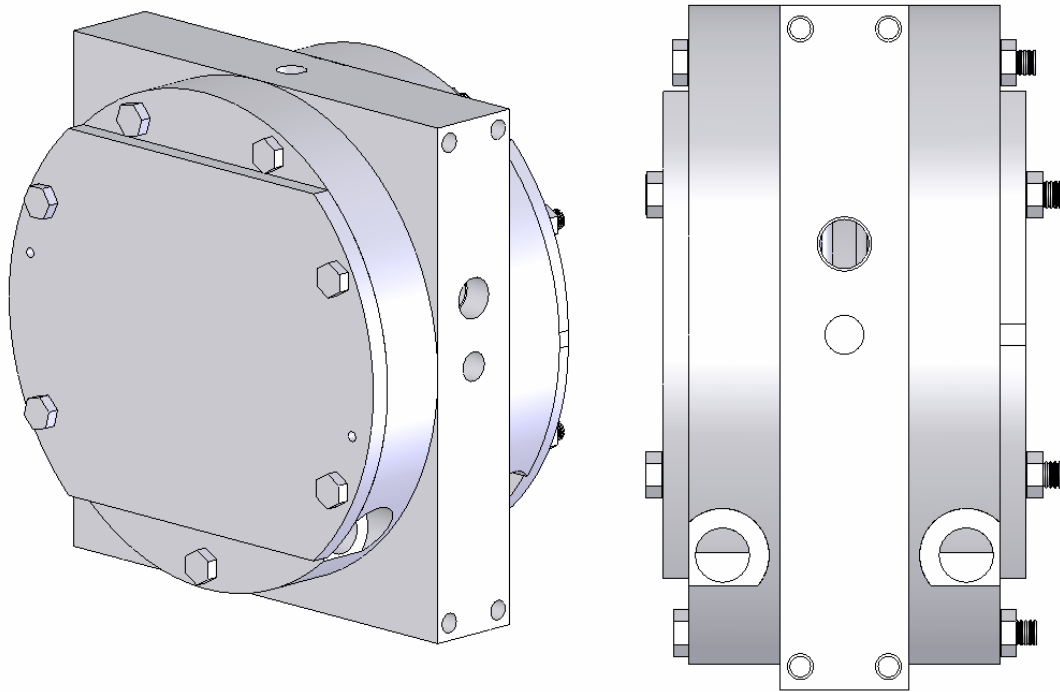
Figure 2.7 Seal housing assembly

Oil is pumped into the inlet cavity of the adaptor where the high pressure is obtained. As a consequence of the pressure difference between the inlet cavity and the outer side of the seal rings, pressure driven leakage flow occurs in the axial direction. On the other hand, Couette flow occurs in the direction of rotor rotation in addition to Poiseuille flow. Rotor surface speed is the reason for velocity driven circumferential flow. Cross-sectional view of the seal housing where rotor and brush seals are located is given in Figure 2.8.
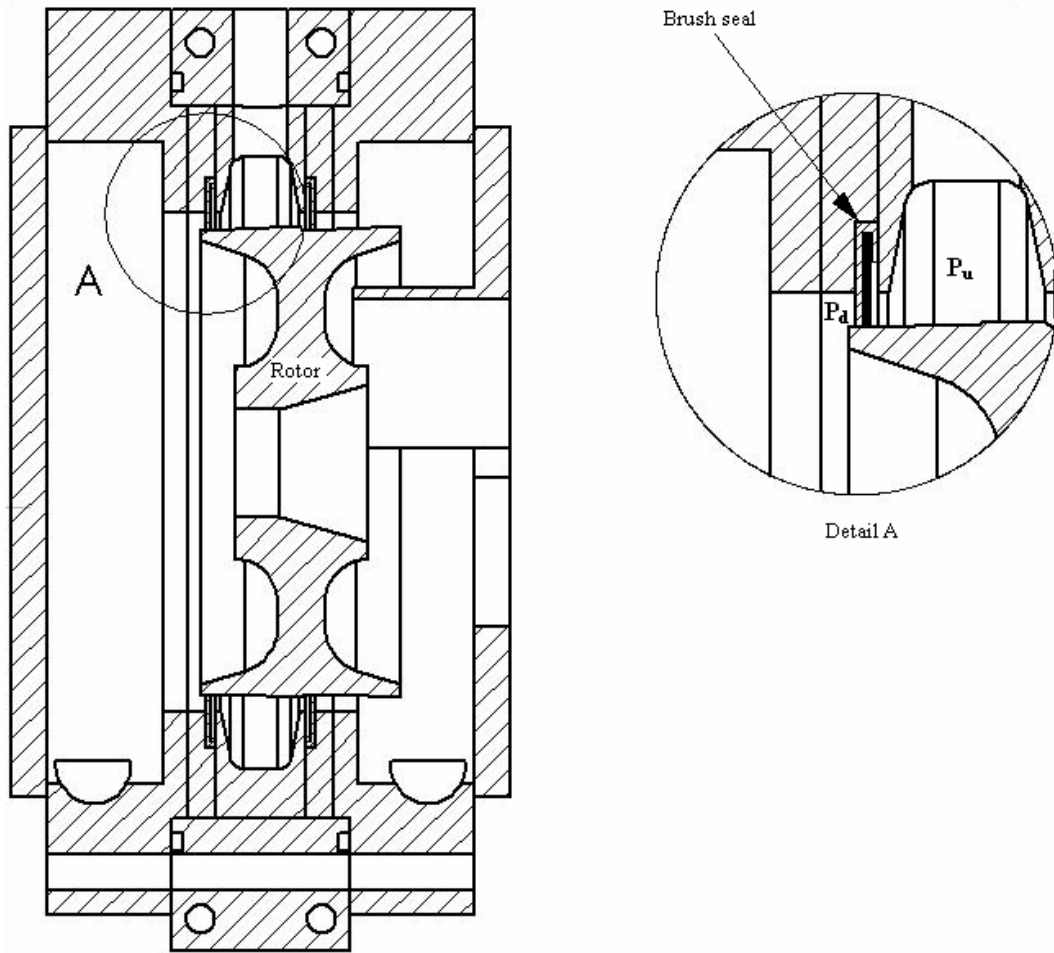
Figure 2.8 Cross-sectional view of the seal housing assembly

2.1.2 Spindle Holder Design

Spindle is the part which supplies power for the shaft rotation. Rotational motion of the spindle is transmitted to the rotor through a connection rod. Balancing of the rotor has an extreme importance as small imbalance together with high rotor speeds may cause serious problems. Therefore, centering of the rotor and stabilization of the spindle is critical. Spindle stabilization is achieved by tightening it between two clamps, one of which is assembled onto a moveable slide. As shown in Figure 2.9, spindle holder consists of five main components: Spindle, upper clamp, lower clamp, connection rod and rotor.
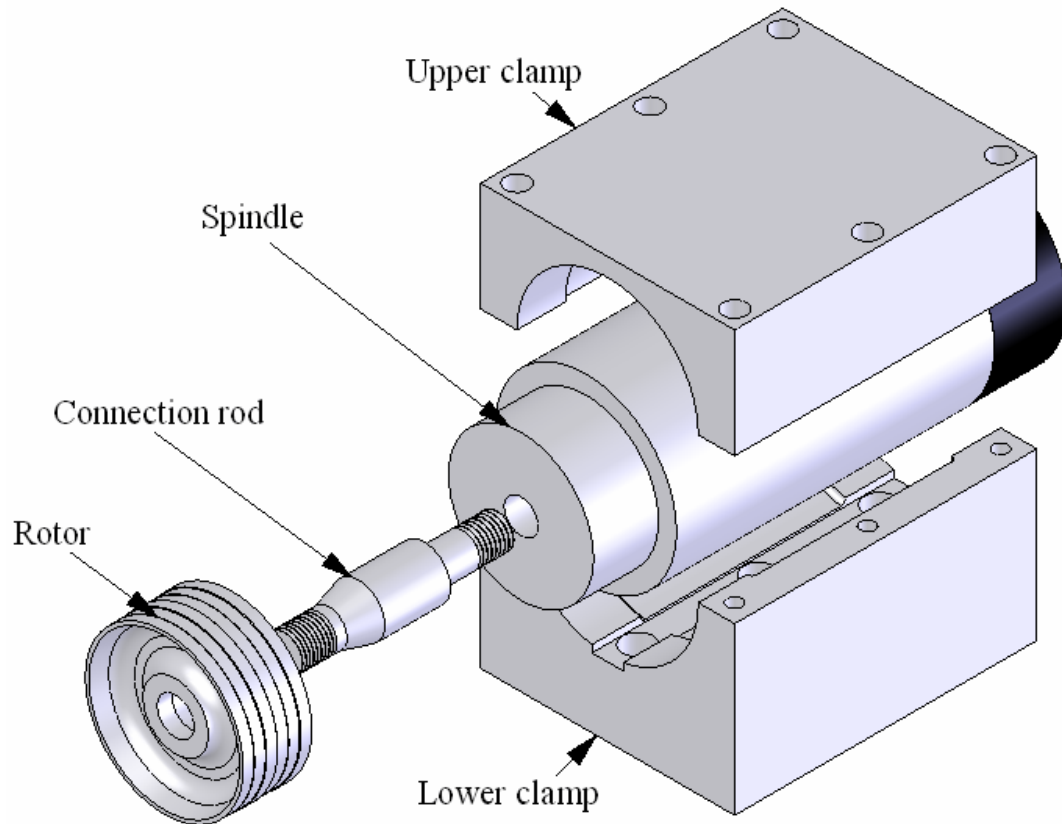
Figure 2.9 Exploded view of spindle holder assembly

2.1.2.1   Clamps

Spindle is mounted between upper and lower clamp, and tightened with the aid of six M12 imbus bolts. Radii of the inner surface of clamps are 75mm, which equals to spindle radius. In order to obtain sufficient tightness to fix the spindle, lower surface of the upper clamp is machined around 0.4mm so that contact of upper and lower clamp is hindered. As a result of this, inner surfaces of both clamps perfectly touch the surface of the spindle. As clamps are bolted, they tend to approach each other. However, contact between spindle surface and inner surfaces of clamps avoid this movement so that all compression force acts on the spindle, and desired tightness can be obtained.

Since the parallelism and the stabilization of the spindle are critical, inner surfaces of the clamps are manufactured with tight tolerances and small surface roughness.

Middle parts of both clamps are produced with the radius of 79mm in order to make clamping insensitive to any possible form errors.

Lower clamp is placed onto a moveable slide, and fixed with three M16 imbus bolts. The channel on the inner surface of the lower clamp is opened to embed bold heads within the lower clamp.
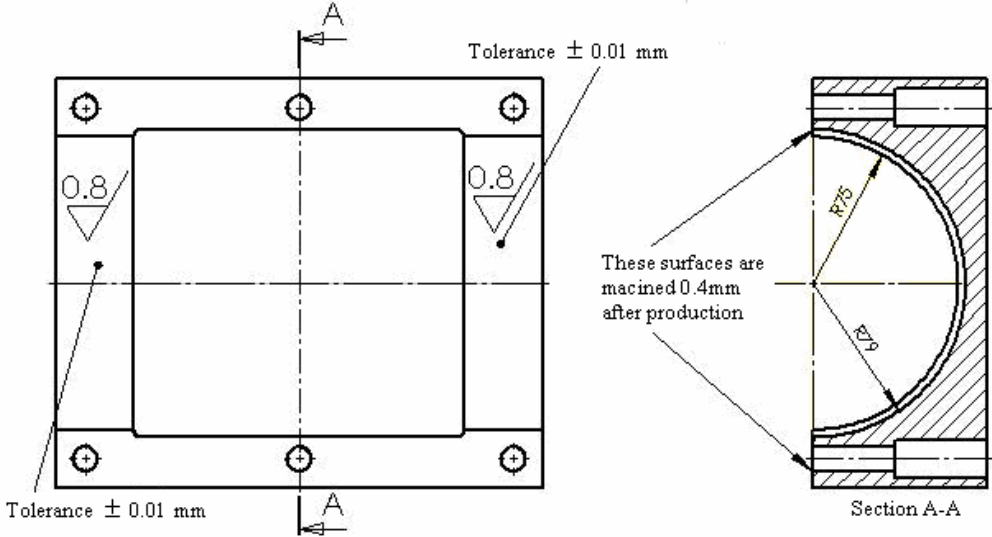
Figure 2.10 Detailed view of upper clamp
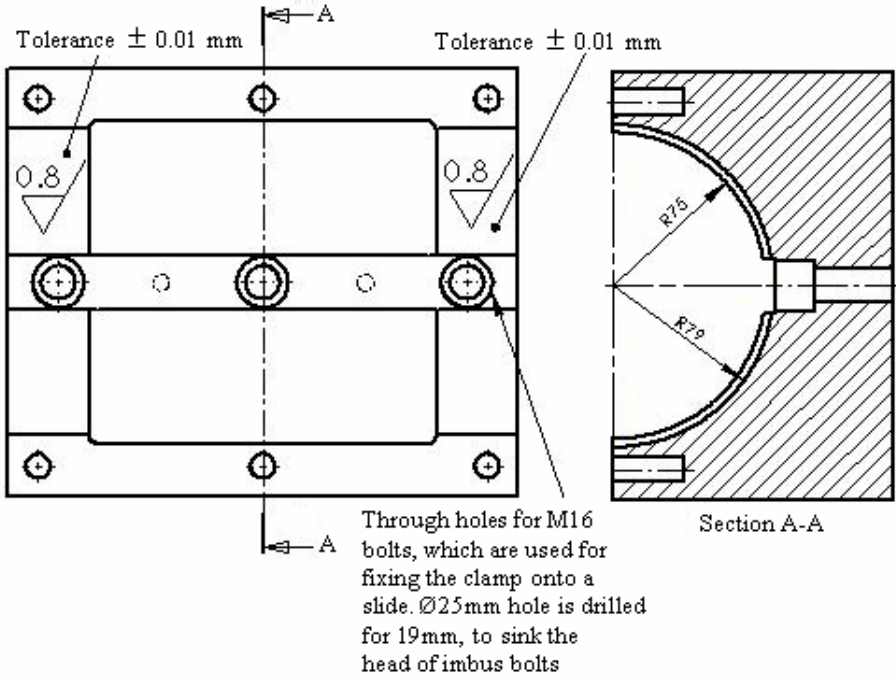
Figure 2.11 Detailed view of lower clamp

2.1.2.2 Spindle and Connection Rod

Rotor rotation is powered by GMN-High frequency spindle. Model of the spindle is HV-X 150-45000/25, with 150mm diameter, 45000rpm maximum rotational speed and 25kW output rating.

Power of the spindle is transmitted to the rotor by a connection rod, which is produced from the runout test rod supplied with the spindle. Original test rod gives 8μm run-out at 10 cm from spindle end. This tight run-out value helps a great deal in balancing the rotor. Original test rod has 28mm diameter at the spindle side, which is completely bolted into the spindle head. Its diameter increases to the value of 48.2mm as moved away from spindle. Test rod is threaded to provide assembly with spindle head. This threaded connection permits tightening in one direction.

In order to achieve accurate centering of the rotor, original test rod is machined with 15° cone angle, and its diameter is reduced to 30mm. This reduced section is threaded after cutting the unnecessary length. Rotor is also bored with same cone angle so that the inner surface of the rotor becomes coincident with the conical surface of the connection rod. M30 nuts are used to tighten the rotor on the connection rod.
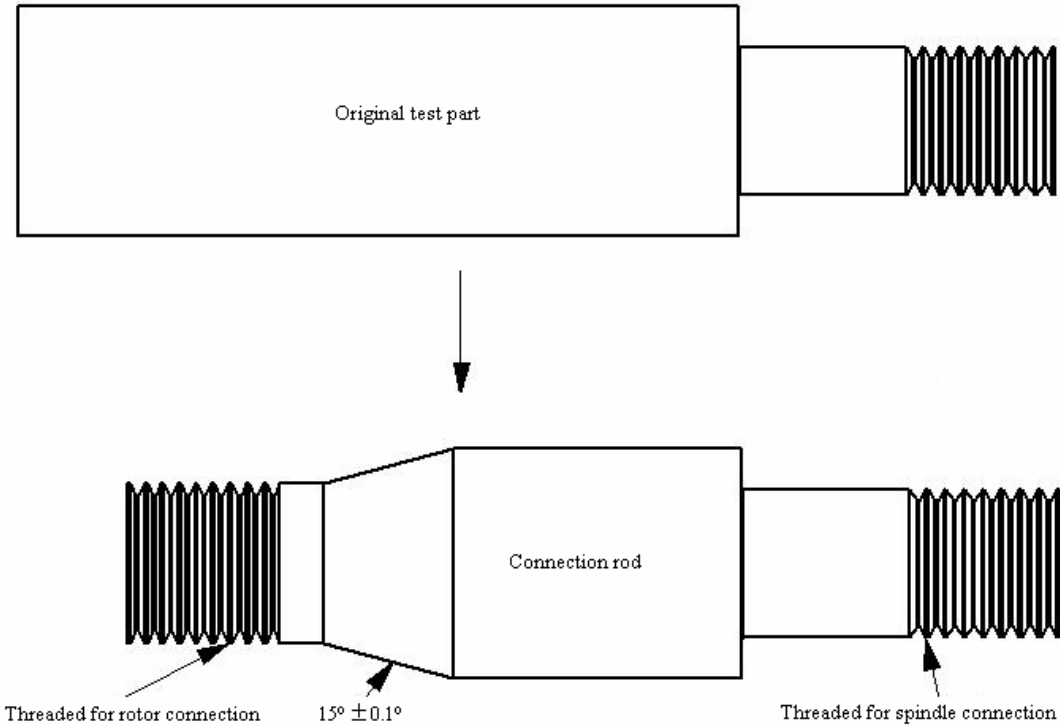
Figure 2.12 Drawings of original test part and connection rod

2.1.2.3 Rotor

Shaft and brush seals contact in the engine is simulated by the test rotor. As mentioned before, rotor is placed and rotated at the bore of the seal and the housing. Each seal faces three radial rotor steps. Varying diameter of the rotor surface allows testing the brush seals under different seal interferences. Center of the rotor is drilled with 15° cone angle down to a diameter of 30.5mm, and thereafter has a bore with constant diameter. Cross-sectional view of the rotor and detailed view of connection rod-rotor assembly is given in Figures 2.13 and 2.14 respectively.
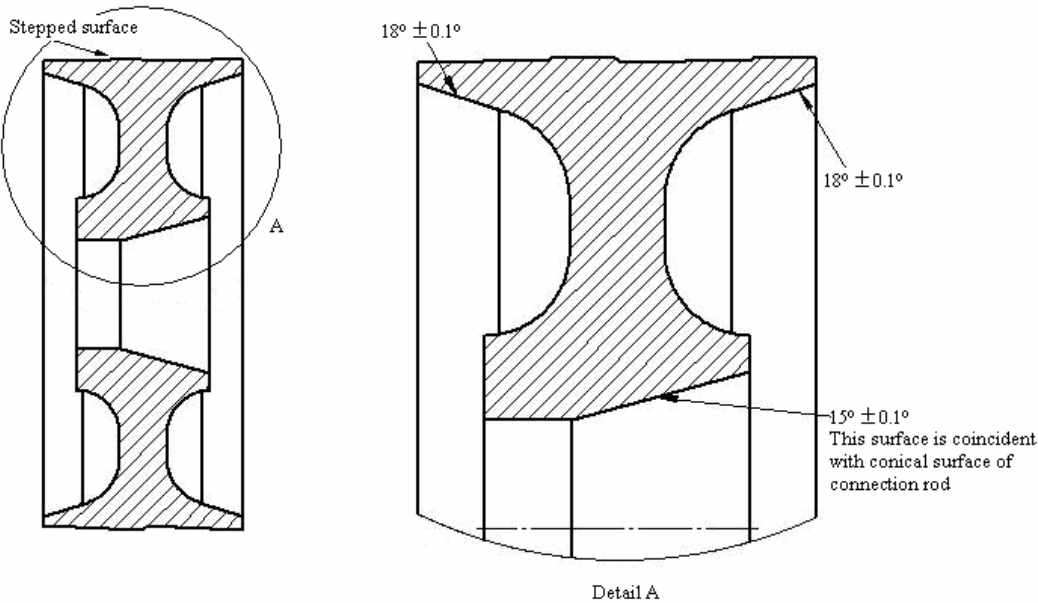
Figure 2.13 Cross-sectional view of the rotor
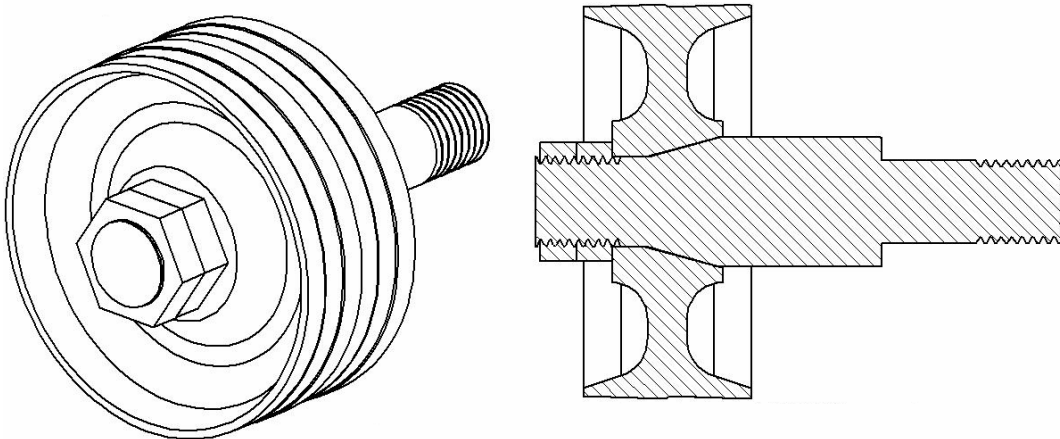
Figure 2.14 Detailed view of connection rod-rotor assembly

2.1.2.4 Spindle Holder Assembly

Spindle is successfully fixed with the given spindle holder design. Isometric view of spindle holder is given in Figure 2.15.
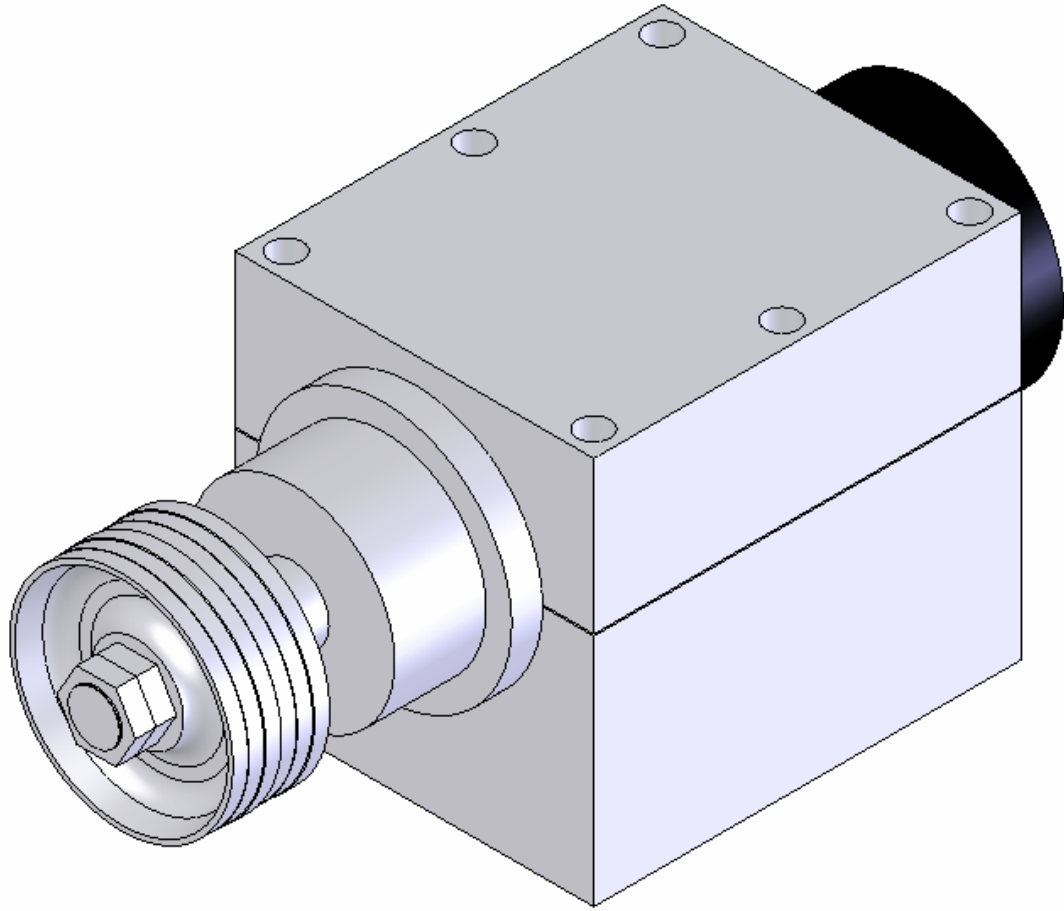
Figure 2.15 Spindle holder assembly

2.1.3 Test Rig

Seal housing and spindle holder are mounted on slides, which are positioned using dowel pins, and bolted onto a stainless steel platform. Usage of a platform brings the advantages of added stiffness, further damping of vibration and ease of portability for the test rig. Assembly process starts with mounting the brush seals into the housing with

the aid of adaptor and seal rings, and assembling the components of seal housing instead of cover sheets. Then, rotor is placed into the seal housing using the slide.
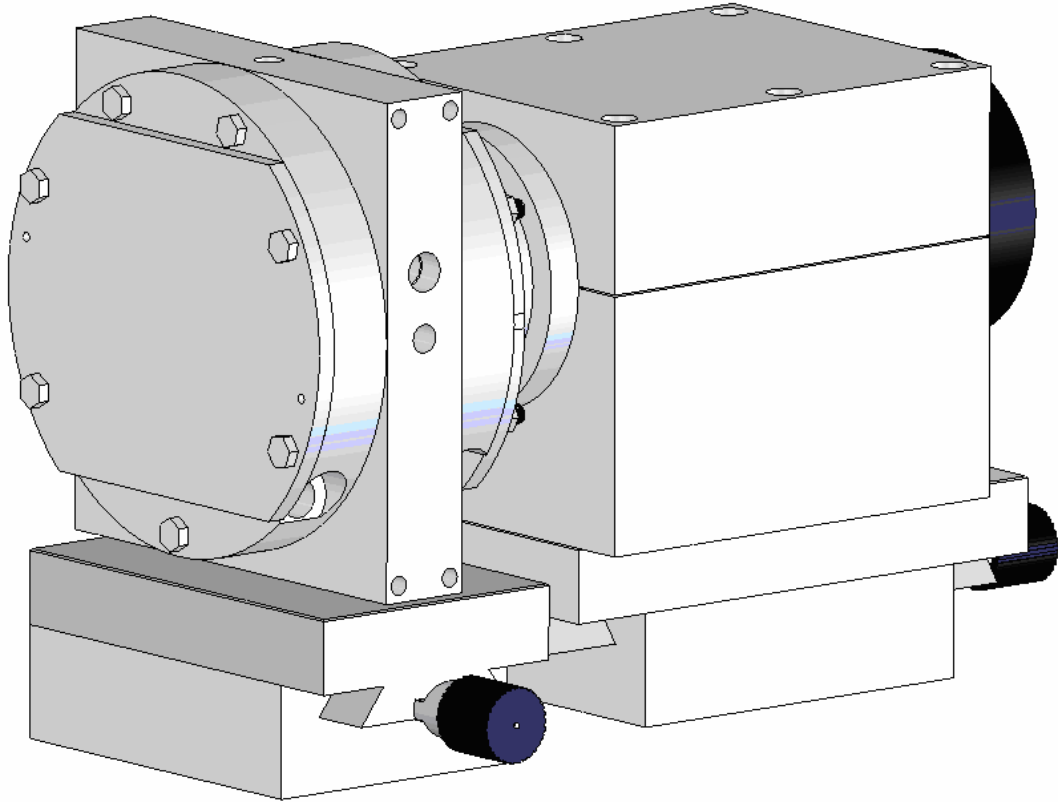
a)
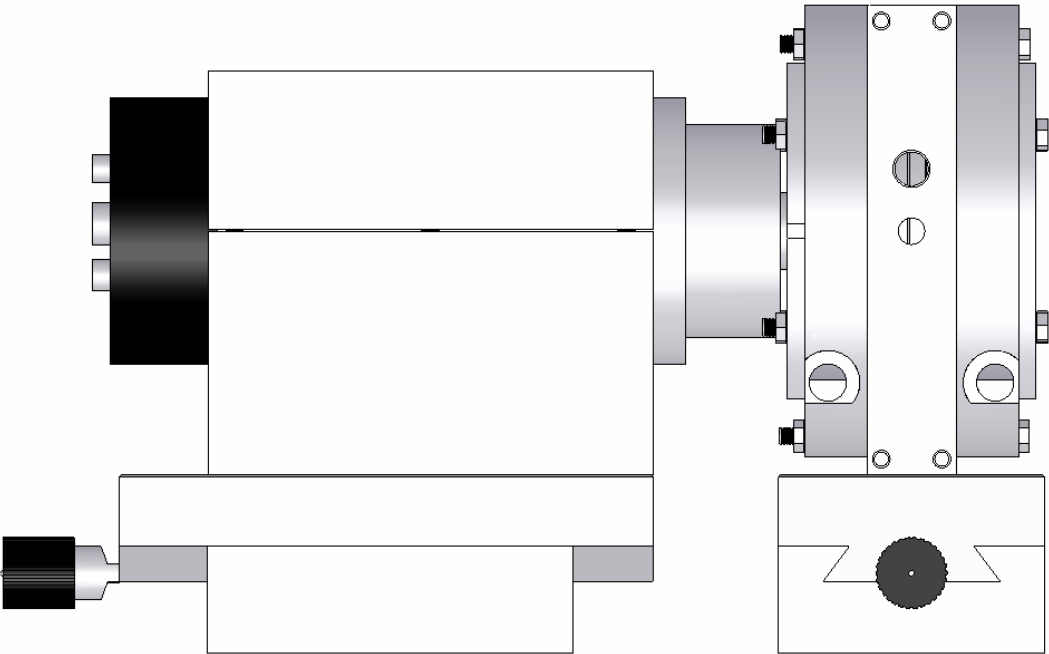
b)

Figure 2.16 Different views of test rig: a) Isometric view b) Front view
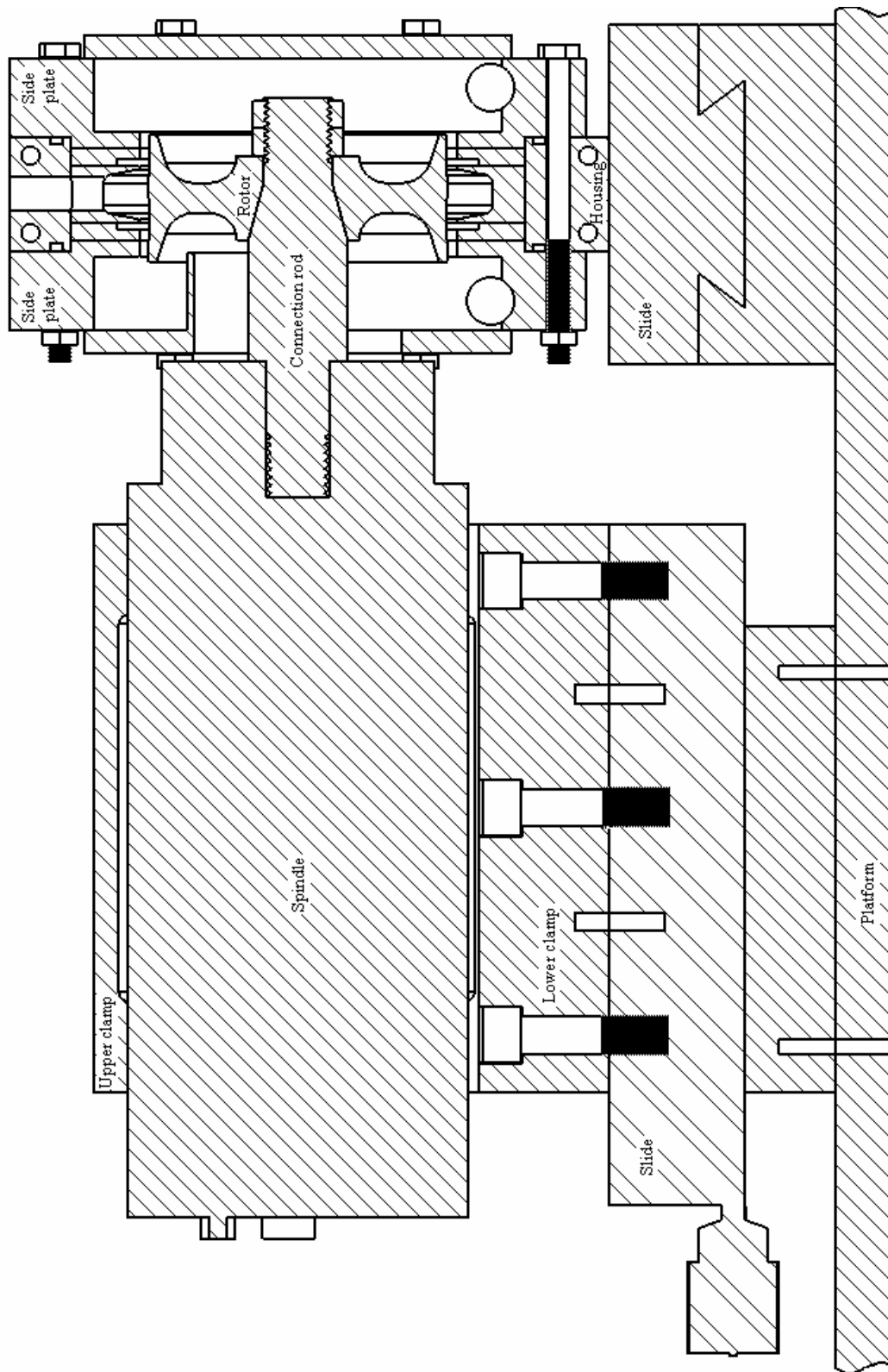
Figure 2.17 Cross-sectional view of the test rig

Axial motion of the rotor is achieved by the slide under the lower clamp whereas housing motion, which is vertical to the rotor axis, is achieved by the slide mounted under housing. This motion of the housing permits performing leakage tests for eccentric rub conditions.
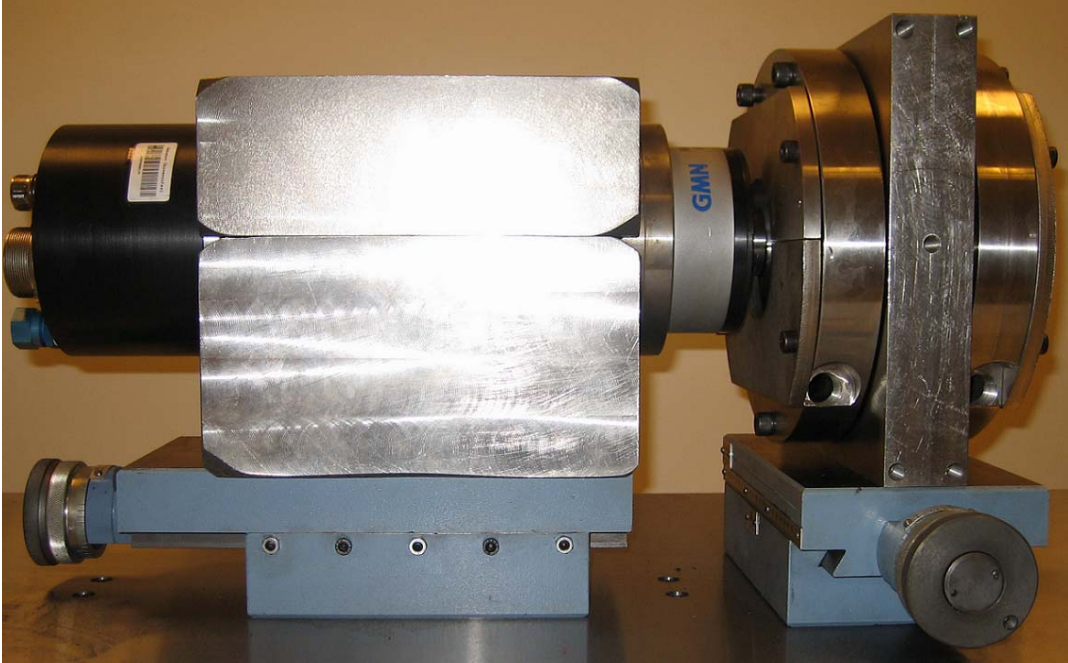
Figure 2.18 Side view photo of test rig
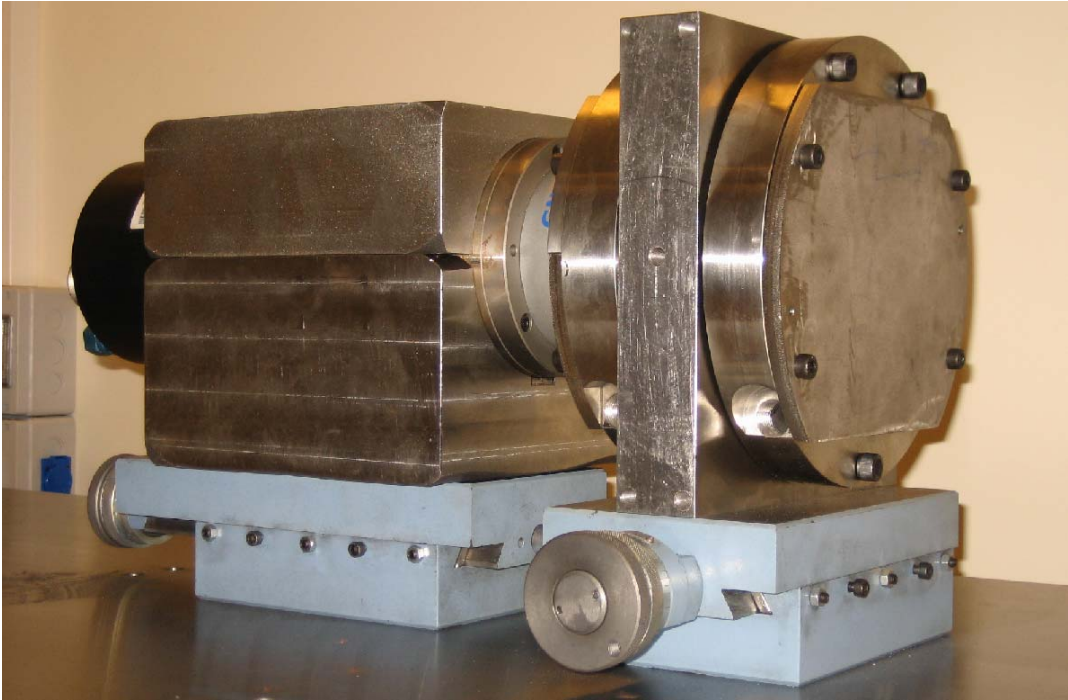
Figure 2.19 Isometric view photo of test rig
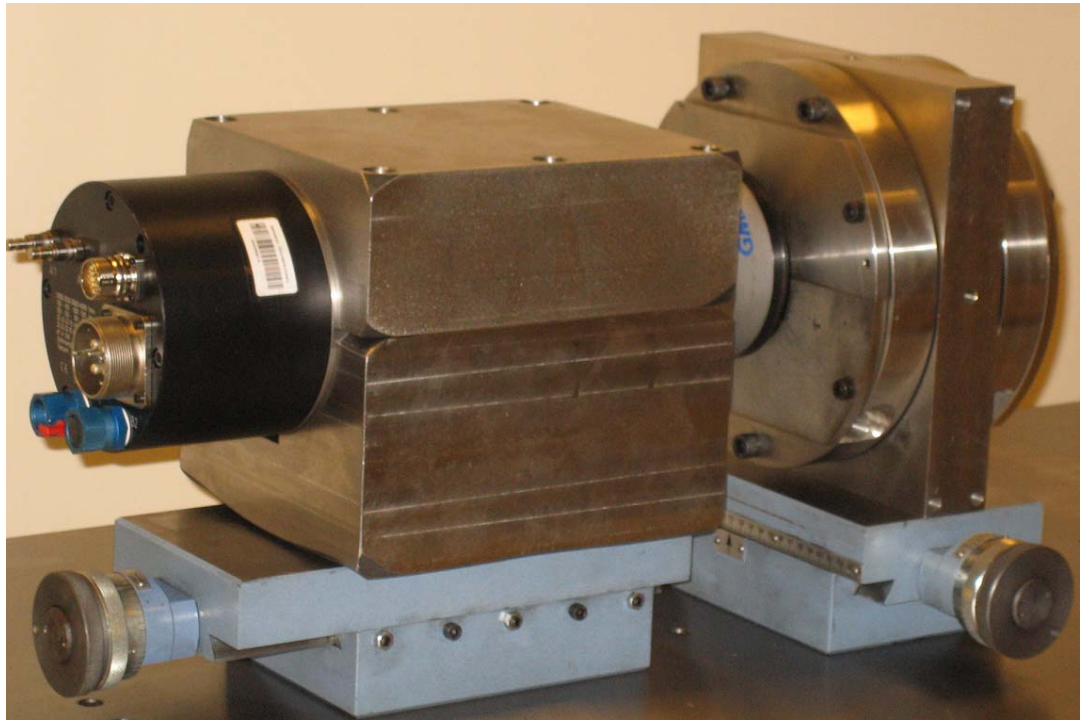
Figure 2.20 Isometric view photo of test rig from different perspective

Stainless steel platform, where test rig is constructed on, is fixed onto a steel table for stability. Oil and water tanks are placed under the table. The control unit for the spindle is hanged onto the platform.

2.2 Experimental Results

Hydrodynamic lift clearance is the most important parameter for oil seal applications in steady state. However, direct measurement of lift clearance is very difficult. Therefore, leakage rate is measured during leakage tests. Since dual brush seal configuration is used in order to avoid axial loading on the rotor, leakage values are averaged.

Flow rate measured for static case represents the leakage through the porous bristle pack. As rotor surface speed increases, additional leakage occurs due to the fact that bristles are lifted of the rotor surface. Flow rate stabilizes after a certain rotor speed which indicates stable hydrodynamic lift clearance formation as a result of shear heating. Due to the fact that manufacturing of the designed seal test rig could not be completed in time for this dissertation, experimental data provided by Aksit et al [16] has been used for verification. Measured flow rate per seal circumferential length change with rotor surface speed for different pressure loads is given in Figure 2.21.
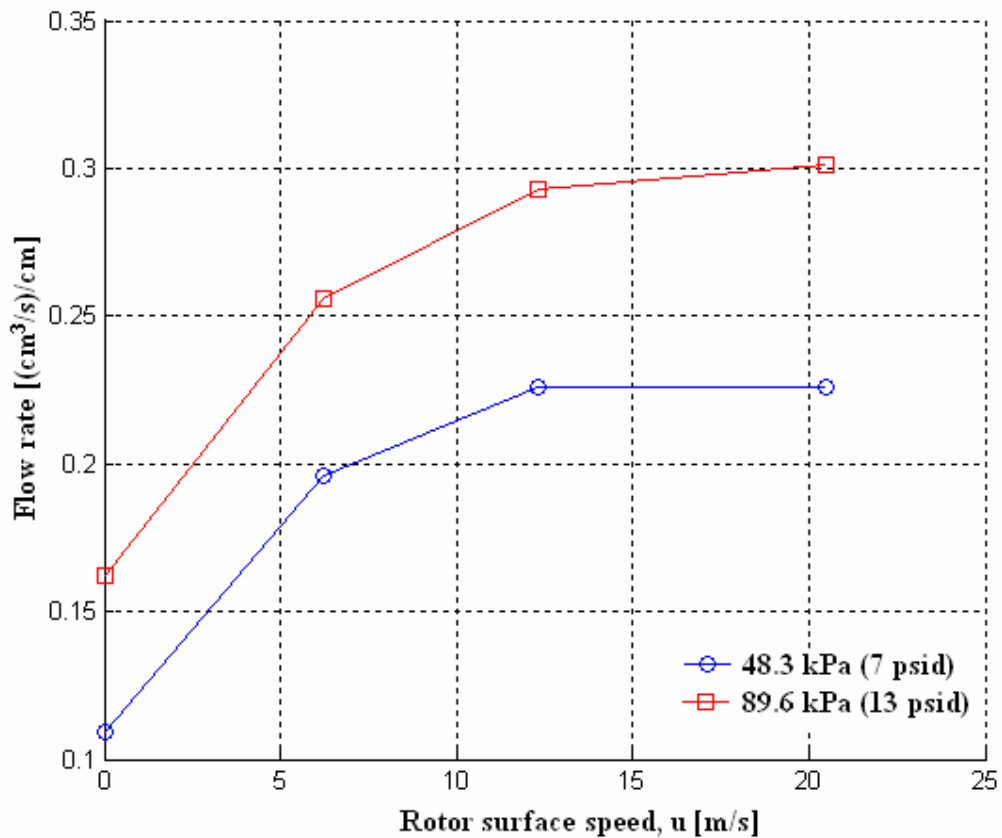
Figure 2.21 Flow rate per seal circumferential length versus rotor surface speed for different pressure loads

	ΔP = 48.3 kPa	ΔP = 89.6 kPa
Rotor surface speed [m/s]	Flow rate [(cm^3/s)/cm]	Flow rate [(cm^3/s)/cm]
0	0.109	0.162
6.2	0.196	0.256
12.3	0.226	0.293
20.5	0.226	0.301

Table 2.1 Experimental flow rate data for different rotor surface speeds and pressure loads

Assuming that the portion of the leakage flow through the porous bristle pack does not change with hydrodynamic lift clearance, which means that pressure difference between upstream and downstream side is remained constant for increasing rotor surface speeds, hydrodynamic lift clearance inducing additional leakage can be calculated.

CFD model of Aksit et al [16] is used for hydrodynamic lift clearance calculations. In his model, Aksit et al [16] define the rotor surface as a non/rotating wall boundary in circumferential direction. In ax-symmetric direction, boundaries of the model domain are defined as symmetric boundaries for non-rotational cases. Cyclically matched boundaries are defined for cases with rotation. In his study, domain is divided into finite volumes, and Navier-Stokes equations are numerically solved for this domain. Aksit et al use the porous medium approach for the bristle pack, which is given by the following equation.

$$-\frac{dP}{dx} = \left(\alpha_i \left| u_i \right| + \beta_i \right) u_i \tag{2.1}$$

In Eq. 2.1, P is pressure, α_i is the effective anisotropic inertial flow resistance, β_i is the effective anisotropic viscous flow resistance and u_i stands for the mean velocity of the fluid. Effective flow resistance coefficients for bristle pack are calibrated to match the experimental leakage data by performing CFD analysis for non-rotating conditions. Rotation and clearance are included into the CFD model after leakage is matched in the first step. The clearance of CFD model is changed until experimental leakage data for a

given pressure load and rotor surface speed is captured. As a result of this, hydrodynamic lift clearance data can be derived from experimental leakage data with the aid of CFD model with calibrated coefficients. Change of hydrodynamic lift clearance with rotor surface speed is given in Figure 2.22 [16].
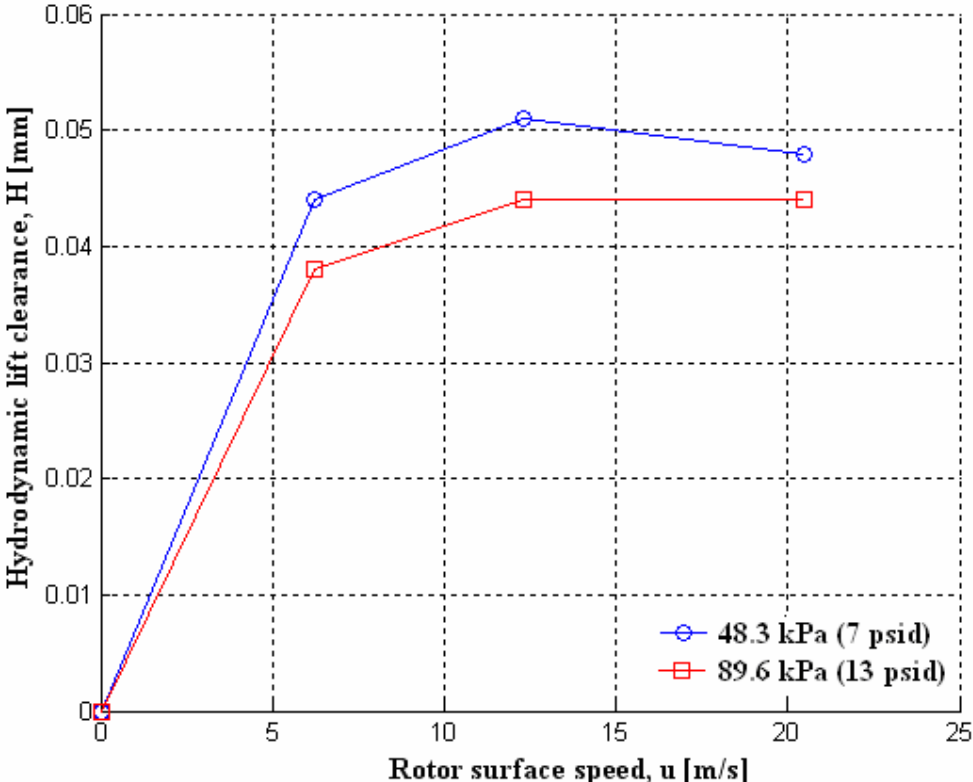
Figure 2.22 Hydrodynamic lift clearance versus rotor surface speed under different pressure loads, based on experimental leakage data, Aksit et al [16]

	ΔP = 48.3 kPa	ΔP = 89.6 kPa
Rotor surface speed [m/s]	Hydrodynamic lift clearance [mm]	Hydrodynamic lift clearance [mm]
0	0	0
6.2	0.044	0.038
12.3	0.052	0.044
20.5	0.048	0.044

Table 2.2 Hydrodynamic lift clearance data for different rotor surface speeds and pressure loads, based on experimental leakage data

As it can be seen from the figure, hydrodynamic lift clearance increases with rotor surface speed, and stabilizes after a certain value of speed. The reason for that stabilization is the shear heating of the oil. Lift clearance is highly dependent on oil viscosity, which is a strong function of temperature. High rotor speed together with small clearance result in oil temperature to rise, which causes shear thinning of the oil by means of decrease in viscosity. This shear thinning effect is the reason for high speed lift clearance stabilization.

3 DERIVATION OF OIL TEMPERATURE DISTRIBUTION FOR BRUSH SEALS IN OIL SEALING APPLICATIONS

Significance of hydrodynamic lift clearance in determining leakage performance of brush seals in oil sealing applications brings up the issue of shear heating effect. As mentioned in the previous chapter, shear heat dissipation, which causes oil viscosity to decrease, is the reason for high speed lift clearance stabilization. Therefore, detailed investigation and theoretical derivation of the oil temperature distribution has a great importance in brush seal applications. In this chapter, temperature distribution analysis is done. Continuity and Navier-Stokes equations are solved with the assumptions which are also given in this chapter. A closed form solution to the temperature distribution of the oil is obtained with the assumption of linear pressure distribution in the axial direction of the rotor. Function of temperature is also derived for nonlinear pressure distribution in the rotor axial direction, and temperature distribution is solved numerically for the nonlinear pressure case. Results of two temperature analyses are also compared.

3.1 Selection of Control Volume

Analysis of boundary layer and thermal energy equations starts with the selection of a control volume. For this purpose, control volume is selected as the volume between the bristle pack and the rotor surface, as shown in Figure 3.1.
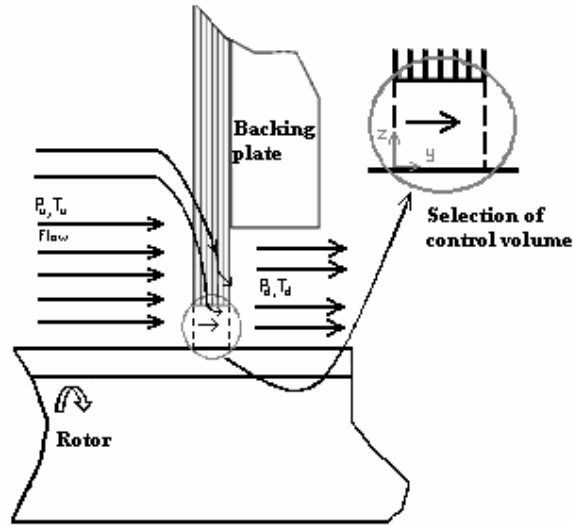
Figure 3.1 Selection of control volume

Due to the fact that the axial leakage flow is dominant, radial flows (flows in z-direction in Figure 3.1) are neglected for the sake of simplicity. To be able to solve thermal energy equation, it is required to solve continuity and Navier-Stokes equations to find the velocity profile for the fluid. These equations are solved under the assumptions of,

1. Steady state
2. Incompressible flow
3. Convection from rotor surface and bristle surfaces to the fluid is neglected.

In the analysis of the boundary layer equations, rotor and bristle surfaces are taken as flat surfaces, and the control volume as the rectangular volume between these surfaces. As shown in Figure 3.2, L is the circumferential length of the rotor surface, w is the width of the bristle pack, H is the hydrodynamic lift clearance, and u is the rotor surface speed. Note that L, w, and H are also the dimensional scales for the control volume. Seal design parameters which are used in analyses as well as the experiments are,

$$R_{rotor} = 67mm$$

$$L = 2 \cdot \pi \cdot R_{rotor} \approx 405 \cdot 10^{-3} m$$

$$w = 25 \cdot 10^{-4} m$$

Hydrodynamic lift clearance changes with pressure difference and rotor speed. Based on the experimental data, amount of lift and the inlet temperature for the initial steps of analysis are taken as,

$$H = 40 \cdot 10^{-6} m$$

$$T_u = 50^\circ C \ \text{(upstream temperature)}$$

Density and the specific heat values for the oil at the upstream temperature are,

$$\rho = 884.61 kg / m^3$$

$$c_p = 2030.5 J / kg^\circ C$$
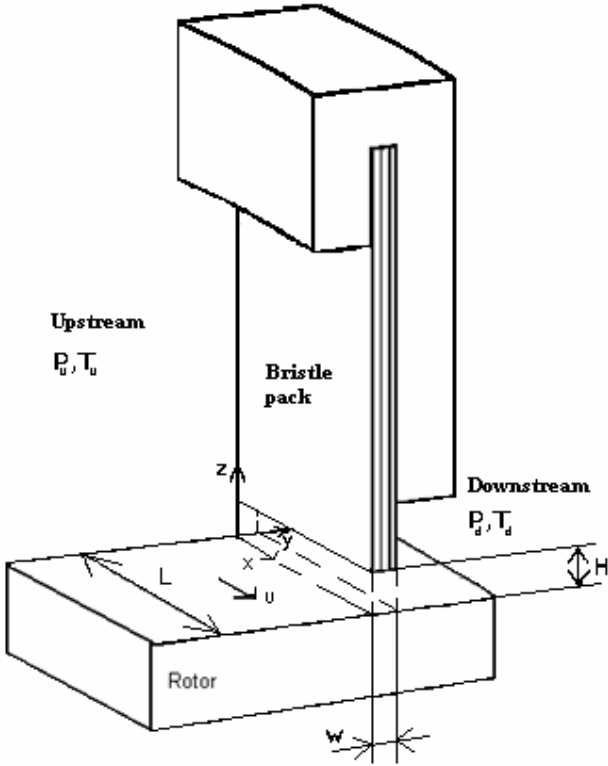
Figure 3.2 Unwrapped brush seal geometry

3.2 Solution to Continuity and Navier Stokes Equations for the Brush Seal

To be able to solve thermal energy equation, velocity profile and pressure distribution for the oil have to be known. Therefore, it is required to solve continuity and Navier-Stokes equations.

The leakage flow through the control volume is a channel flow, and Reynolds number is required to investigate whether the flow is laminar or turbulent. Hydrodynamic lift clearance, which is perpendicular to the flow, is the characteristic length for the Reynolds number.

$$\mathrm{Re}_H = \frac{\rho \cdot \upsilon_f \cdot H}{\mu} \tag{3.1}$$

Where ρ is the density of the fluid, and υ_f is the mean fluid velocity. Viscosity of the oil at 50°C, which is the upstream temperature, is 0.0195Pa.s, and the density of the oil at upstream temperature is 884.61kg/m³. Mean fluid velocity is derived by dividing the flow rate per circumferential length of the rotor with hydrodynamic lift clearance. To match the available data, flow rate per circumferential length of the rotor is taken as 0.4(cm³/s)/cm, and hydrodynamic lift clearance is taken as 40μm. Reynolds number is found with these values as,

$$\mathrm{Re}_H = \frac{\rho \cdot \upsilon_f \cdot H}{\mu} = \frac{884.61 \cdot \dfrac{0.4 \cdot 10^{-4}}{40 \cdot 10^{-6}} \cdot 40 \cdot 10^{-6}}{0.0195} \approx 1.81 << 2300 \tag{3.2}$$

Therefore, the flow is determined to be laminar. Another concern is about whether the flow is fully developed or not. For the flow of interest, starting point for the fully developed region can be calculated by using the equation given below.

$$\left(\frac{y_{fd,h}}{H} \right)_{lam} = 0.05 \cdot \mathrm{Re}_H \Rightarrow y_{fd,h} = 0.05 \cdot 1.81 \cdot 40 \cdot 10^{-6} \approx 3.6 \cdot 10^{-6} m \tag{3.3}$$

As mentioned before, width of the bristle pack is taken as 2.5mm. From Equation (3.3), the starting point of fully developed laminar flow is found as 3.6μm, which is almost thousand times smaller than the width of the bristle pack. As a result of this, the flow is assumed to be fully developed through the bristle pack.

Continuity and Navier-Stokes equations with the assumption of no radial flow (no flow in z-direction) are given through Equations (3.4) to (3.6).

$$\frac{\partial \upsilon_x}{\partial x} + \frac{\partial \upsilon_y}{\partial y} = 0 \tag{3.4}$$

$$\rho \cdot \left(\frac{\partial \upsilon_x}{\partial t} + \upsilon_x \cdot \frac{\partial \upsilon_x}{\partial x} + \upsilon_y \cdot \frac{\partial \upsilon_x}{\partial y} + \upsilon_z \cdot \frac{\partial \upsilon_x}{\partial z} \right) =$$

$$-\frac{\partial P}{\partial x} + \left[\frac{\partial}{\partial x}\left(\mu_{eff_z} \frac{\partial \upsilon_x}{\partial x} \right) + \frac{\partial}{\partial y}\left(\mu_{eff_z} \frac{\partial \upsilon_x}{\partial y} \right) + \frac{\partial}{\partial z}\left(\mu_{eff_z} \frac{\partial \upsilon_x}{\partial z} \right) \right] - \rho \cdot g_x \tag{3.5}$$

$$\rho \cdot \left(\frac{\partial \upsilon_y}{\partial t} + \upsilon_x \cdot \frac{\partial \upsilon_y}{\partial x} + \upsilon_y \cdot \frac{\partial \upsilon_y}{\partial y} + \upsilon_z \cdot \frac{\partial \upsilon_y}{\partial z} \right) =$$

$$-\frac{\partial P}{\partial y} + \left[\frac{\partial}{\partial x}\left(\mu_{eff_z} \frac{\partial \upsilon_y}{\partial x} \right) + \frac{\partial}{\partial y}\left(\mu_{eff_z} \frac{\partial \upsilon_y}{\partial y} \right) + \frac{\partial}{\partial z}\left(\mu_{eff_z} \frac{\partial \upsilon_y}{\partial z} \right) \right] - \rho \cdot g_y \tag{3.6}$$

P is the pressure, υ_x, υ_y, υ_z are the fluid velocity components in x, y and z-directions, $\mu_{eff\text{-}z}$ is the dynamic viscosity of the oil at a certain z coordinate, and g stands for gravitational acceleration. Since gravitational terms are small compared to other terms, they can be neglected. For steady state conditions,

$$\frac{\partial \upsilon_x}{\partial t} = \frac{\partial \upsilon_y}{\partial t} = 0 \tag{3.7}$$

Since there is no flow in z-direction, all related terms takes the value of zero.

$$\upsilon_z = 0, \; \upsilon_z \cdot \frac{\partial \upsilon_x}{\partial z} = \upsilon_z \cdot \frac{\partial \upsilon_y}{\partial z} = 0 \tag{3.8}$$

Following from brush seal geometry relations provided in Equation (3.9) can be stated for dimensional scales of the problem.

$$L \gg w \gg H$$

$$\frac{\partial}{\partial x} \ll \frac{\partial}{\partial y} \ll \frac{\partial}{\partial z} \tag{3.9}$$

which further leads to the following inequality the relations.

$$\frac{\partial^2 \upsilon_x}{\partial x^2}, \frac{\partial^2 \upsilon_x}{\partial y^2} << \frac{\partial^2 \upsilon_x}{\partial z^2}, \text{ neglect } \frac{\partial^2 \upsilon_x}{\partial x^2}, \frac{\partial^2 \upsilon_x}{\partial y^2} \tag{3.10}$$

$$\frac{\partial^2 \upsilon_y}{\partial x^2}, \frac{\partial^2 \upsilon_y}{\partial y^2} << \frac{\partial^2 \upsilon_y}{\partial z^2}, \text{ neglect } \frac{\partial^2 \upsilon_y}{\partial x^2}, \frac{\partial^2 \upsilon_y}{\partial y^2} \tag{3.11}$$

Following the above mentioned simplifications, N-S equations given in Equations (3.5) and (3.6) are reduced to the form given below by using relations given in Equations (3.7) through (3.11).

$$\rho \cdot \left(\upsilon_x \cdot \frac{\partial \upsilon_x}{\partial x} + \upsilon_y \cdot \frac{\partial \upsilon_x}{\partial y} \right) = -\frac{\partial P}{\partial x} + \mu_{eff_z} \cdot \frac{\partial^2 \upsilon_x}{\partial z^2} \tag{3.12}$$

$$\rho \cdot \left(\upsilon_x \cdot \frac{\partial \upsilon_y}{\partial x} + \upsilon_y \cdot \frac{\partial \upsilon_y}{\partial y} \right) = -\frac{\partial P}{\partial y} + \mu_{eff_z} \cdot \frac{\partial^2 \upsilon_y}{\partial z^2} \tag{3.13}$$

In Equations (3.12) and (3.13), $\mu_{eff\text{-}z}$ is taken out from $\partial / \partial z$. In this study, dynamic viscosity is taken as a function of temperature. Temperature field, which is going to be derived in the following sections, varies along y- and z-directions. $\mu_{eff\text{-}z}$ is the value of dynamic viscosity which is calculated for a certain point on z axis. As a result, $\mu_{eff\text{-}z}$ is a function of y, and independent of z.

Terms of modified Navier-Stokes Equations given in Equations (3.12) and (3.13) are non-dimensionalized in order to take the analysis one step further. For this purpose, following normalized parameters are used.

$$x^* = \frac{x}{L}, y^* = \frac{y}{w}, z^* = \frac{z}{H}$$

$$\upsilon_x^* = \frac{\upsilon_x}{u}, \upsilon_y^* = \frac{\upsilon_y}{u} \cdot \frac{L}{w} \tag{3.14}$$

$$P^* = \frac{P}{\mu_{eff_z} \cdot u \cdot L} \cdot H^2$$

Substituting these parameters into the modified N-S Equations (3.12) and (3.13) gives,

$$\text{Re}_{H-u} \cdot \frac{H}{L} \cdot \left(\upsilon_x^* \cdot \frac{\partial \upsilon_x^*}{\partial x^*} + \upsilon_y^* \cdot \frac{\partial \upsilon_x^*}{\partial y^*} \right) = -\frac{\partial P^*}{\partial x^*} + \frac{\partial^2 \upsilon_x^*}{\partial z^{*2}} \tag{3.15}$$

$$\mathrm{Re}_{H-u} \cdot \frac{H}{L} \cdot \left(\upsilon_x^* \cdot \frac{\partial \upsilon_y^*}{\partial x^*} + \upsilon_y^* \cdot \frac{\partial \upsilon_y^*}{\partial y^*} \right) = -\frac{\partial P^*}{\partial y^*} \cdot \frac{L^2}{w^2} + \frac{\partial^2 \upsilon_y^*}{\partial z^{*2}} \tag{3.16}$$

Re_{H-u} stands for Reynolds number for which the characteristic length is the hydrodynamic lift clearance and the velocity is the rotor surface speed. To match the available data, Re_{H-u} is calculated for 10m/s rotor surface speed using the above mentioned viscosity, density and H values.

$$\mathrm{Re}_{H-u} \cdot \frac{H}{L} = \frac{\rho \cdot u \cdot H}{\mu_{eff_z}} \cdot \frac{H}{L} \approx 1.86 \cdot 10^{-3} << 1 \tag{3.17}$$

Since the Re_{H-u} is much smaller than unity, inertia terms can be neglected. Therefore, left hand sides of the Navier-Stokes equations drop leading to reduced Navier-Stokes equations (3.18) and (3.19) as,

$$-\frac{\partial P}{\partial x} + \mu_{eff_z} \cdot \frac{\partial^2 \upsilon_x}{\partial z^2} = 0 \text{, with the boundary conditions}$$

$$z = 0, \upsilon_x = u$$
$$z = H, \upsilon_x = 0 \tag{3.18}$$

$$-\frac{\partial P}{\partial y} + \mu_{eff_z} \cdot \frac{\partial^2 \upsilon_y}{\partial z^2} = 0 \text{, with the boundary conditions}$$

$$z = 0, \upsilon_y = 0$$
$$z = H, \upsilon_y = 0 \tag{3.19}$$

Velocity profiles for the fluid in x and y directions are found by solving reduced Navier-Stokes Equations (3.18) and (3.19) respectively.

$$\upsilon_x = \frac{1}{2\mu_{eff_z}} \cdot \frac{\partial P}{\partial x} \cdot \left(z^2 - z \cdot H \right) + u \cdot \left(1 - \frac{z}{H} \right) \tag{3.20}$$

$$\upsilon_y = \frac{1}{2\mu_{eff_z}} \cdot \frac{\partial P}{\partial y} \cdot \left(z^2 - z \cdot H \right) \tag{3.21}$$

Substituting υ_x and υ_y into the continuity equation (Equation (1)) yields,

$$\frac{\partial}{\partial x}\left(\frac{H^3}{\mu_{eff_z}} \cdot \frac{\partial P}{\partial x}\right) + \frac{\partial}{\partial y}\left(\frac{H^3}{\mu_{eff_z}} \cdot \frac{\partial P}{\partial y}\right) = 0 \qquad (3.22)$$

Since $L >> w$, which means $\dfrac{\partial}{\partial x^2} << \dfrac{\partial}{\partial y^2}$, Equation (3.22) reduces to,

$$\frac{\partial}{\partial y}\left(\frac{H^3}{\mu_{eff_z}} \frac{\partial P}{\partial y}\right) = 0 \qquad (3.23)$$

Equation (3.23) is the differential equation governing the variation in hydrodynamic pressure in axial (y) direction. Pressure takes the value of upstream pressure for y equals to zero, and takes the downstream pressure value at the end of bristle pack, where y equals to the width of the bristle pack, w. These two values of the pressure set the boundary conditions for Equation (3.23). Downstream pressure value equals to atmospheric pressure. Upstream pressure value is determined per pressure load value, ΔP, which changes from design to design.

3.3 Solution to the Thermal Energy Equation with Linear Pressure Distribution Assumption

The term $\mu_{eff\text{-}z}$ in Equation (3.23) depends on y, and can not be taken out. However, for the sake of simplicity, and to be able to find a closed form solution to the temperature distribution, pressure gradient along y-axis is assumed to be constant. As stated by Bhate et al [10], axial pressure drop is almost linear. Therefore, Equation (3.23) reduces to,

$$\frac{\partial P}{\partial y} = C_1,$$

B.C's:
$$y = 0, P = P_u$$
$$y = w, P = P_d$$

(3.24)

Pressure distribution can be obtained by solving this differential equation with the given boundary conditions as,

$$P = -\frac{\Delta P}{w} \cdot y + P_u$$

(3.25)

where $\Delta P = P_u - P_d$

All required information to solve thermal energy equation has been obtained. In most general form, 3-D thermal energy equation for an incompressible flow is given below.

$$\rho c_p \left(\upsilon_x \frac{\partial T}{\partial x} + \upsilon_y \frac{\partial T}{\partial y} + \upsilon_z \frac{\partial T}{\partial z} \right) = \frac{\partial}{\partial x}\left(k \frac{\partial T}{\partial x} \right) + \frac{\partial}{\partial y}\left(k \frac{\partial T}{\partial y} \right) + \frac{\partial}{\partial z}\left(k \frac{\partial T}{\partial z} \right) + \mu \cdot \phi + q'''$$ (3.26)

where ϕ is the dissipation function defined as,

$$\phi = 2\left[\left(\frac{\partial \upsilon_x}{\partial x}\right)^2 + \left(\frac{\partial \upsilon_y}{\partial y}\right)^2 + \left(\frac{\partial \upsilon_z}{\partial z}\right)^2 \right] + \left(\frac{\partial \upsilon_x}{\partial y} + \frac{\partial \upsilon_y}{\partial x}\right)^2 + \left(\frac{\partial \upsilon_z}{\partial y} + \frac{\partial \upsilon_y}{\partial z}\right)^2$$

$$+ \left(\frac{\partial \upsilon_x}{\partial z} + \frac{\partial \upsilon_z}{\partial x}\right)^2 - \frac{2}{3}\left(\frac{\partial \upsilon_x}{\partial x} + \frac{\partial \upsilon_y}{\partial y} + \frac{\partial \upsilon_z}{\partial z}\right)^2$$

(3.27)

In thermal energy equation (3.26), q''' stands for heat input per volume and equals to zero for the control volume of interest. Since the circumferential length of the rotor *(L)* is much larger than the bristle pack width *(w)* and hydrodynamic lift clearance *(H)*, temperature of the oil can be assumed to be lumped in *x*-direction. In addition, dissipation function terms, $\partial \upsilon_x/\partial x$, $\partial \upsilon_x/\partial y$ drops out when compared to $\partial \upsilon_x/\partial z$, and $\partial \upsilon_y/\partial x$, $\partial \upsilon_y/\partial y$ drops out when compared to $\partial \upsilon_y/\partial z$. Since υ_z is zero, all related terms on the left hand side of the thermal energy equation and in the dissipation function drop out. . Assuming that there is no convection from the rotor and the bristle surfaces to the fluid, and neglecting the heat conduction, thermal energy equation reduces,

$$\rho c_p \upsilon_y \frac{\partial T}{\partial y} = \mu\left(\left(\frac{\partial \upsilon_x}{\partial z}\right)^2 + \left(\frac{\partial \upsilon_y}{\partial z}\right)^2 \right)$$

(3.28)

Based on the experimental leakage data, flow rate in y-direction is taken around 0.4cm^3/sec. Taking the value of thermal conductivity as 0.145 W/m-K, using other oil properties for the test conditions, the Peclet number, which is the ratio of forced convection to heat conduction, takes a value around 495. Since the contribution of heat conduction to energy transfer is small in comparison to convection terms, conduction terms are neglected in this study.

Note that dynamic viscosity, μ appears in thermal energy equation (3.28) instead of $\mu_{eff\text{-}z}$, which is defined earlier and used in the continuity and N-S equations. $\mu_{eff\text{-}z}$ is used in these equations in order to get rid of z dependency of μ. However, there is no difference between using μ or $\mu_{eff\text{-}z}$ in thermal energy equation since the differential of temperature is taken only with respect to y (z behaves as a constant when integrating it with respect to y, so there is no difference in using z or any other constant number).

Thermal energy equation given in Equation (3.28) is first order differential equation, where its boundary condition is the upstream temperature; T_u. Due to their weak dependence on temperature, density and specific heat of the fluid are assumed to be constant at their values at upstream temperature. After adjustments given below, thermal energy equation of (3.28) takes the form given in Equation (3.29).

$$\mu = \mu_0 e^{-\beta(T-T_0)}$$

$$\frac{\partial \upsilon_x}{\partial z} = -\frac{u}{H}$$

$$\frac{\partial \upsilon_y}{\partial z} = \frac{1}{2\mu}\cdot\frac{\partial P}{\partial y}\cdot(2z - H)$$

$$\theta = T - T_0$$

$$\left(\frac{1}{2\mu_0^2}\cdot e^{2\beta\theta}\right)\cdot\partial\theta + \frac{1}{\rho c_p\left(z^2 - zH\right)}\cdot\left[\frac{u^2 w}{H^2 \Delta P} + \frac{\Delta P}{w}\cdot\frac{(2z - H)^2}{4\mu_0^2}e^{2\beta\theta}\right]\partial y = 0$$

$$\text{B.C: } T = T_u \text{ at } y = 0 \tag{3.29}$$

μ_o, β are oil properties, and for the oil of interest, β is 0.0294 and μ_o is 0.028Pa.s for $T_o = 37.78^\text{o}$C. This differential equation is of the form,

$$M(\theta, y)\cdot\partial\theta + N(\theta, y)\cdot\partial y = 0 \tag{3.30}$$

41

$$M_{,y} = 0$$

$$N_{,\theta} = \frac{2\beta}{\rho c_p \left(z^2 - zH\right)} \cdot \frac{\Delta P}{w} \cdot \frac{\left(2z - H\right)^2}{4\mu_0^2} \cdot e^{2\beta\theta}$$

Since $M_{,y}$ does not equal to $N_{,\theta}$, the differential equation is not an exact differential equation. An integration factor must be found to make it exact. Integration factor, which is only function of y, can be found after making calculations given below.

$$\frac{d\eta}{\eta} = \frac{N_{,\theta} - M_{,y}}{M} = \frac{\left(2z - H\right)^2}{\rho \cdot c_p \cdot \left(z^2 - zH\right)} \cdot \frac{\Delta P}{w} \cdot \beta \cdot dy$$

$$\int \frac{d\eta}{\eta} = \int \frac{\left(2z - H\right)^2}{\rho \cdot c_p \cdot \left(z^2 - zH\right)} \cdot \frac{\Delta P}{w} \cdot \beta \cdot dy$$

$$\ln\left[\eta(y)\right] = \frac{\left(2z - H\right)^2}{\rho \cdot c_p \cdot \left(z^2 - zH\right)} \cdot \frac{\Delta P}{w} \cdot \beta \cdot y$$

$$\Downarrow$$

$$\eta(y) = \exp\left[\frac{\left(2z - H\right)^2}{\rho c_p \left(z^2 - zH\right)} \cdot \frac{\Delta P}{w} \cdot \beta \cdot y\right] \tag{3.31}$$

An exact differential equation can be obtained by multiplying the Equation (3.29) with the integration factor $\eta(y)$. After multiplication, the following relations are obtained.

$$\partial F = F_{,\theta} \partial \theta + F_{,y} \partial y = 0 \tag{3.32}$$

$$F_{,y} = \frac{\exp\left[\dfrac{\left(2z - H\right)^2}{\rho c_p \left(z^2 - zH\right)} \cdot \dfrac{\Delta P}{w} \cdot \beta \cdot y\right]}{\rho c_p \left(z^2 - zH\right)} \cdot \left[\frac{u^2 w}{H^2 \Delta P} + \frac{\Delta P}{w} \cdot \frac{\left(2z - H\right)^2}{4\mu_0^2} e^{2\beta\theta}\right] \tag{3.33}$$

$$F_{,\theta} = \frac{1}{2\mu_0^2} \cdot e^{2\beta\theta} \cdot \exp\left[\frac{\left(2z - H\right)^2}{\rho c_p \left(z^2 - zH\right)} \cdot \frac{\Delta P}{w} \cdot \beta \cdot y\right] \tag{3.34}$$

Integrating $F_{,y}$ with respect to y yields,

$$F(\theta, y) = \left[\frac{u^2 w}{H^2 \Delta P} + \frac{\Delta P}{w} \cdot \frac{(2z - H)^2}{4\mu_0^2} e^{2\beta\theta} \right] \cdot \frac{w}{\Delta P \beta (2z - H)^2} \cdot \exp\left[\frac{(2z - H)^2}{\rho c_p (z^2 - zH)} \cdot \frac{\Delta P}{w} \cdot \beta \cdot y \right] + C(\theta)$$

(3.35)

After taking the derivative of $F(\theta, y)$ with respect to θ and equating it to Equation (3.34), $C(\theta)_{,\theta}$ is obtained as zero, which means that $C(\theta) = C$, which is a constant. Now, solution to function $F(\theta, y)$ is found. However, it is required to find θ in order to find temperature. It is known from the differential equation (3.32) that ∂F equals to zero, which means $F(\theta, y)$ is a constant. As a result, solution to differential equation is obtained as,

$$\left[\frac{u^2 w}{H^2 \Delta P} + \frac{\Delta P}{w} \cdot \frac{(2z - H)^2}{4\mu_0^2} e^{2\beta\theta} \right] \cdot \frac{w}{\Delta P \beta (2z - H)^2} \cdot \exp\left[\frac{(2z - H)^2}{\rho c_p (z^2 - zH)} \cdot \frac{\Delta P}{w} \cdot \beta \cdot y \right] + C_2 = 0$$

(3.36)

C_2 is a constant other than C. After applying temperature boundary condition, $T = T_u$ at $y = 0$, C_2 is obtained as,

$$C_2 = -\left(\frac{u^2}{H^2} \cdot \frac{w}{\Delta P} + \frac{\Delta P}{w} \cdot \frac{(2z - H)^2}{4\mu_0^2} e^{2\beta\theta_u} \right) \cdot \frac{w}{\Delta P \beta (2z - H)^2}$$

(3.37)

After substituting this constant into the Equation (3.36) and rearranging, temperature distribution is reached as,

$$T = T_0 + \frac{1}{2\beta} \ln\left(\frac{f_1}{f_2} + f_3 \cdot f_4 \right)$$

(3.38)

43

$$f_1 = \exp(2\beta(T_u - T_0))$$

$$f_2 = \exp\left[\frac{(2z-H)^2}{\rho c_p(z^2 - zH)} \cdot \frac{\Delta P}{w} \cdot \beta \cdot y\right]$$

$$f_3 = \frac{4(u \cdot w \cdot \mu_0)^2}{[H \cdot \Delta P \cdot (2z-H)]^2}$$

$$f_4 = \exp\left[-\frac{(2z-H)^2}{\rho c_p(z^2 - zH)} \cdot \frac{\Delta P}{w} \cdot \beta \cdot y\right] - 1$$

Temperature distribution under the bristle pack along y and z axes is obtained as a function of pressure difference (ΔP), upstream temperature (T_u) rotor surface speed (u), hydrodynamic lift clearance (H), bristle pack width (w) and oil properties$(\rho,\ c_p,\ \mu_o,\ \beta)$. Pressure load and upstream temperature are design parameters and known. Oil properties are also known. Hydrodynamic lift clearance changes with rotor surface speed and pressure difference. Relation between lift clearance and rotor surface speed can be obtained from experimental leakage data given in Chapter 2. To compare the results with the hydrodynamic lift data following seal parameters are used in the analyses,

Bristle radius, $R_b = 0.051\ mm$

Elasticity modulus of the bristle, $E = 2.07 \times 10^{11}\ Pa$

Cant angle, $\theta = 45^o$

Viscosity constants for the fluid, $\beta = 0.0294$, $\mu_o = 0.028 Pa.s$ at $T_o = 37.78^o$

Free bristle height, $BH = 16mm$.

As it can be seen from the temperature function (3.38), it gives $0/0$ uncertainty for value of $H/2$ for z. Uncertainty of the temperature function at $z = H/2$ is removed by applying L'Hopital's Rule. Temperature function at $z = H/2$ is obtained as given in Equation (3.39).

$$T\left(y, z = \frac{H}{2}\right) = T_0 + \frac{1}{2\beta} \cdot \ln\left\{\exp[2\beta(T_u - T_0)] + \frac{16(u \cdot w \cdot \mu_o)^2 \cdot \beta \cdot y}{\rho \cdot c_p \cdot \Delta P \cdot w} \cdot \frac{1}{H^4}\right\} \qquad (3.39)$$

Since convection from bristles and rotor surfaces is neglected, temperature distribution goes to infinity at both ends for z, which does not reflect the real case. Therefore, mean value of temperature with respect to z is used for temperature analysis.

$$T_{mean-z}(y) = \frac{1}{H} \int_0^H T(y,z) \cdot dz \qquad (3.40)$$

T_{mean-z} is the mean temperature in z-axis. Temperature is a complex function of z, which makes taking its integral with respect to z almost impossible. Therefore, numerical integration methods are used. Trapezoid rule as given by Equation (3.41) is employed as the numeric integration method.

$$\int_0^H T(y,z) \cdot dz = \frac{l}{2} \cdot \left[T(y,z_1) + 2T(y,z_1+l) + \ldots + T(y,z_2) \right] \qquad (3.41)$$

l, the rise of z for each step, is taken as $H/80$, which is around 5×10^{-7} m. In Equation (3.41), z_1 takes the value of zero, and z_2 stands for H, where temperature goes to infinity. To be able to get over this problem, values of the temperature at both ends are taken as equal to the temperature values at $H/80$ further from these ends for the numeric integration. After the integral is taken, mean temperature value with respect to z at any y point can be derived by simply dividing it by H, as given in Equation (3.40).A simple MATLAB code is written to compute the numeric integration and mean-z temperature values along y-axis. Mean-z temperature distribution along y-axis is given in Figure 3.3 for different pressure loads and rotor surface speeds.

As it can be observed in Figure 3.3, temperature distribution along y-direction yields consistent results with real life applications. Temperature of the fluid at $y = 0$ equals to upstream temperature, 50°C. As the fluid under the bristle pack flows to the downstream side, temperature of the fluid increases, and takes its maximum value at the downstream end. The reason for this temperature rise is mostly related to viscous forces in the fluid causing shear heat dissipation. Shear heating has great influence on hydrodynamic lifting force at moderate and high rotor surface speeds.
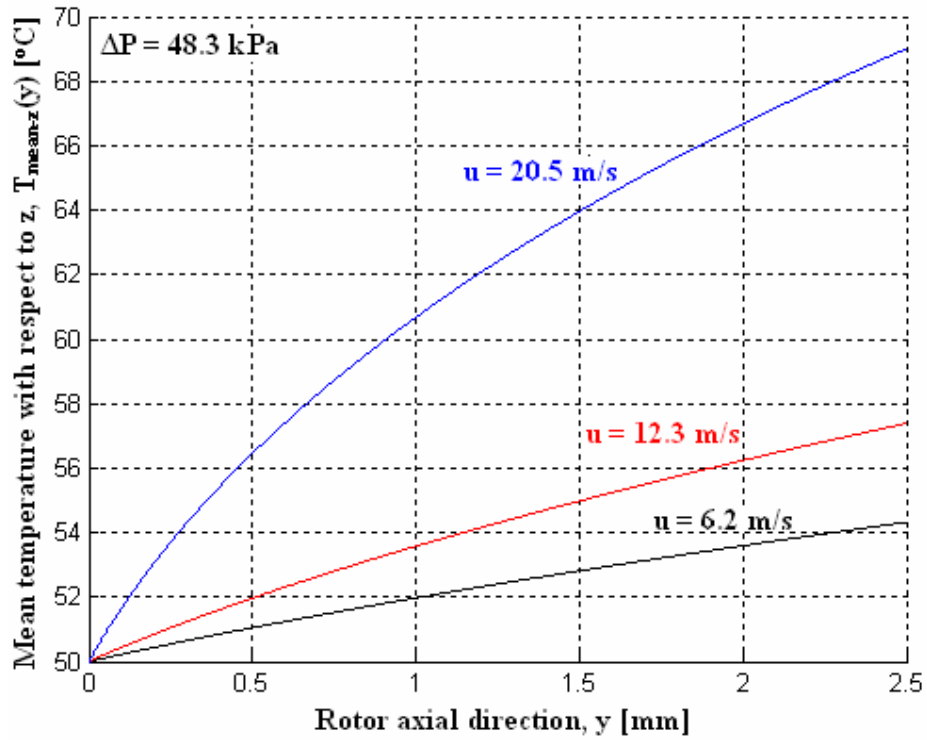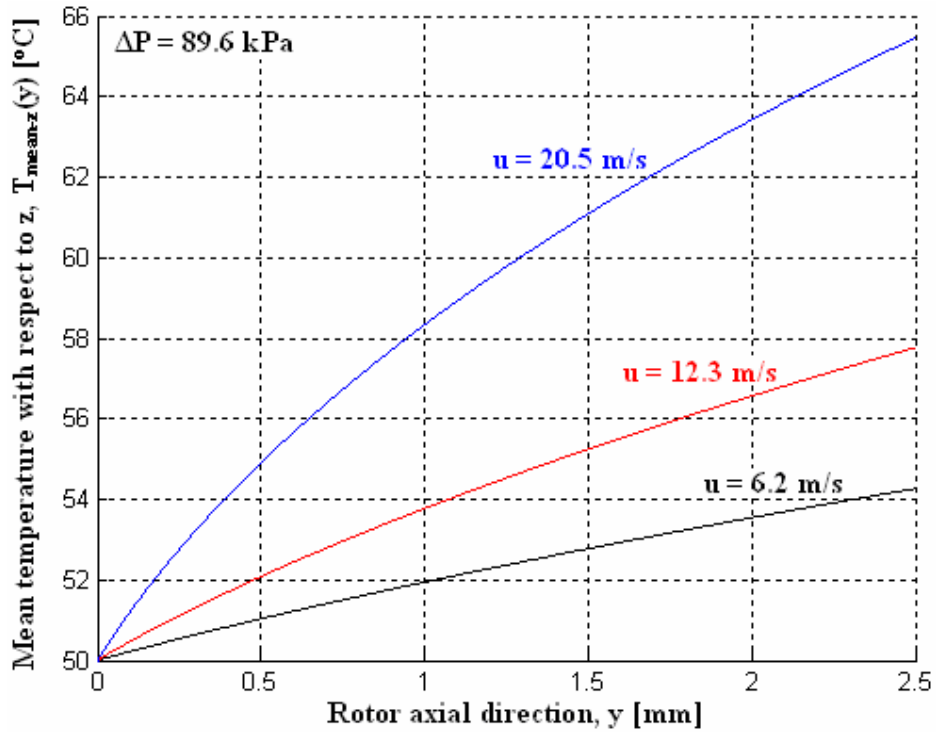
Figure 3.3 Mean-z temperature, $T_{mean-z}(y)$, distribution along y-axis (in the direction of leakage flow (rotor axial direction)) for different pressure loads and rotor surface speeds
a) $\Delta P = 48.3$ kPa, b) $\Delta P = 89.6$ kPa

Temperature rise along y-axis for different rotor surface speeds are also obtained, and results are presented below. Temperature rise along the *y*-axis is defined as the difference between the mean value of the downstream temperature with respect to *z* and the upstream temperature.

$$T_{d_{mean-z}} = T_{mean-z}(y = w) = \frac{1}{H}\int_0^H T(w,z) \cdot dz$$

$$\Downarrow$$

$$\Delta T = T_{d_{mean-z}} - T_u \tag{3.42}$$

Rotor surface speed [m/s]	ΔP = 48.3 kPa Temperature rise along y-axis, ΔT	ΔP = 89.6 kPa Temperature rise along y-axis, ΔT
0	0	0
6.2	4.3 ℃	4.2 ℃
12.3	7.4 ℃	7.7 ℃
20.5	19 ℃	15.4 ℃

Table 3.1 Temperature rise along y-axis for rotor surface speeds and different pressure loads

3.4 Solution to the Thermal Energy Equation for Nonlinear Pressure Distribution

In the previous section, a closed form solution for the temperature distribution is obtained based on the assumption of linear pressure distribution along y-axis. In this section, temperature function is derived using a nonlinear pressure distribution by solving reduced continuity equation (3.23) and thermal energy equation (3.28) simultaneously. Steps of temperature analysis for nonlinear pressure distribution are given in this chapter.

After the implementing assumptions given in Chapter 3.2, substituting values of v_x and v_y into the continuity equation and making necessary simplifications, reduced continuity equation (3.23) was obtained as,

$$\frac{\partial}{\partial y}\left(\frac{H^3}{\mu_{eff_z}}\frac{\partial P}{\partial y}\right) = 0$$

If the pressure distribution is assumed to be linear along y-axis, Equation (3.23) can be reduced to Equation (3.24). However, $\mu_{eff\text{-}z}$ depends on y, and can not be taken out from the differentiation. If the dependency of the $\mu_{eff\text{-}z}$ to y is included, Equation (3.23) yields,

$$\frac{\partial}{\partial y}\left(\frac{1}{\mu_{eff_z}}\frac{\partial P}{\partial y}\right)=0$$

B.C's:

$$y=0, P=P_u$$

$$y=w, P=P_d$$

(3.43)

As it does not depend on y, hydrodynamic lift clearance, H can be taken out of the parenthesis and it drops out. Integrating Equation (3.43) with respect to y gives,

$$\frac{\partial P}{\partial y}=C\cdot\mu_{eff_z}$$

(3.44)

where C is the integration constant. Substituting it into the v_y given in Equation (3.21) yields,

$$v_y=\frac{C}{2}\cdot\left(z^2-z\cdot H\right)$$

(3.45)

Substituting this v_y and other necessary parameters into the thermal energy equation (3.28) gives,

$$\rho c_p v_y \frac{\partial T}{\partial y}=\mu\left(\left(\frac{\partial v_x}{\partial z}\right)^2+\left(\frac{\partial v_y}{\partial z}\right)^2\right), \text{ thermal energy equation (3.28)}$$

$$\frac{\partial v_x}{\partial z}=-\frac{u}{H}$$

$$\frac{\partial v_y}{\partial z}=\frac{C}{2}\cdot\left(2z-H\right)$$

$$v_y=\frac{C}{2}\cdot\left(z^2-z\cdot H\right)$$

$$\Downarrow$$

$$\frac{1}{\mu}\frac{\partial T}{\partial y}=\frac{2}{\rho\cdot c_p\cdot\left(z^2-z\cdot H\right)\cdot C}\cdot\left(\frac{u^2}{H^2}+\frac{C^2}{4}\cdot\left(2\cdot z-H\right)^2\right)$$

(3.46)

Equation (3.46) represents the differential equation for the temperature for nonlinear pressure distribution along y-axis.

Further substituting temperature dependant viscosity, $\mu = \mu_0 e^{-\beta(T-T_0)}$, into the Equation (3.46) and making necessary arrangements following differential equation is obtained.

$$e^{\beta(T-T_0)} \cdot \partial T = \frac{2\mu_0}{\rho \cdot c_p \cdot (z^2 - z \cdot H) \cdot C} \cdot \left(\frac{u^2}{H^2} + \frac{C^2}{4} \cdot (2 \cdot z - H)^2 \right) \cdot \partial y$$

B.C:

$$y = 0, T = T_u$$

(3.47)

Solving this differential equation with the given boundary condition results in the temperature distribution as given below.

$$\int e^{\beta(T-T_0)} \cdot \partial T = \int \frac{2\mu_0}{\rho \cdot c_p \cdot (z^2 - z \cdot H) \cdot C} \cdot \left(\frac{u^2}{H^2} + \frac{C^2}{4} \cdot (2 \cdot z - H)^2 \right) \cdot \partial y$$

$$\Downarrow$$

$$T = T_0 + \frac{1}{\beta} \cdot \ln \left\{ e^{\beta(T_u - T_0)} + \frac{2\mu_0 \cdot \beta}{\rho \cdot c_p \cdot (z^2 - z \cdot H) \cdot C} \cdot \left(\frac{u^2}{H^2} + \frac{C^2}{4} \cdot (2 \cdot z - H)^2 \right) \cdot y \right\} \quad (3.48)$$

Temperature function for nonlinear pressure distribution is derived as in Equation (3.48). However, the integration constant, C, which appears in the temperature function and it is still unknown. Value of this integration constant can be determined by substituting temperature function into the viscosity, and plugging this viscosity into the pressure distribution. As the first step, viscosity is found as,

$$\mu = \mu_0 \cdot \exp\left[-\beta \cdot (T - T_0) \right]$$

$$= \mu_0 \cdot \exp\left\{ -\beta \cdot \left[\frac{1}{\beta} \cdot \ln \left\{ e^{\beta(T_u - T_0)} + \frac{2\mu_0 \cdot \beta}{\rho \cdot c_p \cdot (z^2 - z \cdot H) \cdot C} \cdot \left(\frac{u^2}{H^2} + \frac{C^2}{4} \cdot (2 \cdot z - H)^2 \right) \cdot y \right\} \right] \right\}$$

$$\Downarrow$$

$$\mu = \mu_0 \cdot \left\{ e^{\beta(T_u - T_0)} + \frac{2\mu_0 \cdot \beta}{\rho \cdot c_p \cdot (z^2 - z \cdot H) \cdot C} \cdot \left(\frac{u^2}{H^2} + \frac{C^2}{4} \cdot (2 \cdot z - H)^2 \right) \cdot y \right\}^{-1} \quad (3.49)$$

After arranging Equation (3.49), the viscosity relation becomes,

$$\mu = \mu_0 \cdot \frac{g_2 \cdot C}{g_1 \cdot g_2 \cdot C + \left(g_3 \cdot C^2 + g_4\right) \cdot y}$$

$$g_1 = e^{\beta(T_u - T_0)}$$

$$g_2 = \rho \cdot c_p \cdot \left(z^2 - z \cdot H\right)$$

$$g_3 = \frac{\mu_0 \cdot \beta \cdot (2z - H)^2}{2}$$

$$g_4 = \frac{2\mu_0 \cdot \beta \cdot u^2}{H^2}$$

(3.50)

Substituting viscosity in Equation (3.50) into the Equation (3.44) yields,

$$\frac{\partial P}{\partial y} = \mu_0 \cdot \frac{g_2 \cdot C^2}{g_1 \cdot g_2 \cdot C + \left(g_3 \cdot C^2 + g_4\right) \cdot y}$$

B.C's:

$$y = 0, P = P_u$$

$$y = w, P = P_d$$

(3.51)

Pressure distribution can be found by integrating Equation (3.51) with respect to y.

$$\int_{P_u}^{P} \partial P = \int_0^y \left(\mu_0 \cdot \frac{g_2 \cdot C^2}{g_1 \cdot g_2 \cdot C + \left(g_3 \cdot C^2 + g_4\right) \cdot y} \cdot dy \right)$$

$$\Downarrow$$

$$P(y) = \mu_0 \cdot g_2 \cdot C^2 \cdot \int_0^y \left(\frac{1}{g_1 \cdot g_2 \cdot C + \left(g_3 \cdot C^2 + g_4\right) \cdot y} \cdot dy \right) + P_u$$

$$\Downarrow$$

$$P(y) = \frac{\mu_0 \cdot g_2 \cdot C^2}{g_3 \cdot C^2 + g_4} \cdot \left\{ \ln \left[\frac{g_1 \cdot g_2 \cdot C + \left(g_3 \cdot C^2 + g_4\right) \cdot y}{g_1 \cdot g_2 \cdot C} \right] \right\} + P_u$$

(3.52)

Second boundary condition, $P = P_d$ for $y = w$, is applied to Equation (3.52) to find the value of C. Applying this boundary condition yields,

$$f(C) = \frac{\mu_0 \cdot g_2 \cdot C^2}{g_3 \cdot C^2 + g_4} \cdot \ln \left[\frac{g_1 \cdot g_2 \cdot C + \left(g_3 \cdot C^2 + g_4\right) \cdot w}{g_1 \cdot g_2 \cdot C} \right] + \Delta P = 0$$

(3.53)

Temperature distribution for nonlinear pressure distribution can be obtained after finding C by solving Equation (3.53). However, it is too difficult to solve the Equation

(3.53) with respect to C. Therefore, iterative methods are used to find the value of C. Newton-Raphson method is used as an iteration method. For the given values of u and ΔP, C can be found. For the sake of simplicity, value of C is evaluated for $z = H/2$. Details for the application of Newton-Raphson method is given below.

$$f(C) = \frac{\mu_0 \cdot h_2 \cdot C^2}{h_3 \cdot C^2 + h_4} \cdot \left\{ \ln\left[\frac{h_1 \cdot h_2 \cdot C + \left(h_3 \cdot C^2 + h_4\right) \cdot w}{h_1 \cdot h_2 \cdot C} \right] \right\} + \Delta P$$

$$
\begin{aligned}
h_1 &= g_1 \\
h_2 &= g_2(z = H/2) \\
h_3 &= g_3(z = H/2) \\
h_4 &= g_4
\end{aligned}
$$

(3.54)

$$f'(C) = h_5 \cdot h_6 + h_7 \cdot \frac{h_8}{h_9}$$

$$h_5 = \frac{2\mu_0 h_2 C\left(h_3 C^2 + h_4\right) - 2\mu_0 h_2 h_3 C^3}{\left(h_3 C^2 + h_4\right)^2}$$

$$h_6 = \ln\left[\frac{h_1 \cdot h_2 \cdot C + \left(h_3 \cdot C^2 + h_4\right) \cdot w}{h_1 \cdot h_2 \cdot C} \right]$$

(3.55)

$$h_7 = \frac{\mu_0 \cdot h_2 \cdot C^2}{h_3 \cdot C^2 + h_4}$$

$$h_8 = \left(h_1 \cdot h_2 + 2h_3 \cdot C \cdot w\right) \cdot h_1 \cdot h_2 \cdot C - \left[h_1 \cdot h_2 \cdot C + \left(h_3 \cdot C^2 + h_4\right) \cdot w\right] \cdot h_1 \cdot h_2$$

$$h_9 = \left[h_1 \cdot h_2 \cdot C + \left(h_3 \cdot C^2 + h_4\right) \cdot w\right] \cdot h_1 \cdot h_2 \cdot C$$

$$C_{i+1} = C_i - \frac{f(C_i)}{f'(C_i)}$$

(3.56)

To start the iterations a C value is assumed, and iterations are carried on per Equation (3.56) until $f(C_k)=0$ is reached. Experimental leakage data given in Table 2.2 are used for the values of u, ΔP and H. Iteration steps and values for C and $f(y)$ for each step are given below. A MATLAB code is written in order to evaluate the iteration.

	ΔP = 48.3 kPa, u = 6.2 m/s	
i	**C**	**f(C)**
1	$-1.467190032478470 \times 10^{17}$	$-7.170613863850467 \times 10^{12}$
2	$-1.622604627200000 \times 10^{10}$	$-7.431177179456878 \times 10^{5}$
3	$-1.020919675799299 \times 10^{9}$	-57.24674198166031
4	$-1.019746870394267 \times 10^{9}$	$-7.891775021562353 \times 10^{-5}$
5	$-1.019746868777486 \times 10^{9}$	$7.275957614183426 \times 10^{-11}$

	ΔP = 48.3 kPa, u = 12.3 m/s	
i	**C**	**f(C)**
1	$-2.958904348221451 \times 10^{17}$	$-1.446107662728780 \times 10^{13}$
2	$4.346580761600000 \times 10^{10}$	$2.175957942153573 \times 10^{6}$
3	$-1.056944999159943 \times 10^{9}$	$-2.771599680559739 \times 10^{2}$
4	$-1.051247524913726 \times 10^{9}$	-0.00639666891948
5	$-1.051247393413701 \times 10^{9}$	$-7.275957614183426 \times 10^{-12}$

	ΔP = 48.3 kPa, u = 20.5 m/s	
i	**C**	**f(C)**
1	$-1.071895903042292 \times 10^{18}$	$-5.238688195543623 \times 10^{13}$
2	$-2.762253053440000 \times 10^{11}$	$-1.343888531736573 \times 10^{7}$
3	$-1.249907927827210 \times 10^{9}$	$-2.706902437069635 \times 10^{3}$
4	$-1.192548816797807 \times 10^{9}$	-3.53490875660646
5	$-1.192473712509011 \times 10^{9}$	$-6.515794666483998 \times 10^{-6}$
6	$-1.192473712370573 \times 10^{9}$	0

Table 3.2 Iteration steps for ΔP = 48.3 kPa, for different rotor speeds

ΔP = 89.6 kPa, u = 6.2 m/s		
i	C	f(C)
1	$-4.765982124671900 \times 10^{17}$	$-2.329282787733927 \times 10^{13}$
2	$2.689013201280000 \times 10^{11}$	$1.323452623375372 \times 10^{7}$
3	$-1.892342866748383 \times 10^{9}$	$-1.161821916631016 \times 10^{2}$
4	$-1.889962829877517 \times 10^{9}$	$-1.655978412600234 \times 10^{-4}$
5	$-1.889962826485172 \times 10^{9}$	$1.891748979687691 \times 10^{-10}$

ΔP = 89.6 kPa, u = 12.3 m/s		
i	C	f(C)
1	$-1.040328040209791 \times 10^{18}$	$-5.084405550921667 \times 10^{13}$
2	$3.558414656000000 \times 10^{10}$	$1.835259805359471 \times 10^{6}$
3	$-1.968093846392174 \times 10^{9}$	$-6.026381985460321 \times 10^{2}$
4	$-1.955700519338615 \times 10^{9}$	-0.01763559535902
5	$-1.955700156639186 \times 10^{9}$	$-2.910383045673370 \times 10^{-11}$

ΔP = 89.6 kPa, u = 20.5 m/s		
i	C	f(C)
1	$-2.560836574902911 \times 10^{18}$	$-1.251560122492059 \times 10^{14}$
2	$4.396122685440000 \times 10^{11}$	$2.159152323314469 \times 10^{7}$
3	$-2.175514578239014 \times 10^{9}$	$-2.869161751936306 \times 10^{3}$
4	$-2.115506616109094 \times 10^{9}$	-1.46474330038473
5	$-2.115475949613914 \times 10^{9}$	$-4.004687070846558 \times 10^{-7}$
6	$-2.115475949605530 \times 10^{9}$	0

Table 3.3 Iteration steps for ΔP = 89.6 kPa, for different rotor speeds

After finding values of *C* for different pressure gradients and rotor surface speeds, temperature distribution of the oil along *y*-axis can be found by using Equation (3.48). Temperature distributions along *y*-axis at *z = H/2* are compared for both linear and nonlinear pressure distributions in Figures 3.4a through 3.4f.
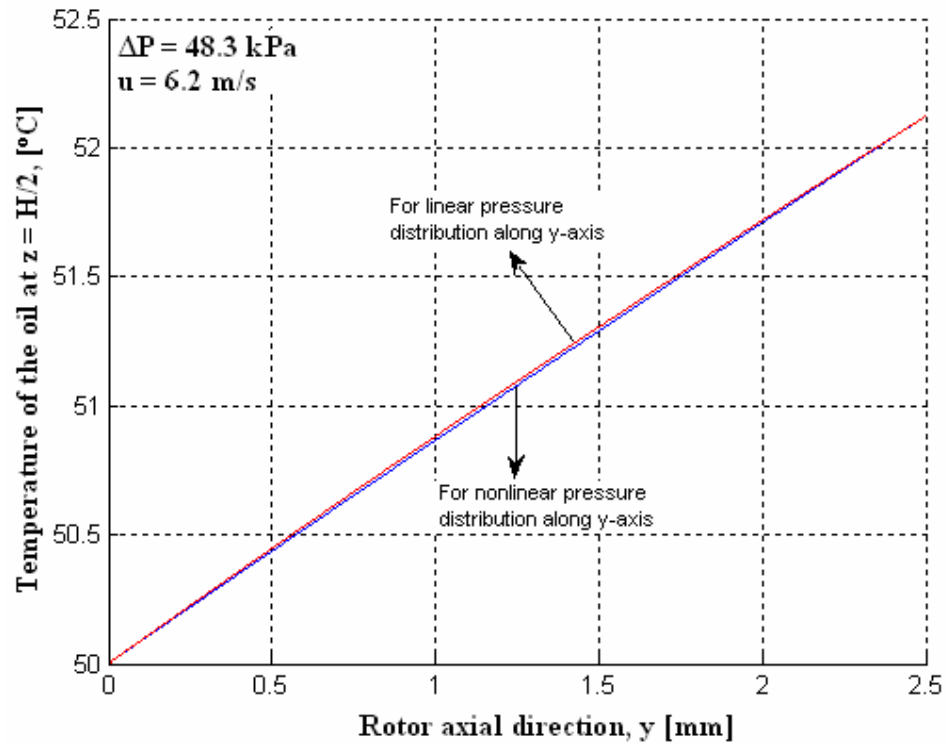
a)
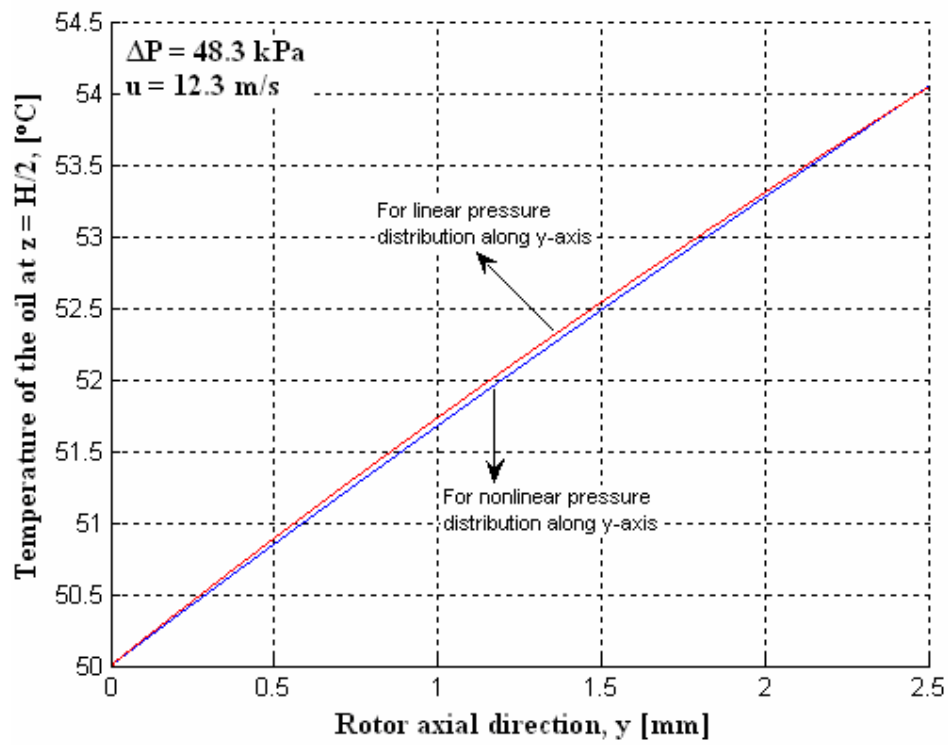
b)
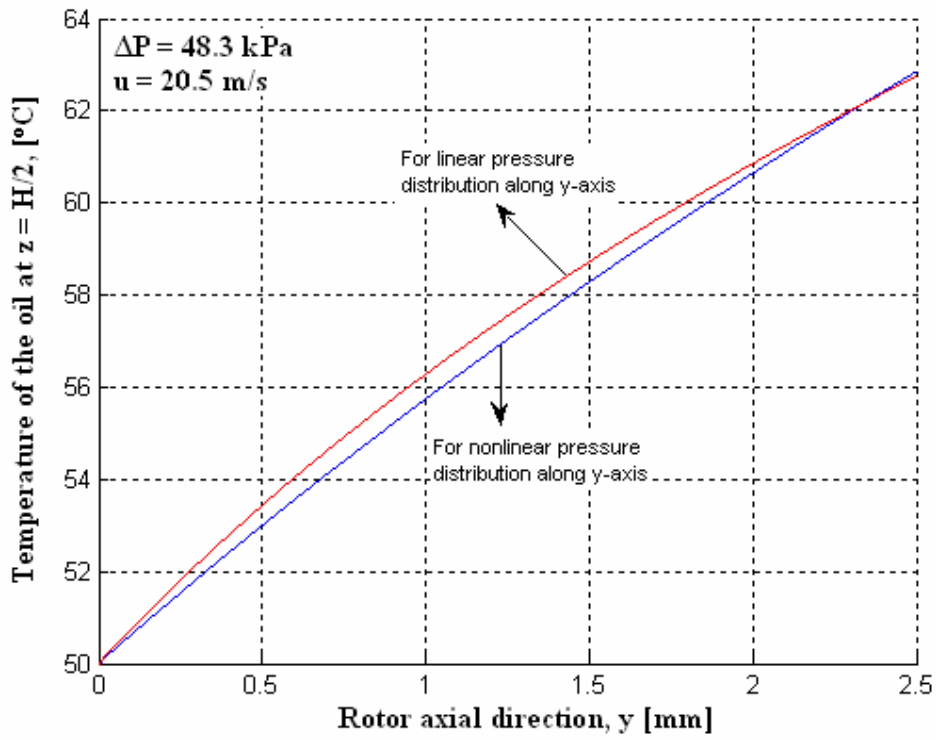
c)
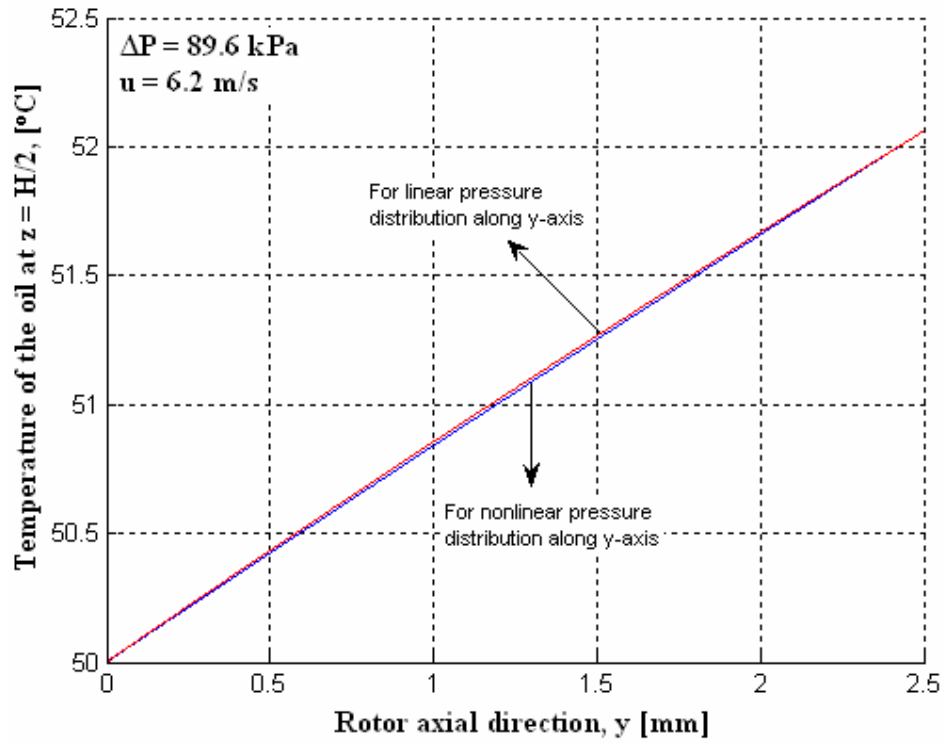
d)
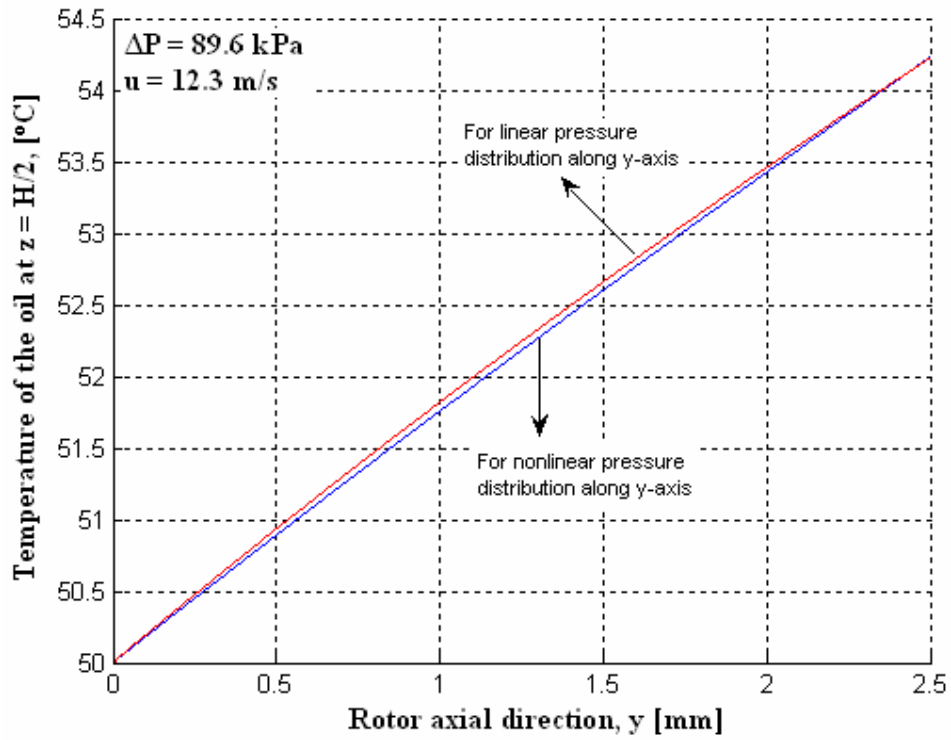
e)
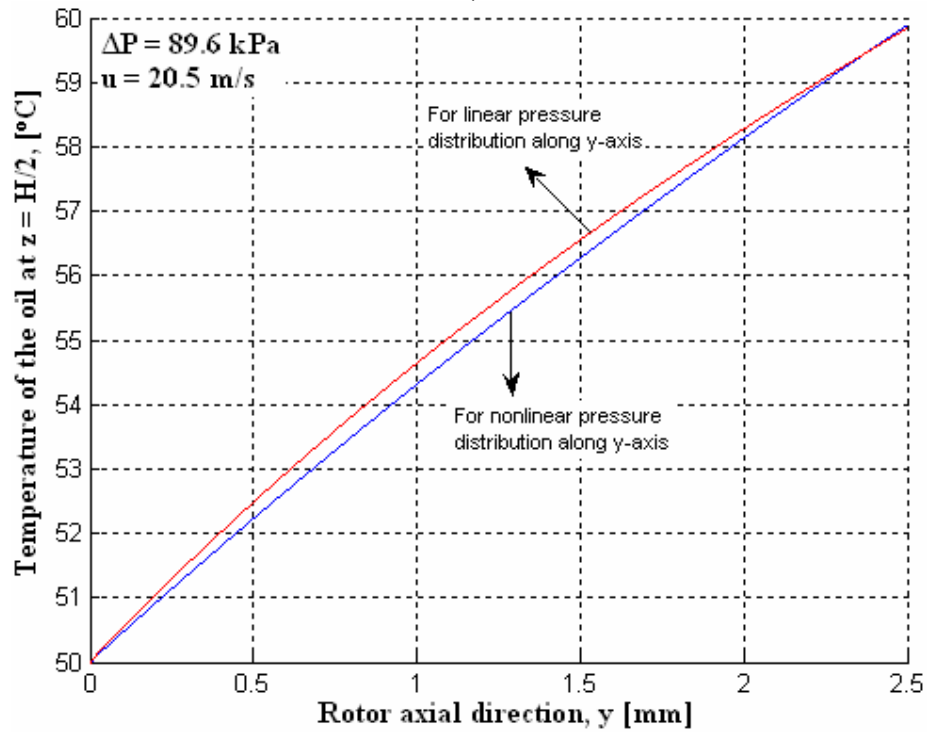
f)

Figure 3.4 Comparison of the temperature distribution of the oil along y-axis with linear

pressure distribution assumption and for nonlinear pressure distribution,

a) ΔP=48.3kPa, u=6.2m/s, b) ΔP=48.3kPa, u=12.3m/s, c) ΔP=48.3kPa, u=20.5m/s,

d) ΔP=89.6kPa, u=6.2m/s, e) ΔP=89.6kPa, u=12.3m/s, f) ΔP=89.6kPa, u=20.5m/s.

As it can be seen from Figure 3.4, for low rotor surface speeds oil temperature distribution is almost the same for both linear and nonlinear pressure cases, and they slightly differ from each other for moderate rotor surface speeds. When the effective temperature is considered, the slight difference between the linear and nonlinear pressure cases becomes much smaller. As a result, it can be concluded that linear pressure distribution assumption provides a good approximation, and closed form oil temperature solution given in Equation (3.38) is sufficiently accurate for seal analysis and design.

Linear pressure distribution gives pressure as a function of rotor axial direction, y, bristle pack width, w, and pressure load, ΔP. On the other hand, nonlinear pressure distribution, which is given in Equation (3.52), is also function of hydrodynamic lift clearance, H, and rotor surface speed, u. As illustrated in Figure 3.5, nonlinear pressure distribution shows a little change with rotor surface speed. Nonlinear pressure is calculated by substituting C values found by iteration and given in Tables 3.2 and 3.3 and the available data of experimental leakage data given in Table 2.2.
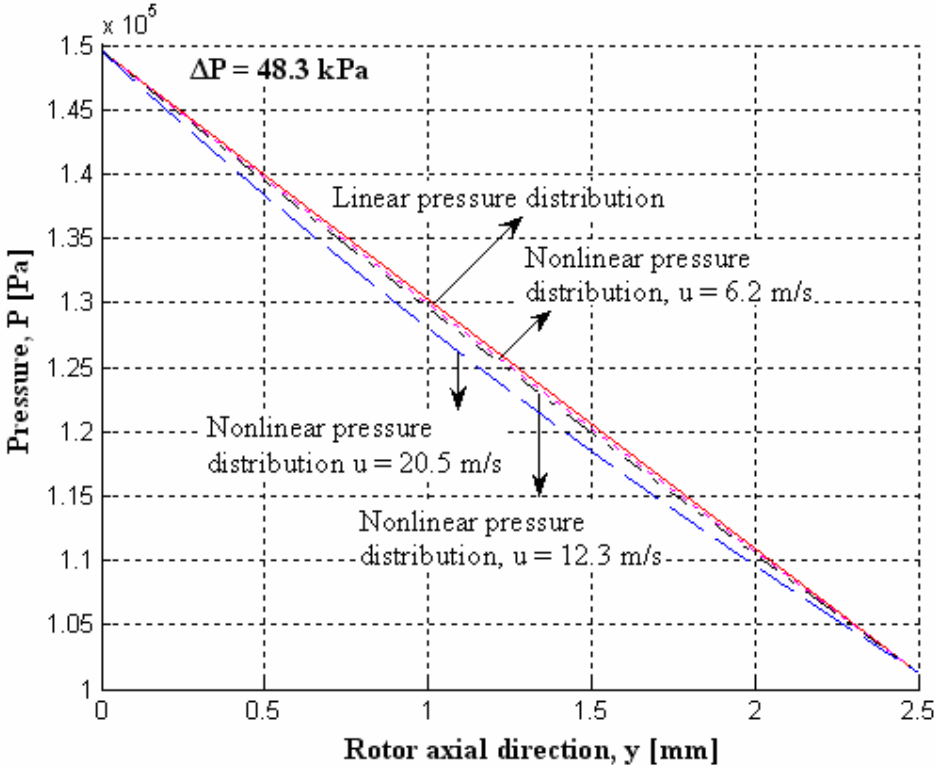
a)
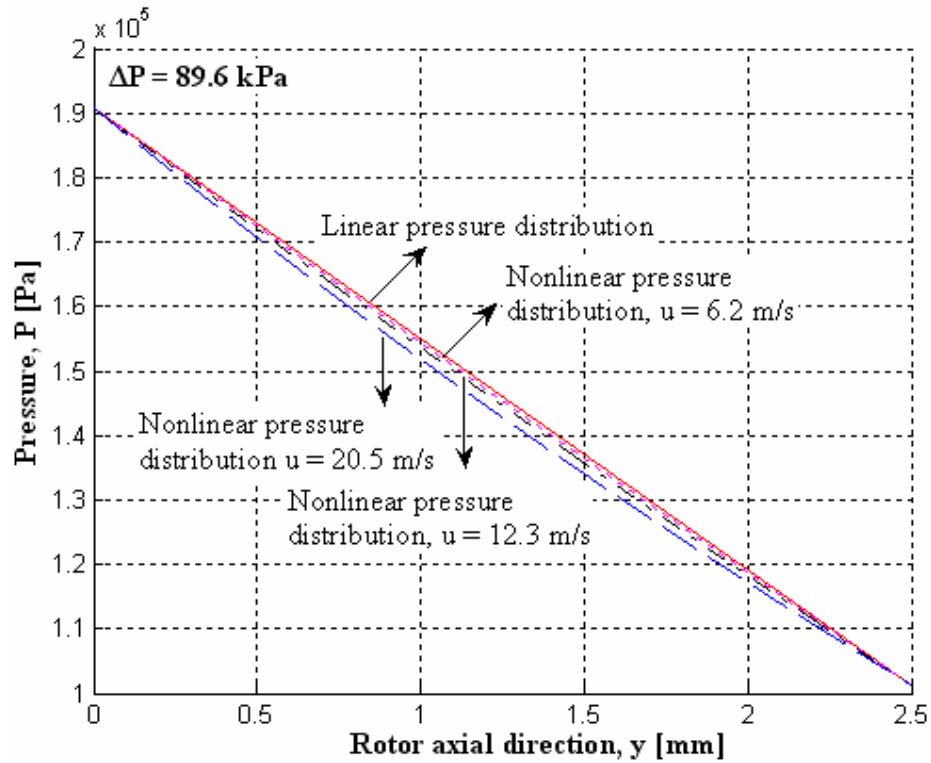
b)

Figure 3.5 Comparison of linear pressure distribution and nonlinear pressure
distribution for different cases, a) ΔP = 48.3 kPa, b) ΔP = 89.6 kPa

Pressure distributions for linear and nonlinear cases show similar characteristic
with temperature distributions. Nonlinear pressure distribution is almost linear for low
rotor surface speeds, and slightly differs from linear pressure for larger rotor surface
speeds.

4 INCLUDING SHEAR HEATING EFFECT INTO LIFT FORCE THEORIES AND VALIDATION WITH OTHER WORKS IN LITERATURE

Shear heat dissipation is an important phenomenon in brush seals since it directly affects the hydrodynamic lift clearance, which determines leakage performance of the seal. Aksit et al. [16] investigate lifting force in two different ways: Simple beam theory and bearing theory. Their studies about simple beam theory underestimates the lifting force since it does not include blow down and friction forces. The force estimated by bearing theory balances all of the reaction force contributions. However, it increases continuously with rotor surface speed since it does not include the shear heating effect. Effect of shear heat dissipation can be included into the bearing theory by means of effective viscosity, which can be evaluated by using the results of thermal analysis given in Chapter 2.

In this chapter, simple beam theory and bearing theory of Aksit et al. [16] are shortly reviewed. Lifting force is evaluated by using shear heat effect included bearing theory, and results are compared with previous studies in the literature.

4.1 Hydrodynamic Lifting Force in Brush Seals

During operation, cant angle and deflection of the bristle together with the contribution from rotor radius are the reasons for the convergent surface formation between bristle and rotor. The fluid is pulled into this wedge by the moving rotor surface, and lifting force is generated as a result of this fluid motion. Convergent surface is called wedge, and the pull of the fluid into this wedge by the rotor generates the wedge action.

When air is the sealing medium, aerodynamic lifting forces, which are generated on very small bearing surface, can not overcome the blow down forces driven by radial

pressure gradients within the brush pack. The small bearing surface and the low viscosity of the air are the reasons for inadequate aerodynamic lift forces.

If the sealing medium is oil, hydrodynamic lifting force becomes dominant, and the associated clearance becomes important. Hydrodynamic lift force acts to deflect bristles off the shaft surface. This force is balanced by a reaction force due to beam/bristle deflection, frictional forces and so called "blow-down" forces occurring due to radial pressure gradient within the bristle pack. During operation, hydrodynamic lift clearance, which is the most important parameter for leakage performance of an oil brush seal, is determined when the lift force becomes equal to the reaction forces.

4.2 Simple Beam Theory

In their study, Aksit et al. [16] calculate lifting force by using simple beam theory. In simple beam theory, lift force is estimated with beam bristle/beam deflection forces.
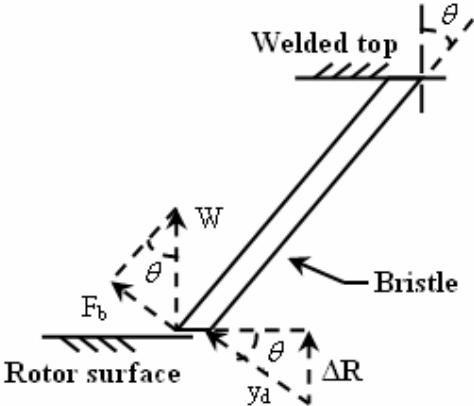
Figure 4.1 Geometric relations for a bristle at an angle, Aksit et al. [16]

F_b is the component of the lifting force normal to the bristle section. Deflection of the beam, y_d, is calculated using the relation,

$$y_d = \frac{\Delta R}{\sin \theta} \tag{4.1}$$

where θ is the cant angle of the brush seal, and ΔR equals to hydrodynamic lift clearance, H. Normal component of the lifting force can be easily obtained by applying beam bending theory.

$$y_d = \frac{F_b L_b^3}{3EI} = \frac{H}{\sin\theta} \Rightarrow F_b = \frac{3EIH}{L_b^3 \sin\theta} \tag{4.2}$$

where E is the modulus of elasticity, I is the second moment of inertia, and L_b is the beam length. Bristles are clamped at the outer end of the free bristle height, and they are supported at this point. Therefore, L_b can be calculated simply by dividing the free bristle height by sine of cant angle.

$$L_b = \frac{BH}{\sin\theta} \tag{4.3}$$

$$I = \frac{\pi(2R_b)^4}{64} \tag{4.4}$$

After substituting second moment of inertia and bristle length into the F_b, lifting force can be evaluated as,

$$W = \frac{F_b}{\sin\theta} = \frac{3\pi}{64} \frac{E(2R_b)^4 H}{L_b^3 \sin^2\theta} \tag{4.5}$$

Values of modulus of elasticity and bristle radius are given in the previous sections. H, hydrodynamic lift clearance values are taken from experimental leakage data given in Table 2.2. For the brush seal of interest, free bristle height, BH, is 16mm and cant angle is 45°.

Due to radial pressure gradients, there is an additional fluid force on bristles which pushes them radially inward. When the inter bristle interlocking and frictional effects are also considered, beam theory always under estimates the actual bristle tip force that will balance the hydrodynamic lift. However, beam theory results are useful to serve as a lower limit or bench mark for the lift force estimates.

4.3 Bearing Theory

Taking advantage of the wedge action, Aksit et al. [16] apply well known Reynolds lubrication theory for bearing surfaces of the brush seals. They apply short bearing theory to a single bristle for hydrodynamic lifting force calculation. In Figure 4.2, simplified bristle geometry is given.
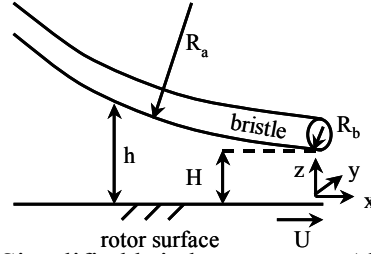
Figure 4.2 Simplified bristle geometry, Aksit et al. [16]

As it can be seen from the figure above, the origin is taken at the projection of the midpoint of the bristle tip on the rotor surface. The distance between the rotor surface and bristle surface is defined by Hertzian contact formulation for two cylinders with inclined axes.

$$h = H + \frac{x^2}{2R_a} + \frac{y^2}{2R_b} \tag{4.6}$$

where H is the hydrodynamic lift clearance, R_a is the equivalent bristle bending curvature for infinite boundary, and R_b is the bristle radius. Equivalent bristle bending curvature is defined as,

$$\frac{1}{R_a} = \frac{1}{R_A} + \frac{1}{R_{rotor}} \tag{4.7}$$

where R_{rotor} stands for rotor radius. Typical Reynolds equation for hydrodynamic bearing is,

$$\frac{\partial}{\partial x}\left[h^3 \frac{\partial P}{\partial x}\right] + \frac{\partial}{\partial y}\left[h^3 \frac{\partial P}{\partial y}\right] = 6\mu u \frac{dh}{dx}, \quad -\infty < x \leq 0 \text{ and } 0 \leq y < \infty \tag{4.8}$$

In their study, Aksit et al. take boundaries as infinity for the sake of simplicity, and with the idea of small contribution of the pressure to lifting force at the outer region of the bristle. As boundary conditions, they take ambient pressure as y goes to infinity, and they assume the derivative of the pressure with respect y as zero due to symmetry. After order of magnitude test, they neglect $\partial/\partial x$ related terms in Equation (4.8), which yields to the reduced differential equation,

$$\frac{\partial}{\partial y}\left[h^3 \frac{\partial P}{\partial y}\right] = 6\mu u \frac{x}{R_a},$$

B.C's:

$$P(y \to \infty) = P_a \text{ and } \left.\frac{\partial P}{\partial y}\right|_{y=0} = 0$$

(4.9)

Equation (4.9) implies the short bearing theory. Integrating once leads to,

$$\int \partial \left[h^3 \frac{\partial P}{\partial y}\right] = \int 6\mu u \frac{x}{R_a} \partial y$$

$$\Downarrow$$

$$h^3 \frac{\partial P}{\partial y} = 6\mu u \frac{x}{R_a} y + C_1$$

(4.10)

where C_1 is an integration constant, which is found as zero upon application the boundary condition $\left.\frac{\partial P}{\partial y}\right|_{y=0} = 0$. Substituting h function defined in Equation (4.6) yields,

$$\frac{\partial P}{\partial y} = \frac{6\mu u}{R_a} \frac{xy}{h^3} = \frac{6\mu u}{R_a} \frac{xy}{\left(H + \frac{x^2}{2R_a} + \frac{y^2}{2R_b}\right)^3}$$

(4.11)

Hydrodynamic fluid pressure can be obtained by integrating again with respect to y.

$$P = \int \frac{\partial P}{\partial y} dy + c_2(x) = \frac{6\mu u x}{R_a}\left[-\frac{R_b}{2}\frac{1}{\left(H + \frac{x^2}{2R_a} + \frac{y^2}{2R_b}\right)^2}\right] + C_2(x)$$

(4.12)

C_2 is the integration constant. Applying second boundary condition, $P(y \to \infty) = P_a$, gives C_2 as ambient pressure, P_a. Substituting this value of integration constant into the Equation (4.12) and rearranging gives hydrodynamic fluid pressure as,

$$P - P_a = -\frac{3\mu u x R_b}{R_a}\frac{1}{h^2} = -3\mu\frac{u}{h}\frac{R_b}{h}\frac{x}{R_a} \tag{4.13}$$

Hydrodynamic lift force is calculated by integrating hydrodynamic fluid pressure over the bristle lift surface.

$$W = 2\int_{-\infty}^{0}\int_{0}^{\infty}(P - P_a)\,dx\,dy$$

$$\Downarrow$$

$$W = \frac{6\mu u R_b}{R_a}\int_{0}^{\infty}\int_{0}^{\infty}\frac{x\,dx\,dy}{\left(H + \dfrac{x^2}{2R_a} + \dfrac{y^2}{2R_b}\right)^2} = \frac{6\mu u R_b}{R_a}\pi R_a\sqrt{\frac{R_b}{2H}} \tag{4.14}$$

$$\Downarrow$$

$$W = \frac{6\pi}{\sqrt{2}}\mu u R_b\sqrt{\frac{R_b}{H}}$$

This lift force is a function of dynamic viscosity, bristle radius rotor surface speed and hydrodynamic lift clearance. Hydrodynamic lift clearance for different rotor surface speeds can be verified from the experimental leakage data given in Table 2.2.

For steady state operation, lift force given by Equation (4.14) is balanced by bristle reaction forces which will include beam deflection as well as the effects of blow-down and frictional forces. However, as the rotor surface speed increases, estimated lift force, which is calculated using bearing theory with constant viscosity, increases continuously. This continuous increase is due to the fact that this formulation does not include oil thinning effect arising from shear heat dissipation. In engine applications, as the test data illustrate in Figure 2.22, increase in rotor speed cause temperature to rise, which results in decrease of dynamic viscosity. This decrease in viscosity is the reason for high speed lift force stabilization.

4.4 Shear Heating Effect Included Bearing Theory

To include the effect of shear heating into the bearing theory, effective temperature is calculated by using temperature distribution given by Equation (3.38). Effective temperature is calculated by using the mean values of the temperature distribution along y and z-axes.

$$T_{mean-z}(y) = \frac{1}{H}\int_0^H T(y,z)\cdot dz$$

$$\Downarrow \qquad\qquad (4.15)$$

$$T_{eff} = \frac{1}{w}\int_0^w T_{mean-z}(y)\cdot dy$$

Numerical integration methods are used again in order to calculate effective temperature. Trapezoidal rule is preferred as the numerical integration method.

$$T_{mean-z}(y) = \frac{1}{H}\int_0^H T(y,z)\cdot dz = \frac{1}{H}\left\{\frac{l}{2}\cdot\left[T(y,z_1)+2T(y,z_1+l)+...+T(y,z_2)\right]\right\}$$

$$\Downarrow$$

$$T_{eff} = \frac{1}{w}\int_0^w T_{mean-z}(y)\cdot dy \qquad\qquad (4.16)$$

$$= \frac{1}{w}\left\{\frac{l_2}{2}\cdot\left[T_{mean-z}(y_1)+2T_{mean-z}(y_1+l_2)+...+T_{mean-z}(y_2)\right]\right\}$$

Parameters l and l_2 are the rise for each step of numeric integration for z and y respectively. l is taken as one eightieth of the hydrodynamic lifting clearance, $H/80$, and l_2 is taken as $w/2500$. Integration steps are taken as small as possible in order to minimize the numerical integration errors. Effective temperature is calculated for the hydrodynamic lift clearance, which is obtained from experimental leakage data for different rotor speeds under various pressure loads. Evaluations of numeric integrals are performed by a code written in MATLAB.

Effect of shear heat dissipation is included into the bearing theory by means of the effective viscosity. Effective viscosity is obtained from the effective temperature as,

$$\mu_{eff} = \mu_0 \cdot e^{-\beta(T_{eff} - T_o)} \tag{4.17}$$

Values of μ_o, T_o and β are provided in the previous sections. Substituting this effective viscosity into the lift force previously derived with constant viscosity yields a lift force formulation that includes the shear heating effect as,

$$W = \frac{6\pi}{\sqrt{2}} \mu_{eff} u R_b \sqrt{\frac{R_b}{H}} \tag{4.18}$$
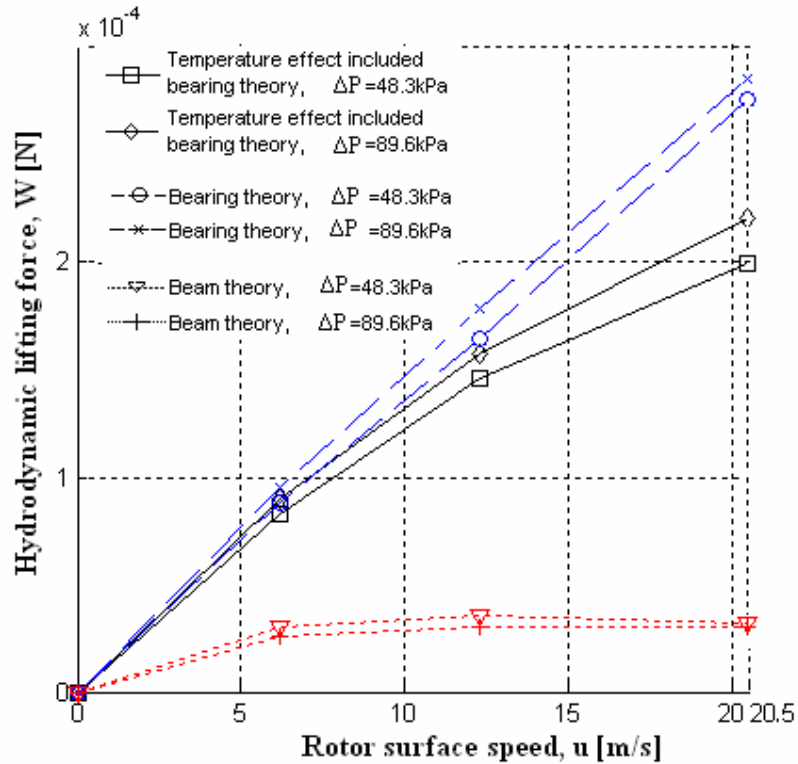
Figure 4.3 Comparison of hydrodynamic lifting force using three different methods

As expected, results in Figure 4.3 illustrates that beam theory underestimates the bristle tip force since it does not include friction, interlocking and blow down forces. Bearing theory works well at low rotor surface speeds, where the temperature rise in the oil is small. As rotor surface speed increases, lifting force of estimated by Aksit et al.

[????]'s constant viscosity formulation increases continuously, and overestimates the lift force. This is somewhat expected. As their analysis does not include temperature effects, lift force does not stabilize. On the other hand, the present formulation including temperature-viscosity effect gives more consistent results with the stabilized lift force trend observed in high speed leakage tests. At low rotor speeds, where the temperature rise is small, both analyses predict similar lift force magnitudes. As rotor speed increases, shear heating becomes dominant, and stabilization of the lift force becomes evident. The effect of shear heating appears in the lift force through effective viscosity. Dynamic viscosity change with rotor speed is given in Figure 4.4.
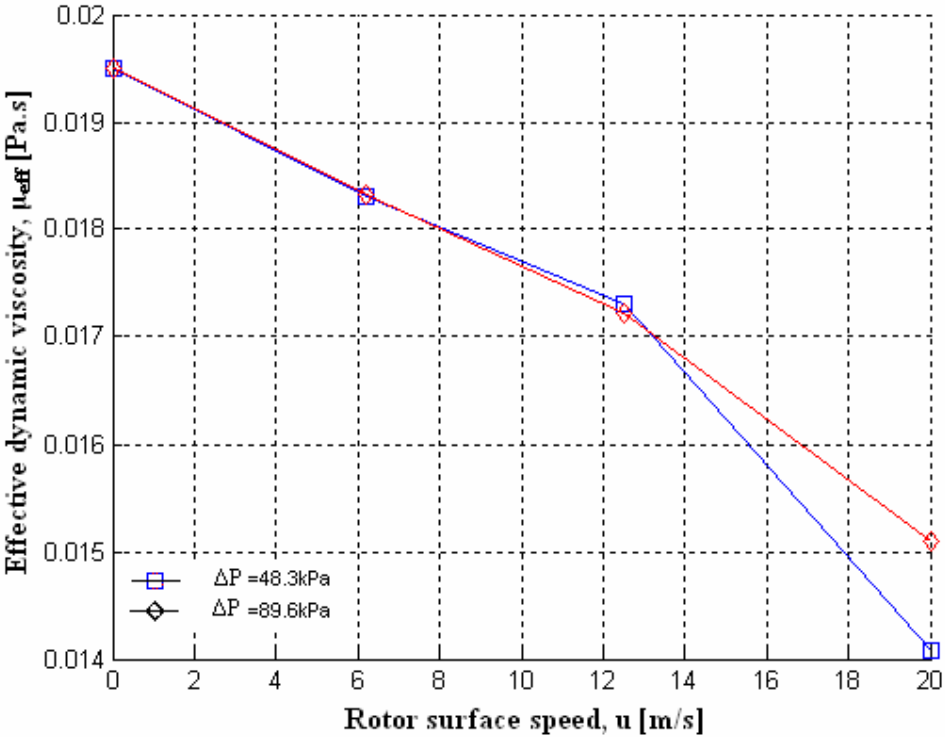
Figure 4.4 Change in effective viscosity with rotor surface speed for different pressure loads

5 DERIVATION OF OIL PRESSURE FOR EACH BRISTLE

In the previous sections, control volume was selected as the oil between the rotor surface and the bristle pack. Pressure distribution was firstly assumed to change linear in the rotor axial direction, and thermal analysis was done with this pressure distribution. Keeping on analysis with the same control volume without constant pressure gradient assumption gave pressure and temperature distribution close to the results of analysis of linear pressure. In the literature, experimental studies suggest almost constant pressure gradient in the rotor axial direction, which is consistent with the results of previous boundary layer analysis of this study.

In this chapter, pressure distribution is found for the control volume which is selected as the oil under each bristle by applying Reynolds bearing theory. Pressure distribution for each bristle of one row in the rotor axial direction is evaluated. Cyclic pressure distribution is assumed for the bristles in the rotor tangential direction (x-direction in Figure 3.2). Later, pressure profiles under each bristle are combined to yield the pressure profile under the brush pack as illustrated in Figure 5.1.

5.1 Selection of Control Volume

Selection of control volume is important since it defines the valid region for the derived pressure distribution. For hydrodynamic bearing theory, control volume for each bristle is selected as given in Figure 5.1. As it can be seen from the same figure, local coordinate system is defined for each control volume of interest. The subscript in the coordinate system stands for the bristle number. First bristle is at the upstream side, and the last bristle is at the downstream side. Number of bristles in one row of the bristle pack is defined by n_r, which generally changes between ten and sixteen. For the brush seal of interest, n_r is 16.
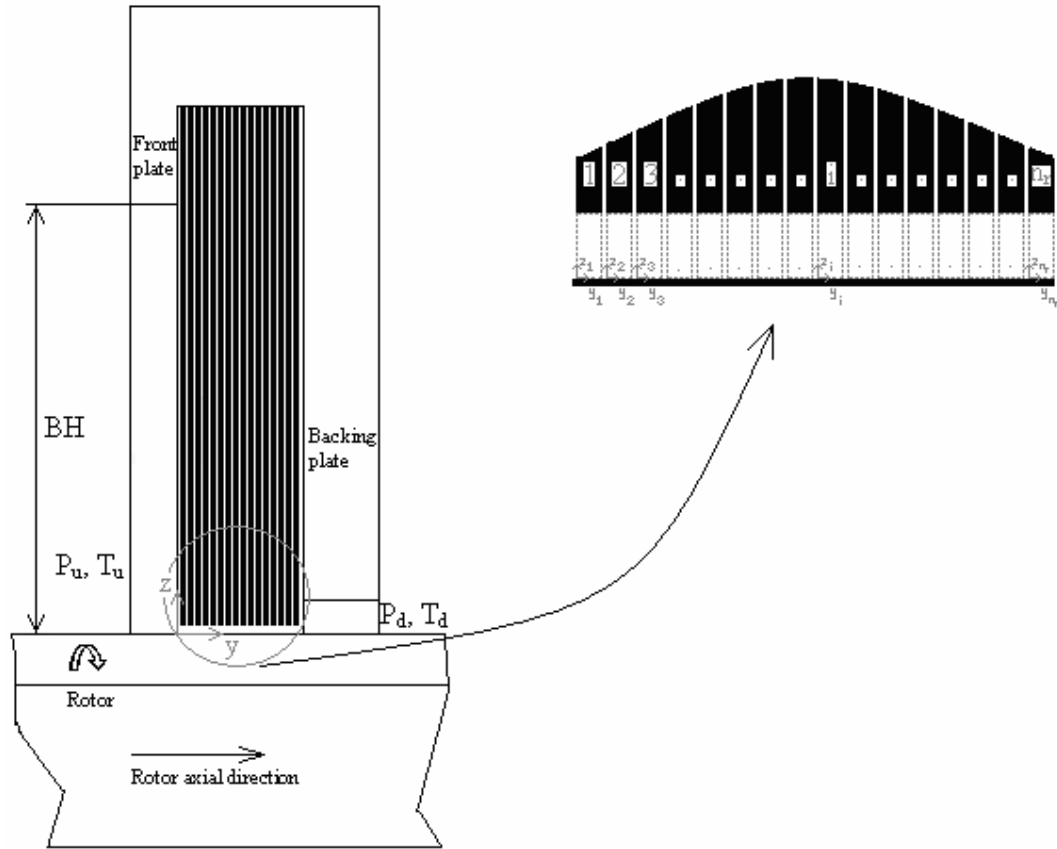
Figure 5.1 Selection of control volume for each bristle

In order to find the pressure distribution, Reynolds bearing theory is applied with the assumptions given below.

1. Steady state
2. Incompressible flow
3. Radial flows are neglected due to the fact that the axial flow is dominant.

Similar to boundary layer analysis in Chapter 3, rotor and bristle surfaces are taken as unwrapped flat surfaces. As given in Figure 5.2, h_i is the distance between the rotor and i^{th} bristle surfaces, and defined by Hertizian contact of two cylinders with inclined axis, as in Equation 4.6. H is the hydrodynamic lift clearance and it is same for every bristle. R_{eq} is the equivalent bristle bending curvature, and R_b is the bristle radius. Hydrodynamic lift clearance and equivalent bristle bending curvature are assumed to be the same for each bristle. Value of bristle radius for the brush seal of interest is 0.051 mm, as defined in the previous sections.

$$h_i = H + \frac{x_i^2}{2R_{eq}} + \frac{y_i^2}{2R_b} \qquad (5.1)$$
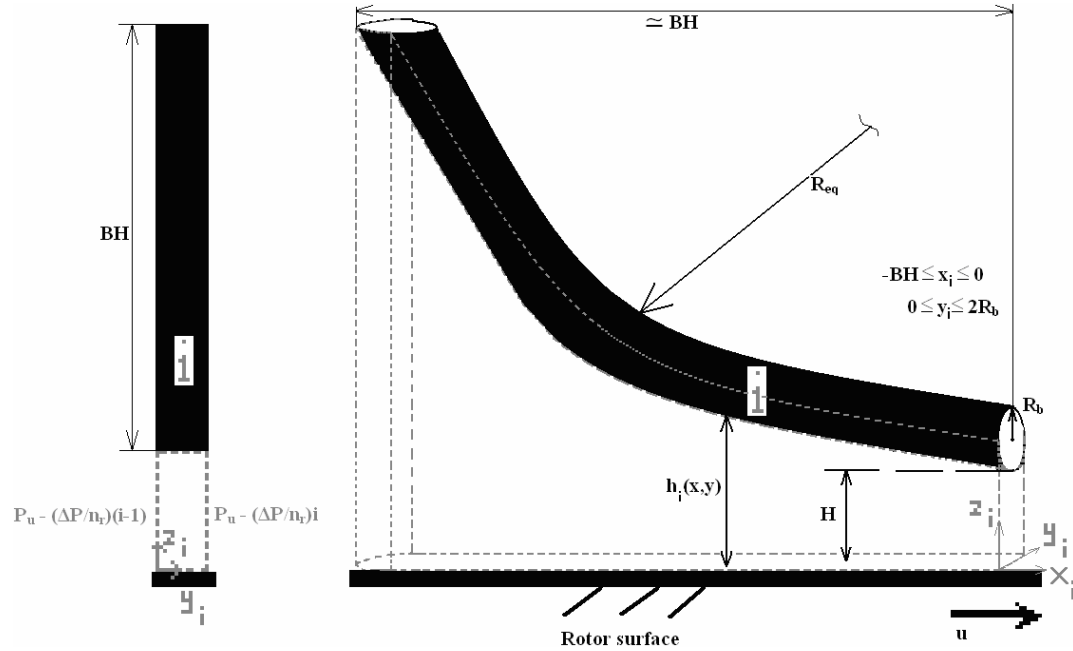
Figure 5.2 Geometry, local coordinate selection and boundaries for ith bristle

Selection of the local coordinates for the ith bristle is illustrated in Figure 5.2. As mentioned before, front plate tightly clamps the bristle. Therefore, bristles are assumed to be supported from the free bristle height, *BH,* and they bend under the effect of hydrodynamic lifting force generated by wedge action. Free bristle height for the bristle is 16mm. Selection of control volume for a bristle can be observed more detailed in Figure 5.2. Boundaries for *y*-coordinate are *0* and *2R_b*. The length of the bristle projection can be taken as *BH* since the cant angle, *Θ*, is 45º. Boundaries for *x*-coordinate are *–BH* and *0.*

The equivalent bristle bending curvature is the radius of bristle where the radii of unwrapped rotor and bent bristle are combined. It can be calculated by using the formula,

$$\frac{1}{R_{eq}} = \frac{1}{R_{bend}} + \frac{1}{R_{rotor}} \qquad (5.2)$$

R_{bend} is the bent bristle radius, and simply taken as equal to free bristle height. Taking this value for R_{bend} brings an acceptable error as it assumes a little larger bristle curvature than the real case. R_{rotor} is the radius of rotor with the same value given in the previous chapters.

5.2   Reynolds Bearing Theory for Each Bristle

As mentioned before, temperature has a great influence on high speed lift clearance stabilization, and the effect of shear heating has to be included into the analysis of brush seals. Effective viscosity derived in Equation (4.17) by using the effective temperature, which is calculated using the temperature function (3.38) *(closed-form solution to temperature with linear pressure distribution under the brush pack)*, gives consistent results with real-life high speed lift-stabilization. Therefore, there is no need to solve thermal energy equation for each bristle. In bearing theory application for each bristle, effective viscosity of Equation (4.17) will be used.

It is known from the previous sections that Re_{H-u} is much smaller than unity so that inertia terms can be neglected. Reynolds bearing theory can be applied to each bristle with the assumptions given before. Typical Reynolds equation for hydrodynamic bearing for the ith bristle is,

$$\frac{\partial}{\partial x_i}\left[h_i^3\frac{\partial P_i}{\partial x_i}\right]+\frac{\partial}{\partial y_i}\left[h_i^3\frac{\partial P_i}{\partial y_i}\right]=6\mu_{eff}u\frac{dh_i}{dx_i}, \quad -BH\le x_i\le 0 \text{ and } 0\le y_i\le 2R_b \tag{5.3}$$

In the equation above, x_i terms can be related with $BH=16\ mm$, and y_i terms can be related with $2R_b=0.102mm$. Since $BH>>2R_b$, $\partial/\partial x_i<<\partial/\partial y_i$, and $\partial/\partial x_i$ terms in above equation can be neglected when compared with $\partial/\partial y_i$ terms. This simplification yields to the differential equation given below.

$$\frac{\partial}{\partial y_i}\left[h_i^3\frac{\partial P_i}{\partial y_i}\right]=6\mu_{eff}u\frac{x_i}{R_{eq}} \tag{5.4}$$

Note that differential equations (5.3) and (5.4) are the Reynolds bearing equations, which are similar to Equations (4.8) and (4.9). However, Aksit et al. [16] take the

boundaries as $-\infty$ to 0 for x, and 0 to ∞ for y. In this study, boundaries are taken as $-BH$ to 0 for x_i, and 0 to $2R_b$ for y_i so that errors coming from infinite boundaries can be neglected. Furthermore, pressure distribution can be obtained for the each bristle in the rotor axial direction *(y-direction in Figure 3.2)*.

Another difference between two analyses is the boundary conditions. In their studies, Aksit et al. [16] assumes the symmetric boundary condition in *y*-direction which gives $\partial P / \partial y$ zero value at $y=0$. Second boundary condition in their studies is $P(y \rightarrow \infty) = P_a$. In this study, different boundary conditions are defined for each bristle in *y*-direction. Boundary conditions for each bristle in a row *(in y-direction)* can be found by using pressure load *(ΔP)* and number of bristles in a row in rotor axial direction *(n_r)*. By doing so, more realistic boundary conditions are defined and interaction between the bristles can be provided. For the first bristle, the left side *(Figure 5.1)*, which corresponds the $y_1=0$, has the pressure value of upstream pressure. The right side pressure *(y_1=2R_b)* for the oil under the first bristle can be calculated by subtracting the pressure decrease portion for a bristle from upstream pressure. Pressure decrease portion for a single bristle can simply be calculated by dividing pressure load, *ΔP*, to *n_r*. The first boundary condition for the second bristle equals to the second boundary condition for the first bristle, and this interaction continuous until the last bristle in rotor axial direction is reached. The boundary conditions for each bristle are given below.

$$i=1, \quad y_1 = 0 \Rightarrow P_1(y_1 = 0) = P_u$$

$$y_1 = 2R_b \Rightarrow P_1(y_1 = 2R_b) = P_u - \frac{\Delta P}{n_r} \tag{5.5}$$

$$i=2, \quad y_2 = 0 \Rightarrow P_2(y_2 = 0) = P_u - \frac{\Delta P}{n_r}$$

$$y_2 = 2R_b \Rightarrow P_2(y_2 = 2R_b) = P_u - \frac{\Delta P}{n_r} \cdot 2 \tag{5.6}$$

$$\cdot$$
$$\cdot$$
$$\cdot$$

$$i, \quad y_i = 0 \Rightarrow P_i(y_i = 0) = P_u - \frac{\Delta P}{n_r} \cdot (i-1)$$

$$y_i = 2R_b \Rightarrow P_i(y_i = 2R_b) = P_u - \frac{\Delta P}{n_r} \cdot i \tag{5.7}$$

$$\cdot$$
$$\cdot$$
$$\cdot$$

$$i=n_r, \quad y_{n_r} = 0 \Rightarrow P_{n_r}(y_{n_r} = 0) = P_u - \frac{\Delta P}{n_r} \cdot (n_r - 1)$$

$$(5.8)$$

$$y_{n_r} = 2R_b \Rightarrow P_{n_r}(y_{n_r} = 2R_b) = P_u - \frac{\Delta P}{n_r} \cdot n_r = P_u - \Delta P = P_d = P_a$$

The inter bristle gap, d_{Ib}, can be defined as the gap between two adjacent bristles. The exact value for inter bristle gap is not know, but it is known that it changes between the one-twentieth and one-fortieth of the bristle diameter. Since the inter bristle gap is very small compared with bristle diameter, it is neglected in this study by implying boundary conditions given through Equations (5.5) to (5.8).

Substituting boundary condition (5.7) into the Equation (5.4) leads to,

$$\frac{\partial}{\partial y_i}\left[h_i^3 \frac{\partial P_i}{\partial y_i}\right] = 6\mu_{eff} u \frac{x_i}{R_{eq}},$$

B.C's:

$$y_i = 0 \Rightarrow P_i(y_i = 0) = P_u - \frac{\Delta P}{n_r} \cdot (i-1) \tag{5.9}$$

and

$$y_i = 2R_b \Rightarrow P_i(y_i = 2R_b) = P_u - \frac{\Delta P}{n_r} \cdot i$$

5.3   Pressure Distribution for Each Bristle

Pressure distribution for the oil under the ith bristle can now be derived by solving the differential equation (5.9) with the given boundary conditions. Integrating with respect to y_i yields,

$$\int \partial\left[h_i^3 \frac{\partial P_i}{\partial y_i}\right] = \int 6\mu_{eff} u \frac{x_i}{R_{eq}} \partial y_i$$

$$\Downarrow$$

$$\frac{\partial P_i}{\partial y_i} = 6\mu_{eff} u \frac{x_i \cdot y_i}{R_{eq}} \cdot \frac{1}{h_i^3} + C_1(x_i)\frac{1}{h_i^3} \tag{5.10}$$

$$\Downarrow$$

73

$$\frac{\partial P_i}{\partial y_i} = 6\mu_{eff} u \frac{x_i \cdot y_i}{R_{eq}} \cdot \frac{1}{\left(H + \dfrac{x_i^{2}}{2R_{eq}} + \dfrac{y_i^{2}}{2R_b}\right)^{3}} + C_1(x_i) \frac{1}{\left(H + \dfrac{x_i^{2}}{2R_{eq}} + \dfrac{y_i^{2}}{2R_b}\right)^{3}}$$

$C_1(x_i)$ is integration constant. Integrating equation above with respect to y_i yields pressure distribution as,

$$P_i = \int 6\mu_{eff} u \frac{x_i \cdot y_i}{R_{eq}} \cdot \frac{1}{\left(H + \dfrac{x_i^{2}}{2R_{eq}} + \dfrac{y_i^{2}}{2R_b}\right)^{3}} \partial y_i$$

$$+ \int C_1(x_i) \frac{1}{\left(H + \dfrac{x_i^{2}}{2R_{eq}} + \dfrac{y_i^{2}}{2R_b}\right)^{3}} \partial y_i + C_2(x_i) \tag{5.11}$$

$C_2(x_i)$ is another integration constant. Evaluation of the integral components of the Equation (5.10) is given in the following.

$$\int 6\mu_{eff} u \frac{x_i \cdot y_i}{R_{eq}} \cdot \frac{1}{\left(H + \dfrac{x_i^{2}}{2R_{eq}} + \dfrac{y_i^{2}}{2R_b}\right)^{3}} dy_i = \frac{6\mu_{eff} \cdot u \cdot x_i}{R_{eq}} \int \frac{y_i}{\left(H + \dfrac{x_i^{2}}{2R_{eq}} + \dfrac{y_i^{2}}{2R_b}\right)^{3}} dy_i$$

$\Downarrow$ Use method of substitution

$$H + \frac{x_i^{2}}{2R_{eq}} + \frac{y_i^{2}}{2R_b} = \gamma \Rightarrow y_i \cdot dy = R_b \cdot d\gamma$$

$\Downarrow$ Substitute

$$\frac{6\mu_{eff} \cdot u \cdot x_i}{R_{eq}} \int \frac{y_i}{\left(H + \dfrac{x_i^{2}}{2R_{eq}} + \dfrac{y_i^{2}}{2R_b}\right)^{3}} dy_i = \frac{6\mu_{eff} \cdot u \cdot x_i}{R_{eq}} \int \frac{R_b}{\gamma^{3}} d\gamma$$

$\Downarrow$ Integrate

$$\frac{6\mu_{eff} \cdot u \cdot x_i}{R_{eq}} \int \frac{y_i}{\left(H + \dfrac{x_i^{2}}{2R_{eq}} + \dfrac{y_i^{2}}{2R_b}\right)^{3}} dy_i = \frac{6\mu_{eff} \cdot u \cdot x_i}{R_{eq}} \cdot \frac{-R_b}{2} \cdot \frac{1}{\gamma^{2}}$$

$\Downarrow$ Substitute γ function $\qquad\qquad$ (5.12)

$$\frac{6\mu_{eff}\cdot u\cdot x_i}{R_{eq}}\int\frac{y_i}{\left(H+\dfrac{x_i^2}{2R_{eq}}+\dfrac{y_i^2}{2R_b}\right)^3}dy_i=\frac{6\mu_{eff}\cdot u\cdot x_i}{R_{eq}}\cdot\left(\frac{-R_b}{2}\right)\cdot\frac{1}{\left(H+\dfrac{x_i^2}{2R_{eq}}+\dfrac{y_i^2}{2R_b}\right)^2}$$

$$\int C_1(x_i)\frac{1}{\left(H+\dfrac{x_i^2}{2R_{eq}}+\dfrac{y_i^2}{2R_b}\right)^3}dy_i=C_1(x_i)\cdot\int\frac{dy_i}{\left[\left(H+\dfrac{x_i^2}{2R_{eq}}\right)\cdot2R_b+y_i^2\right]^3\cdot\dfrac{1}{8R_b^3}}$$

$$\Downarrow$$

Define a function, $\alpha_i^2=2R_b\cdot\left(H+\dfrac{x_i^2}{2R_{eq}}\right)$

$$\Downarrow$$

$$C_1(x_i)\cdot\int\frac{dy_i}{\left[\left(H+\dfrac{x_i^2}{2R_{eq}}\right)\cdot2R_b+y_i^2\right]^3\cdot\dfrac{1}{8R_b^3}}=C_1(x_i)\cdot8R_b^3\int\frac{dy_i}{\left(\alpha_i^2+y_i^2\right)^3}$$

$$\Downarrow$$

Evaluate the integral

$$\Downarrow$$

$$C_1(x_i)\cdot8R_b^3\int\frac{dy_i}{\left(\alpha_i^2+y_i^2\right)^3}=C_1(x_i)\cdot\frac{2R_b^3}{\alpha_i^2}\cdot\left[\frac{y_i}{\left(\alpha_i^2+y_i^2\right)^2}+3\int\frac{dy_i}{\left(\alpha_i^2+y_i^2\right)^2}\right]$$

$$\Downarrow$$

$$C_1(x_i)\cdot\frac{2R_b^3}{\alpha_i^2}\cdot\left[\frac{y_i}{\left(\alpha_i^2+y_i^2\right)^2}+3\int\frac{dy_i}{\left(\alpha_i^2+y_i^2\right)^2}\right]=$$

$$C_1(x_i)\cdot\frac{2R_b^3}{\alpha_i^2}\cdot\left\{\frac{y_i}{\left(\alpha_i^2+y_i^2\right)^2}+\frac{3}{2\alpha_i^2}\left[\frac{y_i}{\left(\alpha_i^2+y_i^2\right)}+\frac{1}{\alpha_i}\arctan\left(\frac{y_i}{\alpha_i}\right)\right]\right\}\quad(5.13)$$

Oil pressure distribution for the oil for i^{th} bristle can be found by substituting Equation (5.12) and (5.13) into the Equation (5.11). After substituting, integration constants can be found by applying boundary conditions given in Equation (5.9).

$$P_i = \frac{6\mu_{eff} \cdot u \cdot x_i}{R_{eq}} \cdot \left(\frac{-R_b}{2}\right) \cdot \frac{1}{\left(H + \dfrac{x_i^2}{2R_{eq}} + \dfrac{y_i^2}{2R_b}\right)^2}$$

$$+ C_1(x_i) \cdot \frac{2R_b^3}{\alpha_i^2} \cdot \left\{ \frac{y_i}{\left(\alpha_i^2 + y_i^2\right)^2} + \frac{3}{2\alpha_i^2}\left[\frac{y_i}{\left(\alpha_i^2 + y_i^2\right)} + \frac{1}{\alpha_i}\arctan\left(\frac{y_i}{\alpha_i}\right)\right]\right\} + C_2(x_i) \qquad (5.14)$$

B.C's:

$$y_i = 0 \Rightarrow P_i(y_i = 0) = P_u - \frac{\Delta P}{n_r} \cdot (i-1)$$

and

$$y_i = 2R_b \Rightarrow P_i(y_i = 2R_b) = P_u - \frac{\Delta P}{n_r} \cdot i$$

⇓ Applying first boundary condition yields $C_2(x_i)$ as,

$$C_2(x_i) = P_u - \frac{\Delta P}{n_r} \cdot (i-1) - \frac{6\mu_{eff} u}{R_{eq}} x_i \left[\frac{-R_b}{2} \cdot \frac{1}{\left(H + \dfrac{x_i^2}{2R_{eq}}\right)^2}\right]$$

⇓ Applying first boundary condition yields $C_1(x_i)$ as,

$$C_1(x_i) = \frac{1}{F_1}\left\{ \frac{-\Delta P}{n_r} - \frac{6\mu_{eff} u}{R_{eq}} x_i \left(\frac{R_b}{2}\right)\left[\frac{1}{\left(H + \dfrac{x_i^2}{2R_{eq}} + 1\right)^2} - \frac{1}{\left(H + \dfrac{x_i^2}{2R_{eq}}\right)^2}\right]\right\} \qquad (5.15)$$

where

$$F_1 = \frac{2R_b^3}{\left(\alpha_i^2\right)}\left\{ \frac{2R_b}{\left(\alpha_i^2 + 4R_b^2\right)^2} + \frac{3}{2\alpha_i^2}\left[\frac{2R_b}{\alpha_i^2 + 4R_b^2} + \frac{1}{\alpha_i}\arctan\left(\frac{2R_b}{\alpha_i}\right)\right]\right\}$$

and $\qquad\qquad (5.16)$

$$\alpha_i^2 = 2R_b \cdot \left(H + \frac{x_i^2}{2R_{eq}}\right)$$

Substituting Equations (5.15) and (5.16) into the pressure equation (5.14) yields,

$$P_i = F_3 + \frac{F_2}{F_1} \cdot F_4 + F_5 \; ,$$

$$F_1 = \frac{2R_b^{\,3}}{\left(\alpha_i^{\,2}\right)} \left\{ \frac{2R_b}{\left(\alpha_i^{\,2}+4R_b^{\,2}\right)^2} + \frac{3}{2\alpha_i^{\,2}}\left[\frac{2R_b}{\alpha_i^{\,2}+4R_b^{\,2}} + \frac{1}{\alpha_i}\arctan\left(\frac{2R_b}{\alpha_i}\right) \right] \right\}$$

$$F_2 = \frac{-\Delta P}{n_r} - \frac{6\mu_{eff}u}{R_{eq}}x_i\left(\frac{R_b}{2}\right)\left[\frac{1}{\left(H+\dfrac{x_i^{\,2}}{2R_{eq}}+1\right)^2} - \frac{1}{\left(H+\dfrac{x_i^{\,2}}{2R_{eq}}\right)^2} \right] ,$$

$$F_3 = \frac{6\mu_{eff}\cdot u\cdot x_i}{R_{eq}}\cdot\left(\frac{-R_b}{2}\right)\cdot\frac{1}{\left(H+\dfrac{x_i^{\,2}}{2R_{eq}}+\dfrac{y_i^{\,2}}{2R_b}\right)^2} , \qquad (5.17)$$

$$F_4 = \frac{2R_b^{\,3}}{\left(\alpha_i^{\,2}\right)} \left\{ \frac{2R_b}{\left(\alpha_i^{\,2}+y_i^{\,2}\right)^2} + \frac{3}{2\alpha_i^{\,2}}\left[\frac{2R_b}{\alpha_i^{\,2}+y_i^{\,2}} + \frac{1}{\alpha_i}\arctan\left(\frac{y_i}{\alpha_i}\right) \right] \right\} ,$$

$$F_5 = P_u - \frac{\Delta P}{n_r}\cdot(i-1) - \frac{6\mu_{eff}u}{R_{eq}}x_i\left[\frac{-R_b}{2}\cdot\frac{1}{\left(H+\dfrac{x_i^{\,2}}{2R_{eq}}\right)^2} \right] ,$$

$$\alpha_i^{\,2} = 2R_b\cdot\left(H+\frac{x_i^{\,2}}{2R_{eq}}\right).$$

Pressure distribution given above includes the effect of shear heating as μ_{eff}, which is found from effective temperature, appears in the pressure function. Pressure is a function of brush seal geometry *(R_b, R_{eq}, n_r)*, pressure load *(ΔP)*, upstream pressure *(P_u)*, rotor surface speed *(u)* and hydrodynamic lift clearance *(H)*. Table 2.2 is used for the experimental hydrodynamic lift clearance values. Note that pressure function derived above is function of both x_i and y_i coordinates. Pressure distribution along x_i direction for *y_i=R_b (middle of the bristle, see Figure 5.2)* of each bristle is given in Figure 5.3 for

48.3 kPa pressure load and 6.2 m/s rotor surface speed. Oil pressure along x_i behaves similarly for different pressure loads and rotor surface speeds, only magnitudes are different. Calculations are performed in MATLAB.
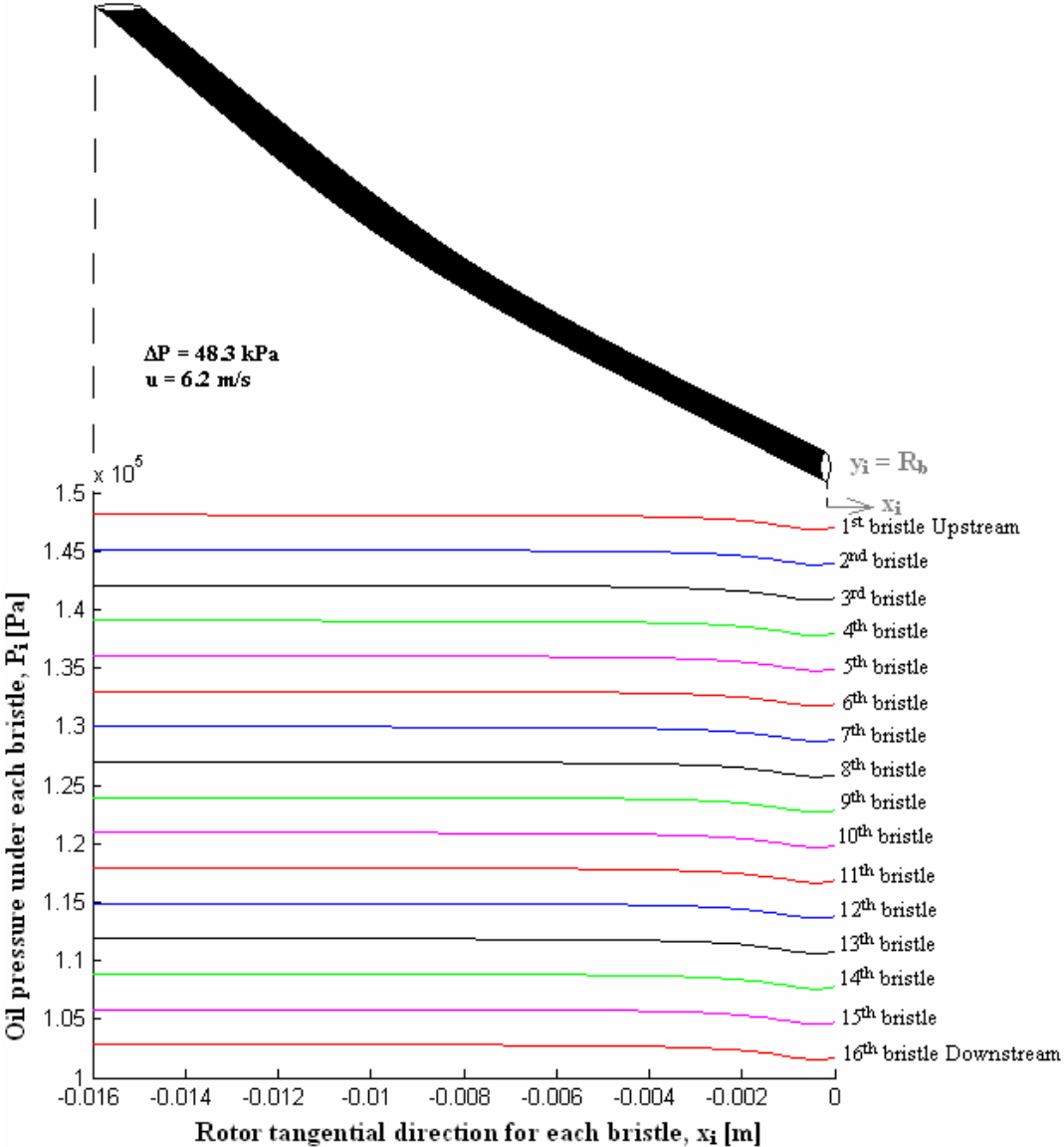
Figure 5.3 Oil pressure distributions along x_i for each bristle, $\Delta P = 48.3$ kPa, $u = 6.2$m/s

As it can be seen from the figure above, pressure change in x_i direction shows similar distribution for each bristle. Plots have same character, but magnitudes are decreasing as going from upstream side to downstream side as it is expected. Oil pressure for the first bristle is around upstream pressure (P_u), whereas it is around

downstream pressure $(P_d=P_a)$ for the oil under the last bristle. There is an evident change in oil pressure between -2mm and 0, which corresponds to length of projection of bristle portion at *"Fence height, FH" (Figure 1.4)* onto the x_i coordinate. After that point, pressure change is almost zero till -7mm, and then oil pressure remains constant. Fence height is the distance between the rotor surface and the backing plate, and bristles have most lack of restriction in that region. Bristles are clamped tighter in the region between free bristle height *(BH)* and fence height *(FH)*, which causes more difficult oil flow. Tightness of bristles increases as approaching to the front plate. Therefore, it is reasonable and consistent with real-life applications to obtain a constant pressure in x_i direction after a certain distance from fence height projection on x_i-axis.

As a representative example, oil pressure distribution along x_i and y_i axes for 89.6kPa pressure load and 20.5m/s rotor surface speed are presented in Figure 5.4.

Figure 5.4 Oil pressure change under each bristle along rotor axial and tangential directions

Combining oil pressure change with respect to local coordinates of bristles (x_i, y_i) gives the pressure distribution under the bristle pack of one row o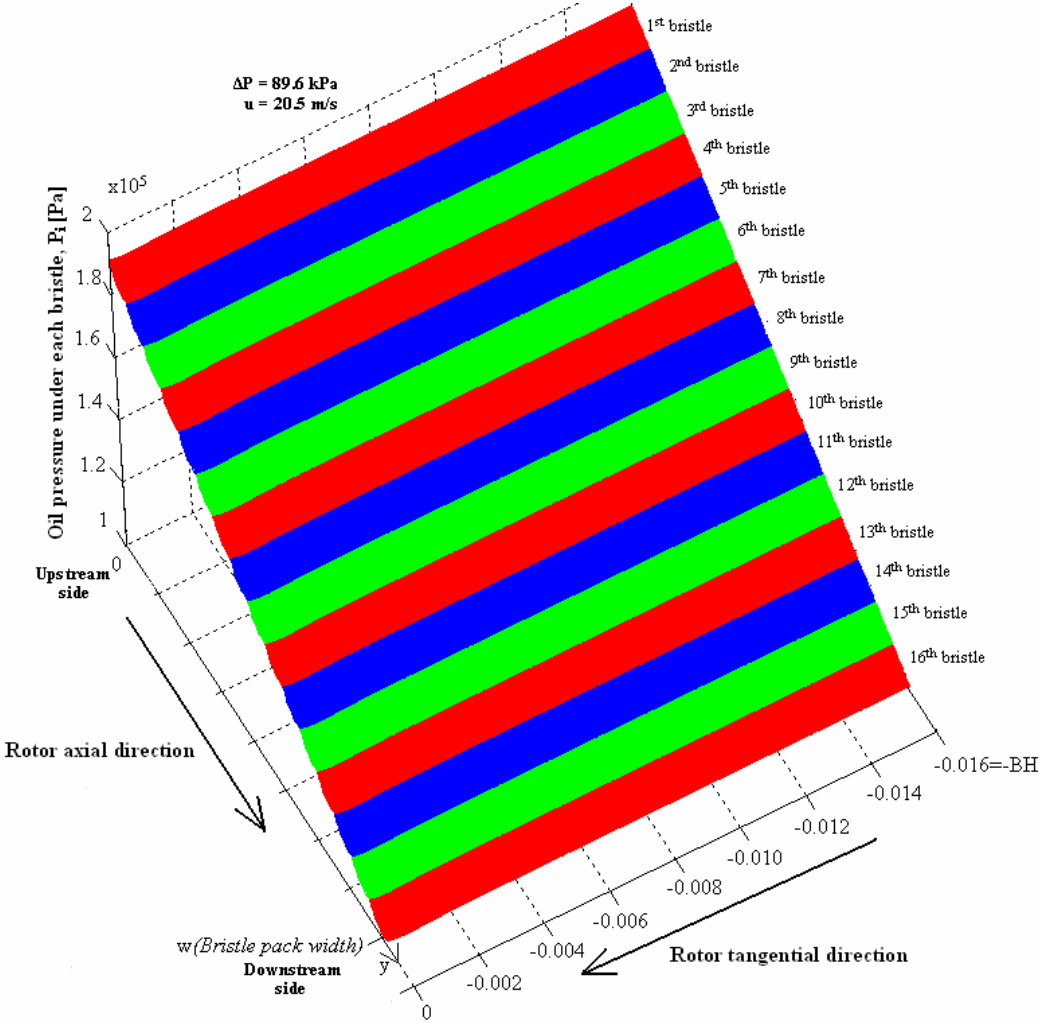f bristles. As it can be observed from the figure above, pressure distribution along rotor axial direction is almost linear for every point in rotor tangential direction as expected. It takes the upstream pressure value for $y = 0$ *(at the upstream side)*, and drops to downstream pressure value for $y = w$ *(at the downstream side)*.

In the previous chapters, analyses have been performed by selecting the control volume between the rotor surface and the bristle pack, and oil pressure distribution along y-axis *(rotor axial direction)* has been found almost linear. Therefore, linear pressure distribution has been accepted for the rotor axial direction. In this chapter, oil pressure has been developed by selecting control volume as the oil under each bristle, and the pressure for each bristle depends on both of the local coordinates, x_i and y_i. From Figure 5.4, comments about almost linear pressure distribution along rotor axial direction can be done. Mean value of oil pressure for each bristle with respect to x_i coordinate is developed in order to make comments on almost linear pressure distribution definite.

$$P_{i_{mean-x_i}}(y_i) = \frac{1}{BH} \int_{-BH}^{0} P_i(x_i, y_i) \cdot dx_i \qquad (5.18)$$

P_i is the oil pressure under each bristle given in Equation (5.17). Again, trapezoid rule is selected as a numeric integration method, and numeric integral is evaluated by writing a MATLAB code.

$$
\begin{aligned}
P_{i_{mean-x_i}}(y_i) &= \frac{1}{BH} \int_{-BH}^{0} P_i(x_i, y_i) \cdot dx_i \\
&= \frac{1}{BH} \left\{ \frac{l}{2} \cdot \left[P_i(x_{i_1}, y_i) + 2P_i\left(x_{i_1} + l, y_i\right) + \ldots + P_i\left(x_{i_2}, y_i\right) \right] \right\}
\end{aligned}
\qquad (5.19)
$$

A step of numeric integration, l, is taken as *BH/1600*. In Figure 5.5, mean-x pressure for the first bristle is given for 89.6 kPa pressure load and 20.5 m/s rotor surface speed. As it can be seen from the figure, pressure distribution along y_i-axis of the first bristle is almost linear. Pressure distribution along y-axis *(rotor axial direction)*, which is given

in Figure 5.6, can be obtained by combining local mean-x_i pressure distribution of each bristle in one row of the bristle pack.
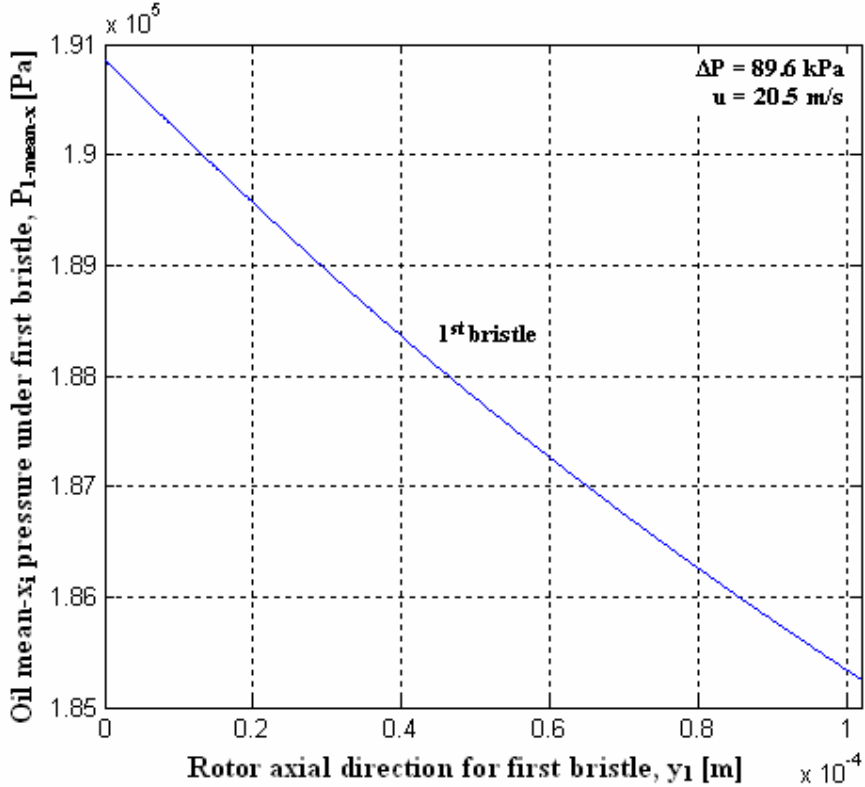
Figure 5.5 Mean-x_i pressure change with rotor axial direction for the first bristle
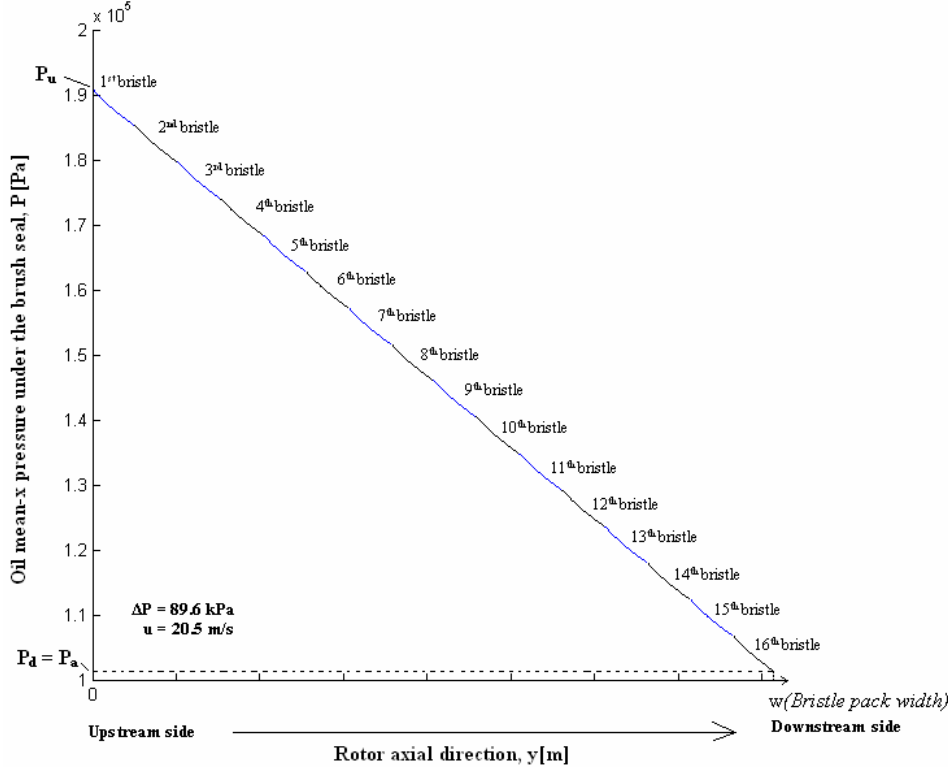
Figure 5.6 Mean-x pressure change with rotor axial direction for the bristle pack

As it can be seen from the Figure 5.6, oil pressure change along rotor axial direction *(y-axis)*, which is found by combining local pressure distributions of Equation (5.19) for each bristle, is almost linear. This result is consistent with pressure distributions derived in Chapter 3 and real-life applications as reported by Braun et al. [30].

6 DERIVATION OF SHEAR HEAT INCLUDED HYDRODYNAMIC LIFT CLEARANCE

Importance of hydrodynamic lift clearance has been stated in the previous sections. Until now, derivation of closed form function for oil temperature has been performed and the shear heat dissipation effect has been successfully integrated into the lift force formulation. Oil pressure is successfully derived by tracking three different ways, all of which give very similar results to each other. All these analyses are advanced fluid mechanics and heat transfer analyses, which give consistent results with real-life applications.

In this chapter, function of shear heating effect included in hydrodynamic lift clearance formulation. For a different pressure loads *(which is design parameter and known)*, change of hydrodynamic lift clearance with rotor surface speed can be found without requiring any experimental leakage data. Furthermore, theoretic lift clearance gives highly accurate results with the experimental lift data given in Table 2.2.

6.1 Theoretic Hydrodynamic Lift Clearance

In the previous chapters, pressure distribution is derived by tracking three different ways and all of three analyses give almost linear pressure distribution along rotor axial direction. In brush seal applications, it is known that pressure changes almost linearly in the direction of rotor axis, which means that analyses of this study gives agreement with real-life applications.

Idea of deriving hydrodynamic lift clearance arises from the almost linear oil pressure. Although oil pressure under each bristle, which is given in Equation (5.17) is found as a complicated function of lift clearance, pressure load, rotor surface, effective viscosity, bristle geometry and local coordinates, it gives almost linear pressure distribution along rotor axial direction *(See Figures 5.5 and 5.6)*. Difference between

the linear oil pressure and pressure given in Equation (5.17) for the ith bristle is defined as error function.

$$\varepsilon_i(u, \Delta P, x_i, y_i) = P_{i-lin} - P_i \tag{6.1}$$

where

$$P_{i-lin} = P_u - \frac{\Delta P}{n_r} \cdot (i-1) - \frac{\Delta P}{2 \cdot R_b \cdot n_r} \cdot y_i$$

and

$$P_i = F_3 + \frac{F_2}{F_1} \cdot F_4 + F_5 \ ,$$

$$F_1 = \frac{2R_b^{\,3}}{\left(\alpha_i^{\,2}\right)} \left\{ \frac{2R_b}{\left(\alpha_i^{\,2}+4R_b^{\,2}\right)^2} + \frac{3}{2\alpha_i^{\,2}} \left[\frac{2R_b}{\alpha_i^{\,2}+4R_b^{\,2}} + \frac{1}{\alpha_i} \arctan\left(\frac{2R_b}{\alpha_i}\right) \right] \right\}$$

$$F_2 = \frac{-\Delta P}{n_r} - \frac{6\mu_{eff}u}{R_{eq}} x_i \left(\frac{R_b}{2}\right) \left[\frac{1}{\left(H + \dfrac{x_i^{\,2}}{2R_{eq}} + 1\right)^2} - \frac{1}{\left(H + \dfrac{x_i^{\,2}}{2R_{eq}}\right)^2} \right] \ ,$$

$$F_3 = \frac{6\mu_{eff} \cdot u \cdot x_i}{R_{eq}} \cdot \left(\frac{-R_b}{2}\right) \cdot \frac{1}{\left(H + \dfrac{x_i^{\,2}}{2R_{eq}} + \dfrac{y_i^{\,2}}{2R_b}\right)^2} \ ,$$

$$F_4 = \frac{2R_b^{\,3}}{\left(\alpha_i^{\,2}\right)} \left\{ \frac{2R_b}{\left(\alpha_i^{\,2}+y_i^{\,2}\right)^2} + \frac{3}{2\alpha_i^{\,2}} \left[\frac{2R_b}{\alpha_i^{\,2}+y_i^{\,2}} + \frac{1}{\alpha_i} \arctan\left(\frac{y_i}{\alpha_i}\right) \right] \right\} \ ,$$

$$F_5 = P_u - \frac{\Delta P}{n_r} \cdot (i-1) - \frac{6\mu_{eff}u}{R_{eq}} x_i \left[\frac{-R_b}{2} \cdot \frac{1}{\left(H + \dfrac{x_i^{\,2}}{2R_{eq}}\right)^2} \right] \ ,$$

$$\alpha_i^{\,2} = 2R_b \cdot \left(H + \frac{x_i^{\,2}}{2R_{eq}}\right).$$

84

$P_{i\text{-}lin}$ gives the linear pressure distribution along rotor axial direction for each bristle. Note that error function of Equation (5.18), $\varepsilon_i(u,\Delta P,x_i,y_i)$, depends on rotor surface speed and pressure load. In Chapter 5, it has been mentioned that hydrodynamic lift clearance is assumed to be same for each bristle in a row of rotor axial direction. Therefore, derivation of lift clearance for any bristle gives the lift data for the brush seal. For this reason, values of error function for the last bristle, which corresponds to 16th bristle since n_r is sixteen, are evaluated for x_{16} = -BH and y_{16} = $R_b/10000$. Values of error functions for different pressure loads and rotor surface speeds are given in Table 6.1.

16th element x_{16} = -BH, y_{16} = $R_b/10000$	ΔP = 48.3 kPa	ΔP = 89.6 kPa
Rotor surface speed [m/s]	Error = $P_{i\text{-}lin}$ -P_i	Error = $P_{i\text{-}lin}$ -P_i
0	0	0
6.2	0.18089160071395	0.18259628994565
12.3	0.37061247121892	0.37043838875252
20.5	0.51292344700778	0.55241753367591

Table 6.1 Error between $P_{i\text{-}lin}$ and P_i for the 16th bristle, where x_i=-BH and y_i=$R_b/10000$

16th element x_{16} = -BH, y_{16} = $R_b/10000$	ΔP = 48.3 kPa	ΔP = 89.6 kPa
Rotor surface speed [m/s]	Error % = 100x($P_{i\text{-}lin}$ -P_i)/$P_{i\text{-}lin}$	Error % = 100x($P_{i\text{-}lin}$ -P_i)/$P_{i\text{-}lin}$
0	0	0
6.2	$1.73361473 \times 10^{-4}$ %	1.707708×10^{-4} %
12.3	$3.55184673 \times 10^{-4}$ %	$3.46447845 \times 10^{-4}$ %
20.5	$4.91571549 \times 10^{-4}$ %	$5.16641552 \times 10^{-4}$ %

Table 6.2 Error% between $P_{i\text{-}lin}$ and P_i for the 16th bristle, where x_i=-BH and y_i=$R_b/10000$

As it can be seen from the Tables 6.1 and 6.2, error function is almost zero so that $P_{i\text{-}lin}$ can be taken equal to P_i. However, for the sake of obtaining more accurate results, error for the 16th bristle, for x_i = -BH and y_i = $R_b/10000$ can be defined. Since there are

two pressure load and three rotor surface speed data, the error function can be found as second degree polynomial of rotor surface speed and first degree polynomial of pressure load. Define an error function for the 16th bristle as,

$$\varepsilon_{16}(u, \Delta P, x_{16} = -BH, y_{16} = R_b / 10000) = \left(a \cdot u^2 + b \cdot u + c\right) \cdot (e \cdot \Delta P + f)$$

$$\Downarrow$$

$$\varepsilon_{16}(u, \Delta P, x_{16} = -BH, y_{16} = R_b / 10000)$$

$$= a \cdot e \cdot u^2 \cdot \Delta P + a \cdot f \cdot u^2 + b \cdot e \cdot u \cdot \Delta P + b \cdot f \cdot u + c \cdot e \cdot \Delta P + c \cdot f$$

Combine the constant coefficients

$$\Downarrow$$

$$\varepsilon_{16}(u, \Delta P, x_{16} = -BH, y_{16} = R_b / 10000) = A \cdot u^2 \cdot \Delta P + B \cdot u^2 + C \cdot u \cdot \Delta P + D \cdot u + E \cdot \Delta P + F$$

(6.2)

A, B, C, D, E and *F* are constant coefficients which can be determined using the data given in Table 6.1. Matrix equation given below is obtained as,

$$\begin{bmatrix} u_1^2 \cdot \Delta P_1 & u_1^2 & u_1 \cdot \Delta P_1 & u_1 & \Delta P_1 & 1 \\ u_2^2 \cdot \Delta P_1 & u_2^2 & u_2 \cdot \Delta P_1 & u_2 & \Delta P_1 & 1 \\ u_3^2 \cdot \Delta P_1 & u_3^2 & u_3 \cdot \Delta P_1 & u_3 & \Delta P_1 & 1 \\ u_1^2 \cdot \Delta P_2 & u_1^2 & u_1 \cdot \Delta P_2 & u_1 & \Delta P_2 & 1 \\ u_2^2 \cdot \Delta P_2 & u_2^2 & u_2 \cdot \Delta P_2 & u_2 & \Delta P_2 & 1 \\ u_3^2 \cdot \Delta P_2 & u_3^2 & u_3 \cdot \Delta P_2 & u_3 & \Delta P_2 & 1 \end{bmatrix} \cdot \begin{bmatrix} A \\ B \\ C \\ D \\ E \\ F \end{bmatrix} = \begin{bmatrix} 0.18089160071395 \\ 0.37061247121892 \\ 0.55410932186351 \\ 0.18180358028621 \\ 0.37152373105346 \\ 0.51383515654015 \end{bmatrix}$$

(6.3)

where

$$u_1 = 6.2 m / s$$
$$u_2 = 12.3 m / s \quad \text{and} \quad \begin{array}{l} \Delta P_1 = 48.3 kPa \\ \Delta P_2 = 189.6 kPa \end{array}$$
$$u3 = 20.5 m / s$$

Matrix equation given above is solved by using MATLAB, which yields,

$$
\begin{bmatrix} A \\ B \\ C \\ D \\ E \\ F \end{bmatrix} = \begin{bmatrix} 0.00000000871259 \\ -0.00138211964675 \\ -0.00000016864155 \\ 0.05703112974953 \\ 0.00000077084728 \\ -0.12156751681664 \end{bmatrix}
$$

$$
\varepsilon_{16}(u, \Delta P, x_{16} = -BH, y_{16} = R_b/10000) = A \cdot u^2 \cdot \Delta P + B \cdot u^2 + C \cdot u \cdot \Delta P + D \cdot u + E \cdot \Delta P + F
$$

(6.4)

$$
= P_{16-lin}(-BH, R_b/10000) - P_{16}(-BH, R_b/10000)
$$

where $x_i = -BH$, $y_i = R_b/10000$, $i = 16$

$$
P_{i-lin} = P_u - \frac{\Delta P}{n_r} \cdot (i-1) - \frac{\Delta P}{2 \cdot R_b \cdot n_r} \cdot y_i
$$

$$
P_i = F_3 + \frac{F_2}{F_1} \cdot F_4 + F_5 \ ,
$$

$$
F_1 = \frac{2R_b^{\,3}}{\left(\alpha_i^{\,2}\right)} \left\{ \frac{2R_b}{\left(\alpha_i^{\,2} + 4R_b^{\,2}\right)^2} + \frac{3}{2\alpha_i^{\,2}} \left[\frac{2R_b}{\alpha_i^{\,2} + 4R_b^{\,2}} + \frac{1}{\alpha_i} \arctan\left(\frac{2R_b}{\alpha_i}\right) \right] \right\}
$$

$$
F_2 = \frac{-\Delta P}{n_r} - \frac{6\mu_{eff} u}{R_{eq}} x_i \left(\frac{R_b}{2}\right) \left[\frac{1}{\left(H + \dfrac{x_i^{\,2}}{2R_{eq}} + 1\right)^2} - \frac{1}{\left(H + \dfrac{x_i^{\,2}}{2R_{eq}}\right)^2} \right] \ ,
$$

$$
F_3 = \frac{6\mu_{eff} \cdot u \cdot x_i}{R_{eq}} \cdot \left(\frac{-R_b}{2}\right) \cdot \frac{1}{\left(H + \dfrac{x_i^{\,2}}{2R_{eq}} + \dfrac{y_i^{\,2}}{2R_b}\right)^2} \ ,
$$

$$
F_4 = \frac{2R_b^{\,3}}{\left(\alpha_i^{\,2}\right)} \left\{ \frac{2R_b}{\left(\alpha_i^{\,2} + y_i^{\,2}\right)^2} + \frac{3}{2\alpha_i^{\,2}} \left[\frac{2R_b}{\alpha_i^{\,2} + y_i^{\,2}} + \frac{1}{\alpha_i} \arctan\left(\frac{y_i}{\alpha_i}\right) \right] \right\} \ ,
$$

$$
F_5 = P_u - \frac{\Delta P}{n_r} \cdot (i-1) - \frac{6\mu_{eff} u}{R_{eq}} x_i \left[\frac{-R_b}{2} \cdot \frac{1}{\left(H + \dfrac{x_i^{\,2}}{2R_{eq}}\right)^2} \right] \ ,
$$

$$
\alpha_i^{\,2} = 2R_b \cdot \left(H + \frac{x_i^{\,2}}{2R_{eq}}\right).
$$

87

Equation (6.4) is a function of ΔP, μ_{eff}, BH, R_b, R_{eq}, n_r, u and H. ΔP is a design parameter and known. BH, R_b, R_{eq}, n_r are brush seal properties and they are also known. μ_{eff} can be calculated from Equation (4.17), by using temperature analysis of Chapter 2. Only u and H is unknown in Equation (6.4), and relation between them can be found by using this equation, without requiring any experimental data. Since the equation (6.4) is a complex function of u and H, closed form solution to H can not be found. Therefore, MATLAB code is used in order to find hydrodynamic lift clearance. The logic of MATLAB code is as given,

1. Start a *"for loop"* for rotor surface speed.
2. Start another *"for loop"* for hydrodynamic lift clearance.
3. For u and H, find effective temperature by using Equation (4.16).
4. Find effective viscosity, μ_{eff}, by using Equation (4.17).
5. Find $P_{16-lin}(-BH, R_b/10000) - P_{16}(-BH, R_b/10000)$ for ever u and H value by using Equation (6.4).
6. Find

   $$\varepsilon_{16}(u, \Delta P, x_{16} = -BH, y_{16} = R_b/10000) = A \cdot u^2 \cdot \Delta P + B \cdot u^2 + C \cdot u \cdot \Delta P + D \cdot u + E \cdot \Delta P + F$$
   by using (6.4)

7. If

   $$\varepsilon_{16}(u, \Delta P, x_{16} = -BH, y_{16} = R_b/10000) = P_{16-lin}(-BH, R_b/10000) - P_{16}(-BH, R_b/10000)$$
   break!

Note that shear heating effect is included into the lift clearance through steps 3 to 4, by using previous thermal analysis.

6.2   Results and Comparison with Experimental Lift Clearance

Comparison of theoretical hydrodynamic lift clearance found by introducing a MATLAB code for Equation (6.4) and experimental hydrodynamic lift clearance data is given in Figures 6.1 and 6.2. As it can be seen from the figures, the lift clearance data gives highly consistent results with experimental lift clearance data. High speed-stabilization in theoretic lift clearance is the result of including shear heating effect by means of effective viscosity.

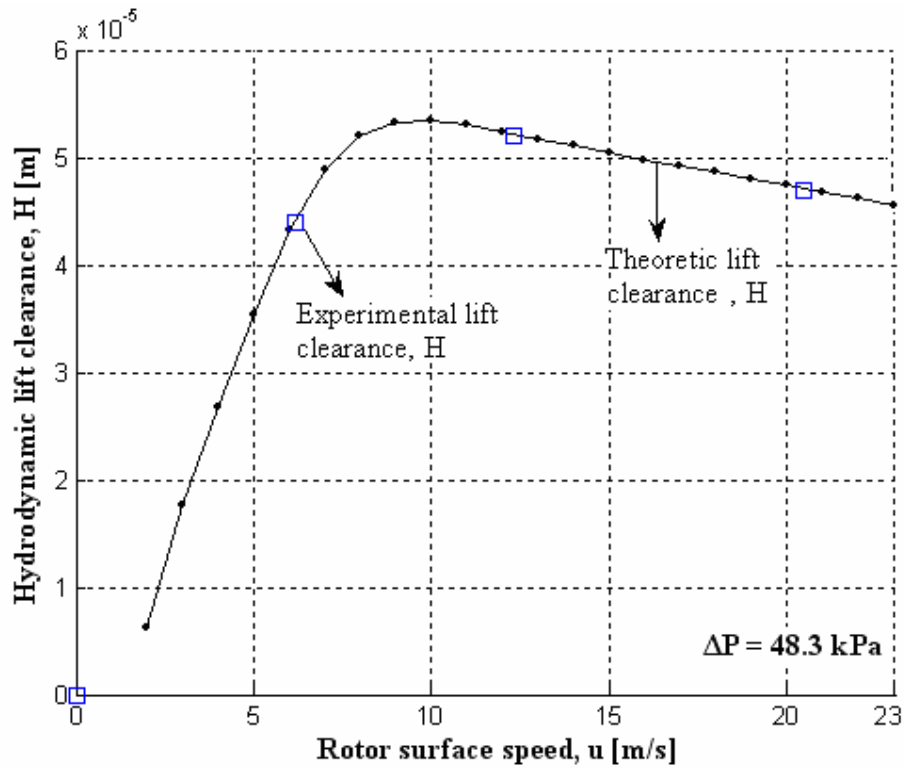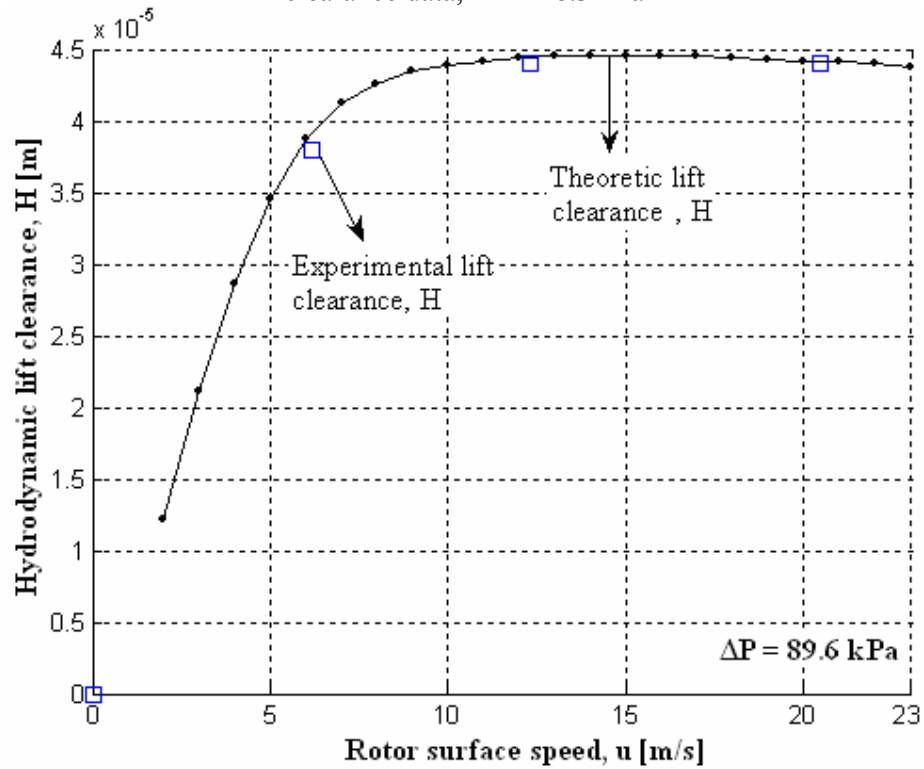Figure 6.1 Comparison of theoretic hydrodynamic lift clearance with experimental lift clearance data, ΔP = 48.3 kPa

Figure 6.2 Comparison of theoretic hydrodynamic lift clearance with experimental lift clearance data, ΔP = 89.6 kPa

Theoretic lift clearance change with rotor surface speeds are given in Figure 6.3 for different pressure loads. As it can be observed form the figure, lift clearance decreases as pressure load increases, which is also the case for real life applications. Oil flow at *y*-direction increases as pressure load increases, which results in more shear in the oil. As a result of increasing shear mechanisms, dissipated heat is higher for large pressure loads. Therefore, effective viscosity takes smaller values for same rotor speeds at higher pressure loads, which degrades the lift ability of the oil.
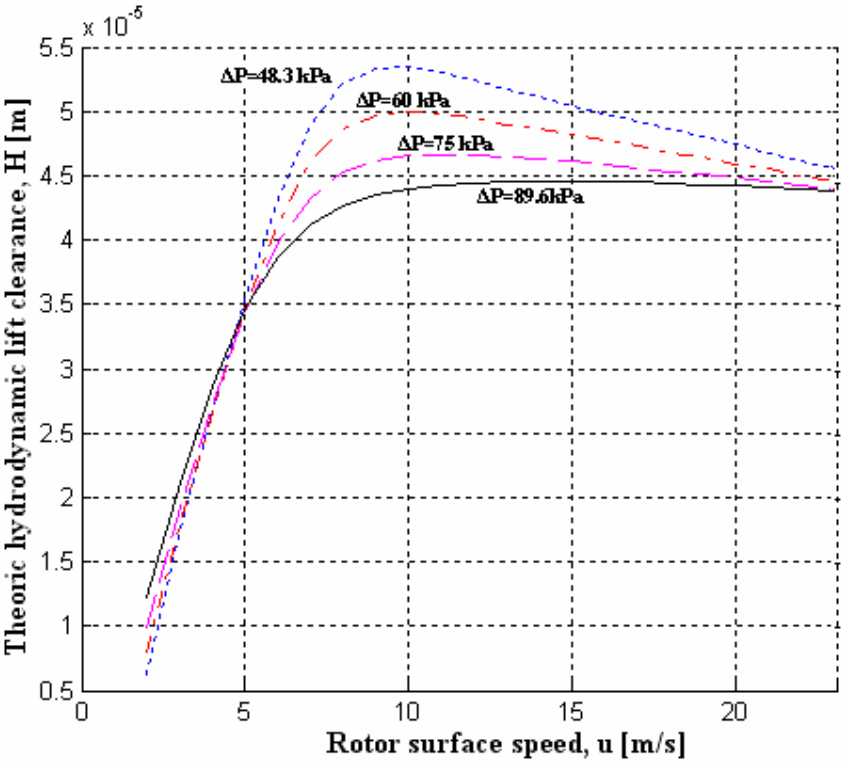

Figure 6.3 Theoretic hydrodynamic lift clearance change with rotor surface speed for different pressure loads

7   CONCLUSION

Shear heating in brush seals has great importance as it affects the hydrodynamic lift clearance and lifting force. This in return, determines the seal leakage performance. In brush seal applications, shear heat dissipation is the reason for stabilization of the lifting force after certain rotor speeds. Until now, suggested theories did not include the shear heating effect, or underestimate the frictional and blow down forces.

In this study, after selecting an appropriate control volume, and analyzing the boundary layer equations, thermal energy equation for the control volume has been derived. A closed-form solution for the temperature distribution of the oil is provided as a function of oil properties, hydrodynamic lift clearance, and pressure difference between upstream and downstream sides. Effect of shear heating on the lifting force is successfully represented by including the temperature effects into the bearing theory. Comparison of analysis results with the available experimental data show reasonable agreement with proper high speed lift stabilization due to shear thinning.

Pressure distribution of the oil is another important task for brush seal applications. Until now, there is no theoretical work on oil pressure for brush seals. This study derives oil pressure by tracing three different ways. As a result of pressure analyses, pressure distribution in rotor axial direction is found almost linear, which is consistent with engine applications.

The most important parameter for leakage performance of the brush seal is hydrodynamic lift clearance. Lifting force theories until now are derived in order to give a sight about lift clearance, and they require experimental leakage data. In this study, theoretic lift clearance is derived by using the similarity between oil pressure under each bristle and linear pressure distribution. Shear heating effect is also included into the lifting clearance analysis by means of effective viscosity. In conclusion, theoretic hydrodynamic lift clearance shows high consistency with experimental leakage data.

REFERENCES

[1] Gorelov, G. M., Reznik, V. E., and Tsibizov, V. I., 1988, "Experimental Study of Brush Seal Flow Characteristics and Comparison with a Labyrinth Seal," Izvestitiya VUZ. Aviatsionnaya Tekhnika, 31, No. 4, pp. 43-46 [Allerton Press].

[2] Hendricks, R. C., Schlumberger, S., Braun, M. J., Choy, F., and Mullen, R. L., 1991, "A Bulk Flow Model of a Brush Seal System," ASME paper no. 91-GT-325.

[3] Owen, A. K., Jones, T. V., Guo, S. M., and Hogg, S., 2003, "An Experimental and Theoretical Study of Brush Seal and Shaft Thermal Interaction," ASME paper no. GT-2003-38276.

[4] Chew, J. W., and Guardino, C., 2004, "Simulation of Flow and Heat Transfer in the Tip Region of a Brush Seal," Int. J. Heat Fluid Flow, 25, No. 4, pp. 649-658.

[5] Demiroglu, M., 2004, "An Investigation of Tip Force and Heat Generation Characteristics of Brush Seals," Ph.D. Thesis, Rensselaer Polytechnic Institute, Troy, NY, USA.

[6] Dogu, Y., and Aksit, M., 2006, "Brush Seal Temperature Distribution Analysis," ASME J. Eng. For Gas Turbines and Power, 128, pp. 599-609.

[7] Scharrer, J. and Hendricks, R. C., "Results of Cyrogenic Brush Seal Testing," Proceedings of NASA Seals Workshop – Seals Flow Code Development 92, Cleveland, OH, August 5-6 1992, NASA-CP-10124, pp.215.

[8] Proctor, M. P., "Brush Seals for Cyrogenic Applications," Proceedings of NASA Seals Workshop – Seals Flow Code Development 93, Cleveland, OH, November 3-4 1993, NASA-CP-10136, pp.119-130.

[9] Ingistov, S., "Power Augmentation and Retrofits of Heavy Duty Industrial Turbines model 7EA," Proceedings of Power-Gen International Conference, Las Vegas, NV, 2001.

[10] Bhate, N., Thermos, A.C., Aksit, M.F., Demiroglu, M., Kizil, H., "Non-Metallic Brush Seals For Gas Turbine Bearings", Proceedings of ASME Turbo Expo 2004, GT2004-54296, 2004.

[11] Bagepalli B.S., Aksit M.F., and Mayer R.R., "Brush seal and rotary machine including such brush seal," US Patent No. US 6257588B1, 2001.

[12] Aksit M.F., Dinc O.S., and Mayer R.R., "Brush seal and machine having a brush seal," US Patent No. US 6406027B1, 2002.

[13] Mayer R.R., Bagepalli B.S., and Aksit M.F., "Low flow fluid film seal for hydrogen cooled generators," US Patent No. US 6378873B1, 2002.

[14] Mayer R.R., Aksit M.F., and Bagepalli B.S., "Brush seal for a bearing cavity," US Patent No. US6502824B2, 2003.

[15] Aksit, M. F., Bhate, N., Bouchard, C., Demiroglu, M., and Dogu, Y., 2003, "Evaluation of Brush Seal Performance for Oil Sealing Applications," AIAA paper no. AIAA-2003-4695.

[16] Aksit, M.F., Dogu, Y., J.A. Tichy and Gursoy M., "Hydrodynamic Lift of Brush Seals In Oil Sealing Applications," Proceedings of 40th AIAA/ASME/SAE/ASEE Joint Propulsion Conference & Exhibit, Fort Lauderdale, Florida, AIAA Paper AIAA-2004-3721, 2004.

[17] Flower R., "Brush Seal Development System," AIAA Paper No. AIAA-90-2143, 1990

[18] Braun, M.J., Canacci, V.A., and Hendricks, R.C, "Flow Visualization and Quantitive Velocity and Pressure Measurements in Simulated Single and Double Brush Seals," Trib. Trans., 34, pp 70-80, 1991

[19] Dogu, Y., "Investigation of Brush Seal Flow Characteristics Using Bulk Porous Medium Approach", ASME Turbo Expo 2003, GT2003-38970

[20] O'Neill, A. T., Hogg, S. I., Withers, P. A., Turner, M. T., and Jones, T. V., "Multiple Brush Seals in Series," ASME Gas Turbine and Aeroengine Congress Paper ASME 97-GT-194, 1997

[21] Ferguson, J. G., "Brushes as High Performance Gas Turbine Seals," ASME Gas Turbine and Aeroengine Congress Paper ASME 88-GT-182, 1988

[22] Hendricks, R. C., Carlile, J. A., Liang, A. D., Steinetz, B. M., Easter, Onstott, J. W., and Howe, H., "Static Brush Seals for Propulsion System Interfaces," 5th Advanced Earth to Orbit Propulsion Technology Conference Paper, NASA CP-3174-VOL-1, pp 243-439, 1992

[23] Dinc, S., Bagepalli, B., Cromer, R., Maynard, J., Calabrese, S. and Aksit, M.F., "High Temperature Vibratory Brush Seals for Gas Turbine Applications," AIAA/SAE/ASME/ASEE 30th Joint Propulsion Conference Paper, AIAA 94-2704, 1994

[24] Mayhew, E. R., Bill, R. C., Voorhees, W. J. and O'Donnell, J., "Military Engine Seal Development: Potential for Dual Use," AIAA/SAE/ASME/ASEE 30th Joint Propulsion Conference Paper, AIAA 94-2699, 1994

[25] Holle, G. F., Khrishnan, M. R., "Gas Turbine Engine Brush Seal Applications," AIAA/SAE/ASME/ASEE 26th Joint Propulsion Conference Paper, AIAA 90-2142, 1990

[26] Short, J. F., Basu P., Datta, A., Loewenthal, R. G. and Prior, R.J., "Advance Brush Seal Development," AIAA/SAE/ASME/ASEE 32nd Joint Propulsion Conference Paper, AIAA 96-2907, 1996

[27] Arora, G. K. and Proctor, M. P., "JTAGG II Brush Seal Test Results," AIAA/SAE/ASME/ASEE 33rd Joint Propulsion Conference Paper, AIAA 97-2632, 1997

[28] Hendricks, R.C., Wilson, J., Wu, T., and Flower, R., "Bidirecitonal Brush Seals," ASME Gas Turbine and Aeroengine Congress Paper ASME 97-GT-256, 1997

[29] Incropera, F. P., DeWitt, D. P., "Fundementals of Heat and Mass Transfer," 4th Edition, John Wiley & Sons, Inc., New York, 1996

[30] Öztürk, A. and Kılıç, A., "Çözümlü Problemlerle Termodinamik," 3rd Edition, Çağlayan Kitabevi, Istanbul, 1998

[31] Öztürk, A., Kılıç, A. and Yavuz, H., "Termodinamik ve Isı Geçişi Tabloları," 4th Edition, Çağlayan Kitabevi, Istanbul, 2001

[32] Öztürk, A. and Yavuz, H., "Uygulamalarla Isı Geçişi: Tanıtım ve Işınım," 1st Edition, Çağlayan Kitabevi, Istanbul, 1995

[33] Aksit, M. F., "A Computational Study of Brush Seal Contact Loads with Friction", PhD thesis, 1998